DISSERTATION ZUR ERLANGUNG DES DOKTORGRADES
DER NATURWISSENSCHAFTEN (DR. RER. NAT.)
DER NATURWISSENSCHAFTLICHEN FAKULTÄT III –
BIOLOGIE UND VORKLINISCHE MEDIZIN DER
UNIVERSITÄT REGENSBURG

Cellular role of the putative Ca^{2+}-dependent Cl^- channel bestrophin

vorgelegt von
René Barro Soria
aus La Habana
Juli/2008

Promotionsgesuch eingereicht am: 28. May 2008

Colloquium: 09. Juli 2008

Die Arbeit wurde angeleitet von: Prof. Dr. K. Kunzelmann

Prüfungsausschuss:

Vorsitzender:	Prof. Dr. R. Warth
1. Prüfer:	Prof. Dr. K. Kunzelmann
2. Prüfer:	Prof. Dr. rer.nat. O. Strauss
3. Prüfer:	Prof. Dr. S. Schneuwly
Ersatzprüfer:	Prof. Dr. G. Längst

Die Dissertation wurde von Prof. Dr. K. Kunzelmann angeleitet.

Summary

Ca^{2+}-activated Cl^- channels (CaCCs) participate in a variety of important physiological processes such as transepithelial transport, olfactory and taste transduction, neuronal and cardiac excitability, fototransduction and fertility. These Cl^- channels also play a key role in diseases such as cystic fibrosis, secretory diarrhea and polycystic kidney disease. Although epithelial CaCCs have been studied for more than two decades, their molecular identity and physiological role remain uncertain. Whereas most candidate molecules have failed to fulfill CaCC requisites, proteins of the bestrophin family have been demonstrated to induce a Ca^{2+}-acitivated Cl^- conductance in expression systems. The properties of this conductance resembled those of Ca^{2+}-activated Cl^- currents (I_{ClCa}) in native tissues. Bestrophin 1 (best1), the gene product of the vitelliform macular dystrophy type 2 (VMD2), is expressed in the retinal pigment epithelium (RPE) where it is thought to underlie the Cl^- conductance that controls retinal homeostasis. Mutations in best1 gene cause the so-called Best disease, a genetic form of retinal macular dystrophy.

There is not yet a consensus as to whether Best disease is caused by Cl^- channel dysfunction, partly because mbest1 knockout mice (best1-/-) have no ocular pathology and normal Cl^- currents can be recorded from the RPE. It has also been shown that best1 regulates voltage-gated Ca^{2+} channels in the RPE. The precise cellular role of bestrophins therefore remains an unresolved question. Most importantly, bestrophins remain to be demonstrated to generate I_{ClCa} in tissues other than the RPE.

The present work demonstrates that best1 is also expressed in other epithelial tissues, such as airways, kidney and colon where it enables Ca^{2+}-activated Cl^- secretion. Endogenous I_{ClCa} coincide with endogenous expression of best1 in murine and human epithelial cells, whereas I_{ClCa} is absent in epithelial tissues lacking best1 expression. Furthermore, I_{ClCa} is shown to be activated by ATP in HEK293 cells overexpressing hbest1. The contribution of bestrophin 1 and 2 to the CaCC current in mouse airways was studied. Ussing chamber recordings showed that low concentrations of the purinergic agonist ATP (0.1-1μM) evoked larger short circuit currents (Isc) in tracheas of wild type (best1+/+) mice, when compared to tracheas of best1 knockout (best1-/-) mice. Patch clamp analysis revealed that ATP-induced whole cell currents in primary epithelial cells from best1-/- tracheas were half as the size of those recorded from best1+/+ cells. Besides, short interfering RNA (siRNA) targeting mbest2 reduced ATP-induced whole-cell currents in both best1-/- and best1+/+ cells. Moreover, siRNAs suppression of mbest1 reduced Ca^{2+}-activated Cl^- currents in best1+/+ cells. Cells patch clamped in the presence of different Ca^{2+}-free intracellular solutions, also showed

larger Ca^{2+}-activated Cl^- currents in best1+/+ than in best1-/- mice. These and other results suggest that bestrophin 1 and 2 are necessary components of the Ca^{2+}-activated Cl^- secretion in mouse trachea.

The quaternary structure of bestrophins as well as their cellular localization is of fundamental importance for the understanding of their physiological role. Here, we show a molecular and functional interaction and a colocalization of hbest1 with hbest2 and hbest1 with hbest4, when overexpressed heterologously in HEK293 cells, or for airway epithelial cells expressing endogenous bestrophins. Immunohistochemistry reveals strong plasma membrane expression of hbest2 and hbest4, but weak plasma membrane expression for hbest1, which seems to be localized in the endoplasmic reticulum according to confocal microscopy. Expression of either hbest2 or hbest4 but not hbest1 or hbest3, induce baseline anion conductances upon expression in HEK293 cells. Upon ATP stimulation, the baseline conductance is increased in cells expressing hbest1 and hbest3 but remains unchanged in hbest2- and hbest4-expressing cells. In addition, coexpression of hbest1 or hbest3 largely attenuated the large baseline conductance induced by hbest2 and hbest4. This indicates that bestrophin paralogs interact with each other and form heterooligomers. Although, hbest1 has been proposed to regulate voltage-gated Ca^{2+} channels, we observed no gross changes in ATP-dependent intracellular Ca^{2+} signaling upon expression of bestrophins.

It is known that ion channels play important roles in cell proliferation. In contrast to K^+ channels, for which vast amounts of information exist regarding their participation in tumorigenesis, and which have even been documented as potential drug targets, involvement of Ca^{2+}-activated Cl^- channels in cell proliferation has been scarcely tackled. A high baseline Cl^- conductance coincides with high endogenous expression of hbest1 in fast-growing colonic carcinoma (T_{84}) cells, whereas low baseline Cl^- conductance and low endogenous hbest1 expression are present in slow-growing T_{84} cells. siRNA for hbest1 inhibits proliferation of fast-growing T_{84} cells, while in slow-growing T_{84} cells siRNA has no effect on proliferation. In contrast, overexpression of hbest1 in slow-growing cells induces fast proliferation.

In summary, the present study examines the physiological role of the putative Ca^{2+}-activated Cl^- channel bestrophin. Our results demonstrate that bestrophins enable Ca^{2+}-activated Cl^- secretion in different epithelia. Although we present clear evidence that bestrophins induce I_{ClCa}, our work does not directly address the question whether these proteins form the CaCC pore themselves or are accessory regulatory proteins. We also present evidence for functional and molecular interaction of bestrophin paralogs, presumably acting as

heterooligomers. Finally, we settle a direct correlation between best1 expression and Cl^- currents and cell proliferation, which may be useful to understand of the role of Ca^{2+} and volume regulated Cl^- channels in cell proliferation.

Zusammenfassung

Ca^{2+}-aktivierbare Cl^--Kanäle (CaCCs) sind an einer Vielzahl wichtiger physiologischer Prozesse beteiligt, wie z.B. transepithelialem Transport, Weiterleitung von Geruchs- und Geschmacksreizen, neuronaler und kardialer Erregbarkeit und Fototransduktion. Diese Cl^- Kanäle spielen ebenso eine Rolle bei Krankheiten wie der Mukoviszidose, der sekretorischen Diarrhoe und der polyzystischen Nierenerkrankung. Obwohl epitheliale CaCCs seit mehr als zwei Jahrzehnten untersucht werden, ist über ihre molekularen Eigenschaften und ihre physiologische Rolle noch sehr wenig bekannt. Bisher vermutete Kandidatenproteine erfüllten nicht die nötigen Anforderungen, um sie als CaCCs in Betracht zu ziehen. Im Gegensatz dazu konnte gezeigt werden, dass Proteine der Bestrophinfamilie eine Ca^{2+}-aktivierte Cl^- Leitfähigkeit in Expressionssystemen induzieren. Die Eigenschaften dieser Leitfähigkeit sind denen der Ca^{2+}-aktivierten Cl^- Leitfähigkeit in nativen Geweben sehr ähnlich. Bestrophin 1 (best1), das Genprodukt der „vitelliform macular dystrophy type 2“ (VMD2), ist im Pigmentepithel der Retina (RPE) exprimiert, wo es vermutlich die Cl^- Leitfähigkeit und damit die Homöostase der Retina reguliert. Mutationen des Bestrophin 1-Gens führen zur so genannten Bestschen Maculadystrophie.

Allerdings herrscht noch Unklarheit darüber, ob die Ursache für die Bestsche Erkrankung tatsächlich eine Cl^- Kanal-Dysfunktion ist, unter anderem deshalb, weil mbest1 Knockoutmäuse (best1-/-) keinen pathologischen ophthalmologischen Phänotyp aufweisen und normale Cl^- Ströme im RPE zeigen. Andererseits wurde vermutet, dass die Aktivität von spannungsabhängigen Ca^{2+} Kanälen im RPE durch Bestrophin reguliert wird. Es ist somit ein wichtiges Anliegen, die exakte zelluläre Rolle der Bestrophine zu klären und zu untersuchen, ob Bestrophine auch zur Funktion der Ca^{2+}-aktivierten Cl^--Kanäle in anderen Geweben beitragen könnten. Diese Fragen wurden in der vorliegenden Arbeit untersucht.

Wir konnten zeigen, dass Bestrophin 1 neben dem Pigmentepithel auch in anderen epithelialen Geweben, wie den Luftwegen, der Niere und im Colon exprimiert wird, wo es zur Ca^{2+}-aktivierbaren Cl^- Sekretion beiträgt. Die endogene Expression von best1 in humanen und murinen Epithelzellen ging mit endogenen Ca^{2+}-aktivierbaren Cl^- Strömen (I_{ClCa}) einher, wohingegen in epithelialen Geweben ohne best1-Expression kein I_{ClCa} messbar war. Darüber hinaus ließ sich I_{ClCa} in HEK293 Zellen, welche hbest1 überexprimierten, durch ATP aktivieren. In sogenannten Ussing-Kammer Experimenten wurde beobachtet, dass geringe Konzentrationen des purinergen Rezeptoragonists ATP größere Kurzschlussströme (Isc) im Trachealepithel von Wildtypmäusen (best1+/+) erzeugte als in Geweben von

Knockoutmäusen (best1-/-). Patch-Clamp Messungen zeigten, dass die ATP-induzierten Ganzzellströme in primärkultivierten Epithelzellen der Trachea von Knockouttieren nur halb so groß waren wie die in Zellen von Wildtypmäusen. Untersuchungen mit inhibitorischer siRNA für best1 und best2 deuteten darauf hin, dass in Trachealepithelzellen sowohl best1 als auch best2 an der Entstehung der Ca^{2+}-aktivierten Cl^- -Leitfähigkeit beteiligt sind. Bei Variierung der zytosolischen Ca^{2+}-Aktivität durch die Pipettenlösung zeigte sich, dass der Ca^{2+}-abhängige Cl^- Strom bei Wildtypzellen größer war als bei Knockoutzellen. Zusammenfassend sprechen diese Daten dafür, dass Bestrophin 1 und Bestrophin 2 notwendige Komponenten der Ca^{2+}-aktivierbaren Cl^- Sekretion in der Mäusetrachea darstellen.

Die Quartärstruktur der Bestrophine sowie deren subzelluläre Lokalisation werden derzeit kontrovers diskutiert. Die vorliegenden Ergebnisse zeigen eine molekulare und funktionelle Interaktion und Kolokalisation der Bestrophine 1, 2 und 4 in überexprimierenden HEK293-Zellen und in Epithelzellen der Luftwege, welche Bestrophine endogen exprimieren. In immunhistochemischen Untersuchungen wurde eine deutliche Membranexpression für hbest2 und hbest4 beobachtet, welche für hbest1 kaum vorhanden war. Lokalisationsstudien mit konfokaler Mikroskopie zeigten, dass hbest1 vor allem im endoplasmatischen Retikulum lokalisiert ist und nur im geringen Ausmaß in der Plasmamembran liegt. Gleichwohl induzierte die Expression von hbest1 oder hbest3 eine ATP-stimulierbare Cl^--Leitfähigkeit. Überraschenderweise führte die Expression von hbest2 oder hbest4 zu einer großen basalen Cl^--Leitfähigkeit, die nicht durch ATP-Gabe verändert wurde. Die hbest2/hbest4 induzierte basale Leitfähigkeit wird durch Koexpression mit hbest1 oder hbest3 signifikant verringert. Diese Daten zeigen, dass Bestrophin Paraloge miteinander interagieren und dabei heterooligomere Komplexe ausbilden. Obwohl an anderer Stelle die Regulation von spannungsabhängigen Ca^{2+}- Kanälen berichtet wurde, fanden wir keinen Einfluss der Bestrophin-Expression auf ATP-abhängige intrazelluläre Ca^{2+} Signalwege.

Ionenkanäle spielen eine Rolle bei der Zellproliferation. Während der Einfluss von K^+ Kanälen auf die Tumorgenese gut untersucht ist, gibt es nur wenige Daten zur Beteiligung von CaCCs an der Zellproliferation. Wir untersuchten daher die Rolle von Bestrophinen für die Zellproliferation. Schnell wachsende Kolonkarzinomzellen (T_{84}) mit hoher endogener hbest1-Expression zeigten eine erhöhte basale Cl^- Leitfähigkeit, während langsam wachsende T_{84} Zellen mit geringer endogener hbest1-Expression eine niedrige basale Cl^- Leitfähigkeit aufwiesen. siRNA für hbest1 inhibierte die Proliferation von schnell wachsenden T_{84} Zellen, nicht aber die von langsam wachsenden Kolonkarzinomzellen. Umgekehrt wird die Proliferation von langsam wachsenden Kolonkarzinomzellen durch die Überexpression

von Bestrophin 1 erhöht. Diese Beobachtungen sprechen dafür, dass hbest1 zur Entstehung einer Cl^- Leitfähigkeit in T_{84}-Zellen beiträgt, die vermutlich das Proliferationsverhalten der Zellen beeinflusst.

Zusammenfassend zeigen die vorliegenden Ergebnisse, dass Bestrophine zur Entstehung der Ca^{2+}-aktivierten Cl^--Leitfähigkeit in Expressionssystemen und nativen Epithelien beitragen. Allerdings erlauben die Daten noch keine sicheren Rückschlüsse, ob diese Proteine selbst porenbildend sind oder als Regulatoren oder Adapterproteine funktionieren. Die verschiedenen Mitglieder der Bestrophinfamilie interagieren miteinander und bilden vermutlich heteromere Proteinkomplexe. Eine eindeutige physiologische Funktion konnte den Bestrophinen bisher noch nicht zugeschrieben werden. Unsere Untersuchungen an T_{84}-Kolonkarzinomzellen sprechen dafür, dass Bestrophine nicht nur einen Einfluss auf die Cl^- Leitfähigkeit haben sondern ihre Expression auch das Proliferationsverhalten der Zellen modifizieren kann.

Table of Contents

SUMMARY ..... **I**

ZUSAMMENFASSUNG ..... **IV**

TABLE OF CONTENTS **1**

LIST OF ABBREVIATIONS ..... **I**

CHAPTER 1 ..... **1**

General introduction 1

CHAPTER 2 ..... **21**

Bestrophin 1 enables Ca^{2+} activated Cl^- conductance in epithelia 21

CHAPTER 3 ..... **37**

Bestrophin 1 and 2 are components of the Ca^{2+} activated Cl^- conductance in mouse airways 37

CHAPTER 4 ..... **51**

Functional assembly and purinergic activation of bestrophins 51

CHAPTER 5 ..... **67**

Eag1 and Bestrophin 1 are upregulated in fast growing colonic cancer cells 67

REFERENCES **83**

ACKNOWLEDGEMENTS/ AGRADECIMIENTOS **94**

PUBLICATIONS **95**

List of abbreviations

%	per cent
Δ	delta
μ	micro
Ω	ohm
°	degree
9HTE	human tracheal epithelial cell lline
16HBE	human bronchial epithelial cell line
^{2}	square
aa	amino acid
AB, Ab	antibody
ABC	avidin biotin peroxidase complex
ADE	adenosine
ADVIRC	autosomal dominant vitreoretinochoroidopathy
ANOVA	analysis of variance
ARPE-19	human RPE cell line (arising RPE from a 19 years old male)
ASL	airways surface liquid
Aste	atomizole
ATP	adenosine triphosphate
AVMD	adult-onset vitelliform macular degeneration
A2B	adenosine (A2B) receptor
A9C	anthracene-9-carboxylic acid
Ba^{2+}, Ba	barium
BAPTA	1,2-bis(0-aminophenoxy)ethane-N,N,N',N'-tetraacetic acid
best	bestrophin
bp	base pair
BSA	bovine serum albumin
BVMD	Best Vitelliform Macular Dystrophy
C terminus	carboxyl terminus
C	centigrade
Ca^{2+}	calcium
CaCCs	Ca^{2+}-activated Cl^- channel(s)
Calu-3	human pulmonary adenocarcinoma cell line (airway serous glanular cells)
CAMKII	Ca^{2+}/calmodulin-dependent protein kinase II
cAMP	cyclic adenosine 3',5'-monophosphate

CCD	cortical collecting duct
CCH	carbachol
cDNA	complementary deoxyribonucleic acid
CF	cystic fibrosis
CFTR	cystic fibrosis transmembrane conductance regulator
cGMP	cyclic guanosine monophosphate
Cl^-	chloride
$[Cl^-]_i$	intracellular chloride concentration
CLCA	putative Ca^{2+} activated Cl^- channel family
CLCs	chloride channel(s)
CLICs	intracellular chloride channel(s)
cm	centimetre
Con	control
CO_2	carbon dioxide
CPA	cyclopiazonic acid
CRACM	calcium release-activated calcium modulator
cRNA	complementary ribonucleic acid
d	*Drosophila*
Da	Dalton
DIC	differential interference contrast
DIDS	4-4'-diisothiocyanostilbene-2,2'-disulfonic acid
DMEM	Dulbecco's modified Eagle's medium
DPC	diphenylamine-2-carboxylate
DRG	dorsal root ganglion
Eag	voltage gated ether á gogo K^+ channels
E_{Cl}	equilibrium potential for Cl^-
e.g.	exempli gratia
EGTA	ethylene glycol tetraacetic acid
EGFP	enhanced green fluorescent protein
ER	endoplasmic reticulum
ERG	electroretinogram
etc.	et cetera
FBS	fetal bovine serum
FFA	flufenamic acid
Fig.	figure
G	conductance
g	gram

GABA	glycine or γ-aminobutyric acid
GFP	green fluorescent protein
h	hour, human
H^+	hydrogen, proton
HCO_3^-	bicarbonate
HEK	human embryonic kidney cell line
HEPES	4-(2-Hydroxyethyl) piperazine-1-ethanesulfonic acid
HRP	horseradish peroxidase
HT_{29}	human colorectal carcinoma epithelial cell line
hTTYH3	human tweety homolog 3
H441	human lung papillary adenocarcinoma cell line
I	current
I^-	iodide
I_{ClCa}	Ca^{2+}-activaed Cl^- current
i.e.	id est
IMCD	intramedullary collecting duct
IP_3	inositol 1,4,5-trisphosphate
I_{sc}	short-circuit current
i/v	current/voltage relationship
k	kilo
K^+	Potassium
K_d	dissociation constant
KO	knockout
l	litre
LP	light peak
M	mega, mol
m	milli, metre, mouse
min	minute(s)
mRNA	messenger ribonucleic acid
M1	mouse collecting duct cell line
N terminus	amino terminus
n	nano, number
n.s	no significant
Na^+	sodium
NFA	niflumic acid
NKCC	sodium-potassium-2chloride cotransporter
NPPB	5-nitro-2-(3-phenylpropylamino) benzoic acid

Orai	ORAI calcium release-activated calcium modulator
PBS	phosphate buffered saline
P	pig
PCR	polymerase chain reaction
Pen	penicillin
PGE_2	prostaglandin E2
PKA	protein kinase A
PKC	protein kinase C
PLC	phospholipase C
PP2A	protein phosphatase 2A
P2Y	purinergic receptor P2Y, G-protein coupled
RNAi	ribonucleic acid interfering
RPE	retinal pigment epithelium
RPMI	Roswell park memorial institute medium
RT	reverse transcriptase, room temperature
R_{te}	transepithelial resistance
S	siemens
Scrbled/scrbld	scrambled
SDS-PAGE	sodium dodecyl sulphate polyacrylamide gel electrophoresis
sec, s	second(s)
siRNA	small interfering RNA
SITS	4-acetamido-4'-isothiocyanatostilbene-2,2'-disulfonic acid
SOCs	store operated Ca^{2+} channel(s)
STIM	stromal interaction molecule
Strep	streptomycin
TEA	tetraethylamonium
TMDs	transmembrane domains
T_{84}	human colorectal carcinoma cell line
U	unit(s)
UTP	uridine triphosphate
V	volt, voltage,
V_c	membrane voltaje
VMD2, vmd2	vitelliform macular dystrophy type 2
VRACs	volume-regulated anion channel(s)
V_{te}	transepithelial voltage
WT, wt	wild-type
YFP	Yellow fluorescent protein

Chapter 1

General introduction

Chloride channels

Ion channels are integral membrane proteins which allow the passive flow of ions across biological membranes. Passive diffusion of negatively charged ions along their electrochemical gradient is made possible through anion channels. Because chloride (Cl^-) is the most abundant anion in living organisms and consequently the predominant permeating halide under physiological conditions, anion channels are often referred to as Cl^- channels. Chloride channels can be grouped into the following four categories according to their gating mechanism: voltage-gated Cl^- channels, summarized in the large CLC family of genes; ligand-gated Cl^- channels, which are activated upon extracellular binding of glycine or γ-aminobutyric acid (GABA); cystic fibrosis (CF) transmembrane conductance regulator (CFTR) Cl^- channel, activated upon phosphorylation by protein kinase A and binding of intracellular ATP; volume-regulated anion channels (VRACs) or “swelling-activated” Cl^- channels and Ca^{2+}-activated Cl^- channels (CaCCs) (28;52). To date, little is known about the putative intracellular Cl^- channel (CLICs) family.

Physiological role of chloride channels

The physiological implications of Cl^- channel function can be subdivided into three main groups: (i) regulation of electrical excitability, (ii) cell volume regulation and ionic homeostasis and (iii) transepithelial transport.

(i) regulation of electrical excitability

The voltage-gated Cl^- channel CLC-1 stabilizes the resting potential of skeletal muscle. Thus, the loss of this channel leads to intrinsic muscle hyperexcitability, a condition known as myotonia (52). In contrast, in smooth muscle cells, the opening of Cl^- channels causes membrane depolarization which allows calcium (Ca^{2+}) entry through voltage-gated Ca^{2+} channels (VGCCs). This is particularly important for vascular responses to mechanical stress or modulators such as norepinephrine (53). Furthermore, neuronal responses to neurotransmitters such as glycine and GABA depend on the intracellular Cl^- concentration ($[Cl^-]_i$). Since gycine and GABA receptors are ligand-gated Cl^- channels, passive influx or

efflux of Cl^- can therefore lead to excitatory or inhibitory responses depending on the electrochemical potential for Cl^-.

(ii) cell volume regulation and ionic homeostasis

Cl^- channels play a key role in controlling cell volume. For instance, under extracellular hypotonic stress, the opening of swelling-activated K^+ and Cl^- channels results in a net efflux of salt which ensures that the cells retain their original volume (52). Another important function of Cl^- channels is to maintain the ionic composition of the cytoplasmatic fluid. Na^+/ H^+ and Na^+ HCO_3^-/ H^+ Cl^- exchangers involved in cellular pH control need a parallel Cl^- shunt for Cl^- recycling. In addition, in order to preserve electroneutrality, some H^+-ATPases also need a synchronized Cl^- channel function.

(iii) transepithelial transport

Vectorial movement of salt and fluid across epithelia depends on Cl^- channels and is largely governed by their distribution in the membrane together with active Cl^- uptake mechanisms. For instance, in the thick ascending loop (TAL) of Henle, luminal expression of Na^+-K^+-$2Cl^-$ (NKCC2) cotransporters and K^+ channels causes an increase in intracellular levels of Cl^-, which then leaves the cells through basolateral Cl^- channels, therefore ensuring Cl^- reabsorption in the TAL. In contrast, in secretory epithelia such as airways, acinar cells and intestine, Na^+-K^+-$2Cl^-$ cotransporters together with K^+ channels are located basolaterally (52). Polarized expression allows these tissues to actively secrete Cl^- through apical membrane Cl^- channels. In intestinal crypt cells, Cl^- transport is mediated by apical CFTR Cl^- channels. In acinar cells of most glands, the apical Cl^- channel is activated by intracellular Ca^{2+} (95).

Ca^{2+}-activated Cl^- channels

Unlike the majority of Cl^- channels, the molecular counterpart of CaCCs remains unknown. CaCCs are anion-selective channels that are activated by intracellular increases of Ca^{2+}. They were first described in *Xenopus* oocytes in the early 1980s and later found in many other cell types, such as vascular endothelial cells, neurons, olfactory and photo-receptors, smooth and cardiac muscle cells and in various epithelial cells. A variety of physiological functions has been demonstrated in relation to the widespread expression of CaCCs. These include fertilization of the oocyte, regulation of neuronal and cardiac excitability, taste and olfactory transduction, regulation of smooth muscle tone and transepithelial fluid transport (46;63).

Three main biophysical fingerprints characterize CaCCs. Firstly, they are activated by intracellular Ca^{2+} with half-maximal concentrations for activation in the submicromolar range.

In many epithelial cells, intracellular Ca^{2+} that activates CaCCs is derived from Ca^{2+} release from intracellular stores or Ca^{2+} influx through store-operated Ca^{2+} channels (SOC). Depending on the cell type, Ca^{2+} activates CaCCs either directly by binding to the channel, indirectly through Ca^{2+}-binding proteins or via phosphorylation through Ca^{2+}/calmodulin-dependent protein kinase II (CaMKII). The existence of these mechanisms suggests an underlying molecular diversity of CaCCs. Direct Ca^{2+} gating presumes that the channel contains Ca^{2+}-binding motifs like EF-hands, C2 domains or Ca^{2+}-bowl motifs, similar to those present in large conductance potassium channels. However, this assumption has been questioned because of the apparent lower affinity of CaCCs for Ca^{2+} (8).

Nonetheless, evidence exists in favor of the idea that CaCCs are directly gated by Ca^{2+}. In inside-out and excised membrane patches from hepatocytes, *Xenopus* oocytes and acinar cells isolated from pancreas and parotid glands, rapid application of Ca^{2+} on the cytosolic side of inside-out oriented patches quickly activates CaCCs even in the absence of ATP (65). Further evidences supporting a direct binding of Ca^{2+} to the channel protein are obtained in excised patches from salivary gland acinar cells and pulmonary endothelial cells, in which rundown of channel activity was not observed. Moreover, application of peptide inhibitors of calmodulin (CaM) and CaMKII to rat parotid acinar cells did not prevent Cl^- current activation by ionomycin-mediated $[Ca^{2+}]_i$ increase (46). It has also been reported that some CaCCs are gated by channel phosphorylation involving CaMKII. For instance, it has been shown that in some cell types such as human colonic carcinoma cells (T_{84} or HT_{29}), airway cells, T lymphocytes, human macrophages, biliary epithelial cells and in *Xenopus* oocytes, treatment with calmodulin inhibitors decreased Ca^{2+}-activated Cl^- currents (I_{ClCa}) (46). Interestingly, phosphorylation by CaMKII results in CaCCs inactivation in tracheal smooth muscle (140).

The second main feature that characterizes CaCCs is their poor ion selectivity (52). In general, selectivity is understood as the ability of an ion channel to select among various ions. The binding site for ions and the geometry of the channel seem to be crucial for ion selectivity (144). Unlike voltage-gated K^+ channels that exhibit >100-fold selectivity for ions that differ in radii by less than 0.5 Å, CaCCs select only approximately 10-fold between ions that differ in radii by 1.5 Å (105). Although CaCCs are more selective for anions than for cations, they poorly discriminate between anions, displaying a selectivity sequence similar to that of Eisenman type I ($SCN^- > I^- > Br^- > Cl^- > F^-$) (28;46). In addition, selectivity can also be estimated by comparing permeability or conductance ratios. Briefly, permeability is defined as the ability of an ion to move from the aqueous environment and enter the channel, while conductance is the ability of an ion to pass through the channel and emerge into the aqueous environment on the other side of the membrane (21). For CaCCs, the relative permeability is

related to hydration energy (105). Thus, larger ions which have a lower effective charge density and hence lower hydration energies are relatively more permeant than smaller ions. Yet, in terms of conductance, larger ions are also less conductive than smaller ones because they become stuck in the pore, even though they enter the channel more easily (21). The relative permeability and conductance sequence for CaCCs is quite different. Whereas the conductance exhibits a bell-shaped relationship to hydration energy, permeability displays an exponential dependence on hydration energy. In general, it seems that the ionic selectivity of CaCCs can be explained by a mechanism in which ion entry into the channel is ruled by the partitioning of anions into a barrel with a relatively high dielectric constant (46).

The kinetics of activation by Ca^{2+} constitute the third major biophysical fingerprint characterizing CaCCs. Typical macroscopic currents from CaCCs are voltage- and time-dependent at subsaturating Ca^{2+} concentrations (<1 μM). At these low physiological Ca^{2+} levels, the current activates slowly at positive potentials and deactivates fast at negative potentials (28). The resulting steady-state current/voltage (i/v) relationship is outwardly rectifying at low $[Ca^{2+}]_i$ (<500 nM) (46;65). However, at high Ca^{2+} levels (>1 μM), voltage and time dependence disappear and the current-voltage curve becomes progressively linear. Both, the apparent open probability of CaCCs and the apparent affinity of CaCCs for Ca^{2+} are voltage-dependent. This last feature may explain why at low $[Ca^{2+}]_i$ the shape of the i/v curve is outwardly rectifying. It is possible that positive voltages cause conformational changes of the Ca^{2+}-binding site to favor interaction with Ca^{2+} and thus increase channel opening. In contrast, at high Ca^{2+} levels, Ca^{2+}-dependent gating predominates over the entire voltage range, thereby resulting in a linear i/v relationship (28;65).

Diversity of Ca^{2+}-activated Cl^- channels

Apart from the underlying molecular diversity of CaCCs, suggested by the differences in their mechanisms of regulation, namely their direct gating by Ca^{2+} or by CaMKII phosphorylation, CaCCs widely differ in their single channel conductance properties (1-310 pS) and in their sensitivity to inhibitors. According to the single channel conductance, there appear to be five different types of CaCCs in different cell types. Small-conductance (1-3 pS) CaCCs have been described in various cell types including arterial smooth muscle, endocrine cells, *Xenopus* oocytes and cardiac myocytes (46). 8 pS channels with linear i/v relationships were observed in pulmonary artery endothelial cells (52;88) and hepatocytes (46). Calmidazolium-sensitive CaCCs, exhibiting a 15 pS single channel conductance and a linear i/v relationship, were also found in colon (84). Members of a fourth group, the intermediate conductance (40-50 pS) Cl^- channels, have been observed in Jurkat T cells, *Xenopus* spinal neurons and

airway epithelial cells and are outwardly rectifying (34). The large conductance (310 pS) maxi-CaCC comprises the fifth group and were described in *Xenopus* spinal neurons showing a marked voltage-dependent inactivation above and below +/- 20 mV.

Pharmacology

The molecular identification of CaCC has been seriously hampered in part by the lack of specific and potent channel modulators. In physiology, the foremost application of specific blockers is to selectively suppress one type of ion channel in a complex background of ion conductance. They are also useful in deciphering the pore structure of ion channels as well as in the analysis of tissue distribution. Unlike cation channels, for which highly specific channel blockers are available, the pharmacology of anion channels is quite disappointing.

Among the most common blockers for native CaCCs are the closely related fenamates compounds, such as niflumic acid (NFA) and flufenamic acid (FFA) and the disulfonic stilbene DIDS. In *Xenopus* oocytes, both fenamates inhibit Ca^{2+}-activated Cl^- currents (I_{ClCa}) at concentrations in the range of 10 μM (106). Similarly, 10 μM of NFA significantly reduces the ATP-induced Cl^- transport in mouse tracheal epithelium (11). In contrast to this apparent potency and specificity, studies in guinea-pig and rat myocytes revealed that NFA not only blocks CaCCs but also VRACs and K^+ channels (25). In addition to its blocking effect, in smooth muscle NFA also seems to interact with molecules involved in signal transduction, leading to I_{ClCa} activation at negative voltages (99). Due to these ambiguous effects, NFA is far to be considered a perfect tool to probe endogenous I_{ClCa}. DIDS is another potent blocker commonly used in mammalian cells (11;52). As it will be discussed latter in chapters 2 and 3, DIDS, at micromolar concentrations (100-200 μM), also reduces ATP-induced Cl^- currents in mouse trachea and in 16HBE cells (10;11). Other Cl^- channel blockers, including tamoxifen, glibenclamide, 4-acetamido-4'-isothiocyanatostilbene-2,2'-disulfonic acid (SITS), 5-nitro-2-(3-phenylpropylamino)benzoic acid (NPPB), anthracene-9-carboxylic acid (A9C) and (DPC) are less effective than flufenamate and DIDS in blocking CaCCs. Furthermore, Cl^- channel blockers such as fluoxetine and mefloquine seem to be more effective on VRACs than on CaCCs.

Fortunately, novel chemical classes of CaCCs inhibitors are emerging at the horizon, developed currently in the laboratory of A. Verkman (22). In an ambitious high-throughput screening, they successfully identified two classes of small molecules that potently block endogenous CaCCs from HT_{29} and T_{84} cells. The screening is based on suppression of ATP/carbachol-stimulated iodide influx in the above mentioned cells. Particularly in HT_{29}

cells, the aminothiophenes (3-acyl-2-aminothiophenes) and aminothiazoles (5-aryl-2-aminothiazoles) were able to inhibit more than 95% of the iodide influx in response to multiple Ca^{2+}-enhancing agonists. Interestingly, the inhibition did not interfere with agonist-induced intracellular Ca^{2+} elevation or calmodulin (CaMKII) phosphorylation, suggesting a direct targeting of CaCCs rather than affecting upstream signaling mechanisms (22).

Role of Ca^{2+}-activated Cl^- channels

As briefly outlined above, CaCCs are implicated in a variety of important physiological processes in different tissues and cell types. For instance, in *Xenopus* oocytes, blockade of polyspermy is achieved through activation of I_{ClCa}, which causes the so-called fertilization potential (142). Sperm entry during fertilization triggers Ca^{2+} release from internal stores, which in turn activates CaCCs, producing a depolarization of the cell membrane (the "fertilization potential"). However, Ca^{2+} release from internal stores mediated by inositol 1,4,5-trisphosphate (IP_3) is not sufficient to maintain for sustained periods the depolarization necessary to avoid polyspermy. Continuous depolarization is ensured by a tightly-coupled mechanism that upon Ca^{2+} store depletion activates Ca^{2+} influx through stored-operated Ca^{2+} channels (SOCs), which further contributes to CaCC stimulation (45;65).

CaCCs are also involved in regulating neuronal and cardiac excitability (87;153). They are expressed in a variety of neurons where they are presumably implicated in membrane oscillatory behavior, repolarization of the action potential and generation of after-polarizations. In particular, neurons from the dorsal root ganglion (DRG) that sense skin temperature, touch, muscle tension and pain express CaCCs. Similarly, a fraction of spinal cord neurons express CaCCs suggesting some specific role in neuronal function (33). During the action potential, opening of CaCCs does not dramatically change the membrane potential but it contributes to accelerate repolarization, resulting in limited firing and trains of action potentials (46).

The relevance of CaCCs in controlling cardiac excitability is unquestionable (49;154). For instance, dogs genetically predisposed to cardiac sudden death have abnormal outward currents suggesting a role for CaCCs in cardiac sudden death. Furthermore, during Ca^{2+} overload, arrhythmogenic transient inward currents generated by CaCCs might unleash oscillatory after-potentials resulting in serious cardiac arrhythmias in these animals (49). In smooth muscle cells in which the equilibrium potential for Cl^- (E_{Cl}) is approximately -20 mV, opening of Cl^- channels results in membrane depolarization (133). In these cells, stimulation of adrenergic receptors by norepinephrine increases $[Ca^{2+}]_i$ levels which in turn stimulates Cl^- efflux through CaCCs, leading to membrane depolarization and smooth muscle cell

contraction (46). In a positive feedback loop, this depolarization further activates VGCCs, thereby raising Ca^{2+} entry and additional muscle contraction. The role of CaCCs in smooth muscle contraction has been authenticated by using different CaCC blockers, including A9C and NFA which reduced or blocked muscle contraction (46;68).

CaCCs also play a role in mammalian and amphibian taste transduction (46;114). It is thought that upon taste stimuli, CaCCs may play a role in discriminating chloride salts from salts of other anions and therefore help to shape receptor cell responses elicited by taste stimuli (78). In taste receptor cells from *Necturus maculosus*, activation of CaCCs during action potentials results in a hyperpolarization of these cells since E_{Cl} is between -60 and -80 mV. Hence, it is hypothesized that this hyperpolarization contributes to chemosensory taste adaptation (114). Ciliary membranes of olfactory receptor neurons from a variety of species, including frog, newt, rat, fish and salamander express CaCCs that play a key role in transduction of olfactory stimuli. Odorant molecules bind to G protein-coupled olfactory receptors and this interaction triggers the activation of adenylate cyclase which in turn enhances cAMP levels in the ciliary cells. Cyclic AMP-stimulation of cyclic-nucleotide-gated channels located in the ciliary membrane, leads to a depolarizing influx of Na^+ and Ca^{2+}. Both, depolarization and elevation of $[Ca^{2+}]_i$ cause Cl^- efflux through CaCCs which augments membrane depolarization. It has been postulated that the feedback mechanism ensured by Cl^- efflux upon CaCC stimulation serves as an amplification system of the odorant activated current (98). Physiologically, this amplification could serve to increase the sensitivity to odorants (46). The precise role of CaCCs in photoreceptors remains obscure. It has been suggested however that they could function in membrane potential stabilization by counteracting the depolarization induced by Ca^{2+} entry through VGCC (150). The contribution of CaCCs in rods is unknown but it has been pointed out that in cones they could play a role in modulating lateral inhibition (46).

The presence and role of CaCCs in gland acinar, duct and pancreatic cells are crucial and have been extensively documented (5;79;86). These tissues secrete a NaCl-enriched fluid upon stimulation with the neurotransmitter acetylcholine. Stimulation of the muscarinic receptor increases IP_3 production that triggers a release of Ca^{2+} from the stores. This rise in $[Ca^{2+}]_i$ levels turns on CaCCs and hence a luminal Cl^- secretion. The efflux of Cl^- drives the movement of Na^+ and drags water, resulting in a net salt fluid secretion. Thus, the activation of CaCCs is a key element in the initiation of the secretory process and their opening and closing may explain the oscillations in cell volume observed during stimulation (5).

Contribution of CaCC to epithelial Cl^- secretion

Epithelial salt and fluid transport is a complex phenomenon involving a large number of hormones, serosal and luminal transmembrane receptors, agonists and intracellular signaling molecules involved in downstream regulation of transport proteins and ion channels. The importance of Ca^{2+}-dependent Cl^- channels in this dynamic molecular network is highlighted by its abundance and diversity along most epithelia. In this context, the presence and consequently the role of CaCCs for fluid and salt secretion in epithelia are indisputable (46;63;133) (Fig. 1).

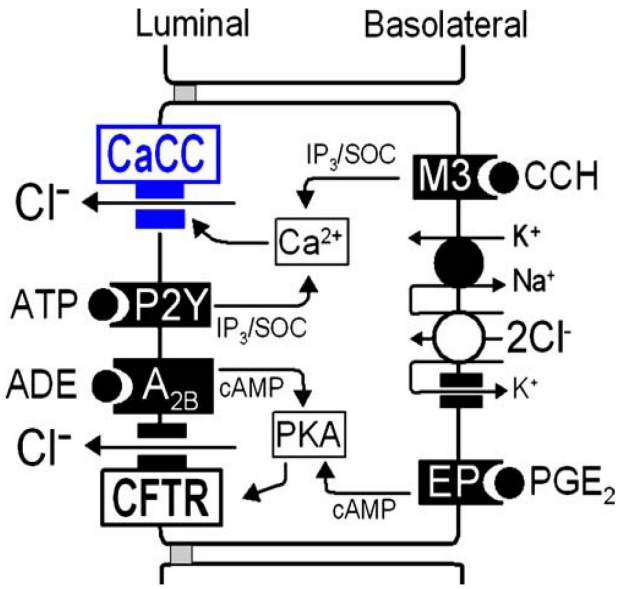

Fig. 1. Cell model for Cl^- secretion in airways and proximal colonic epithelial cells. Two major pathways for salt transport are ensured by cAMP-activated CFTR Cl^- channels [adenosine (ADE) in airways, prostaglandin (PGE_2) in the colon] and by CaCC [$P2Y_2$ in airways, carbachol (CCH) in the colon].

CaCC in the colon

Although colonic epithelium is mainly an absorptive epithelium, electrolyte secretion, that facilitates transport of mucus out of the crypts and maintains its hydration, constitutes also a major task. CaCCs can be easily detected in cultured colonic cells like T_{84} and HT_{29} (60). In murine native colon however, I_{ClCa} can only be found in the proximal section (11;101) whereas Cl^- secretion in rectal and distal colon are governed primarily by CFTR (60). The importance of CaCCs in the intestine became more apparent in a study in which I_{ClCa} was demonstrated in a CFTR knockout (CFTR-/-) mouse model. Despite the lack of CFTR-dependent Cl^- secretion in these mice, a normal survival rate and no signs of any intestinal pathology was observed, most likely due to the presence of CaCCs (116). Finally, it was found that CaCCs follow an age-dependent expression pattern (60). According to this study, in pups of CFRT-/- mice, Cl^- secretion was induced by carbachol in the small intestine, which suggests the presence of a Ca^{2+}-dependant Cl^- secretion. In addition, the rotavirus toxin NSP4, which also induces severe diarrhea in infants and young animals, inhibits absorption and stimulates Ca^{2+}-mediated Cl^- secretion in non-CF and CF mouse pup crypts (7;60). Thus, Cl^- transport induced by NSP4 was largely reduced in CF and non-CF mice, implying an age-dependant expression of CaCC with only a small contribution of these channels to Cl^- secretion in adult mice.

Relevance of CaCC in the kidney

The presence of CaCCs in the renal epithelia is controversially discussed (46;63;69). CaCCs are widely expressed in primary cultures from rabbit distal and proximal convoluted tubule, thick ascending limb and cortical collecting duct; as well as in the mouse collecting duct cell line (M1) and primary and cell-line derived intramedullary collecting duct (IMCD). However, a role of these channels in the native cortical collecting duct (CCD) principal cells is far from being proven (11;69). This situation resembles the above mentioned studies in intact distal colonic epithelia where CFTR is the only luminal Cl^- channel mediating Cl^- secretion, whereas cultured colonic epithelia like HT_{29} and T_{84} cells have Cl^- secretion mediated by CaCCs, in addition to CFTR. Moreover, since CaCCs gating is hormonally controlled, it is speculated that they might play a role in fine-tuning the urine composition.

CaCC in airways

Airway epithelia use active salt transport to modulate the volume of the airway surface liquid (ASL) which in part determines the efficiency of mucus hydration and clearance. Adequate mucus clearance has been proposed as the primary innate defense of airways against infections (54). This is largely accomplished by the active presence and interplay of CFTR and CaCCs, the most abundant Cl^- channels in the apical membrane of airways. Regulation of purinergic P2Y receptors (P2Y-R) plays a crucial role in controlling ion and fluid movement across epithelia. ATP and UTP stimulate G_q-coupled purinergic receptors and this leads to an increase in IP_3 levels, subsequent Ca^{2+} release from the stores and CaCC activation (61). Purinoceptor activation can also lead to CFTR activation through a PKC-dependent mechanism. Furthermore, airflow due to normal tidal breathing confers shear stress on airway surfaces which release ATP. Ecto-5' nucleotidases quickly degrade ATP to adenosine, which also activates CFTR via A2B receptors (136) (Fig. 1). In contrast to CFTR, Ca^{2+}-activated Cl^- secretion is much more transient, in part due to the lack of activation of basolateral Cl^- uptake by the NKCC1 cotransporter. Probably, the basal level of the ASL is controlled by CFTR, whereas CaCCs seem to acutely regulate the height of the liquid layer in response to agonists. The contribution of CaCCs to the airway liquid layer homeostasis in murine airway epithelium could explain the lack of a lung phenotype in CF mouse models (18). One of the hallmarks of CF is the accumulation of viscous, sticky mucus on airway surfaces as a result of Na^+ hyperabsorption because of deinhibition of the epithelial Na^+ channel and hyposecretion of Cl^- due to loss of apical CFTR function (54). It has been postulated that activation of apical CaCCs could be a feasible therapy for cystic fibrosis. However, this idea has been handicapped by the lack of specific activators of CaCCs and the uncertainty of the molecular counterpart of these channels (28;137).

Molecular identity of CaCC

Although Ca^{2+}-activated Cl^- currents (I_{ClCa}) have been studied phenomenologically for more than 20 years and the sequences of genes encoding the mysterious I_{ClCa} are present in the database generated in the course of genome projects, the "real" CaCC has not yet been identified. Considering the wide variety of cation channels that have been cloned and thoroughly characterized, it seems bizarre that the molecular counterpart of CaCC is still a matter of controversy. As previously outlined, there are technical problems that slow the cloning of CaCC. First, expression cloning of CaCC in *Xenopus* oocytes is complicated by the huge background I_{ClCa} present in these cells. Furthermore, the available blockers to discriminate CaCC from other Cl^- currents are rather non-selective and non-specific. None of

the Cl^- channels already cloned, including CFTR, ligand-gated anion channels and the CLC family, have properties resembling those described for CaCCs. There are presumably four molecular prospects intended to be CaCCs.

The putative Ca^{2+} activated Cl^- channel CLCA family, cloned from bovine trachea (20), has been heterologously expressed in different cell types, where it produced an anion current activated by Ca^{2+} (94). However, low voltage and Ca^{2+} sensitivity compared to native I_{ClCa}, and the fact that one of the family member (hCLCA3) is actually secreted, brought about fundamental questions around CLCA being the molecular counterpart of CaCCs (28;46). The relatively newly identified human tweety homologs (hTTYH2 and hTTYH3) genes corresponding to Ca^{2+}-activated maxi-Cl^- channels (>260 pS) are unlikely epithelial CaCCs since native epithelial CaCCs are of small conductance (131). The CLC-3 Cl^- channel, which is regulated by Ca^{2+}, activated by CaMKII and cell swelling has also received attention as a CaCC candidate. However, CLCn3-/- mice exhibit Ca^{2+}-dependent Cl^- conductances similar to those of wild type mice (52). The putative intracellular Cl^- channel (CLIC) parchorin has received little consideration, despite its pronounced expression in secretory tissues. Its amphiphilic properties, small size, a single putative transmembrane domain, and lack of evidences for Ca^{2+} dependency, set this molecule apart from CaCCs (52;83). More than half a decade ago, Nathan's group proposed for the first time that bestrophins comprise a new family of Cl^- channels (130).

Bestrophins

The fact that some members of this family are activated by physiological Ca^{2+} concentrations and mutations of certain amino acids alter the permeability and conductance properties, led to the conclusion that bestrophins comprise the molecular counterpart of at least a subgroup of CaCCs. This conclusion is strengthened by the finding that interfering RNA (RNAi) targeting bestrophin transcripts can suppress endogenous Cl^- currents from different cell types (11;110).

Nomenclature, Bestrophin 1 gene and mutations

The human genome has four bestrophin paralogs (hbest1, hbest2, hbest3, and hbest4) (139). All other mammals have either three or four bestrophin paralogs. For instance, mouse contains three paralogs (mbest1, mbest2, mbest3) and one pseudogene (55). Recently, HUGO Genome Database nomenclature committee has recommended for the mammalian bestrophins the following nomenclature systems: best-1, -2, -3, and -4 (130;139) and VMD2,

VMD2L1 (VMD2-like protein 1), VMD2L2, and VMD2L3 (48;55). Human bestrophin 1 (best1) is encoded by the vitelliform macular dystrophy type 2 (VMD2) gene located on chromosome 11q13 (97). Mutations of best1 gene cause the Best Vitelliform Macular Dystrophy (BVMD) (97), an inherited autosomal dominant macular degeneration. In addition, patients with adult-onset vitelliform macular degeneration (AVMD) and autosomal dominant vitreoretinochoroidopathy (ADVIRC) have mutations in best1 (55;149). Recently Guziewicz and colleagues defined a canine bestrophin-related mutation: the canine multifocal retinopathy (44). To date, there are about 106 best1 mutations that have been associated with diseases.

Structure-function of bestrophins

Two different topology models have been proposed for best1 (81;139). According to the first model, 4 transmembrane domains out of 6 hydrophobic domains predicted by hydropathy profile, (TMD1, 2, 4, 6) cross the membrane, with TMD3 facing the cytosol and TMD5 as a re-entrant loop (139) (Fig. 2A). In the second model, in contrast, TMD1, 2, 5 and 6 are allowed to insert into the membrane while TMD3 and 4 are located in the cytosol (81) (Fig. 2B). Although these two models are basically contradictory, they share common features that aid our understanding of the insertion of best1 in the membrane. Artificial constructs may, however, not fold or enter the membrane like the native protein would. Nonetheless, at least the highly conserved N-terminal 350 amino acids, which include all the predicted TMDs among bestrophins, suggest similar topology for all vertebrate bestrophins (48).

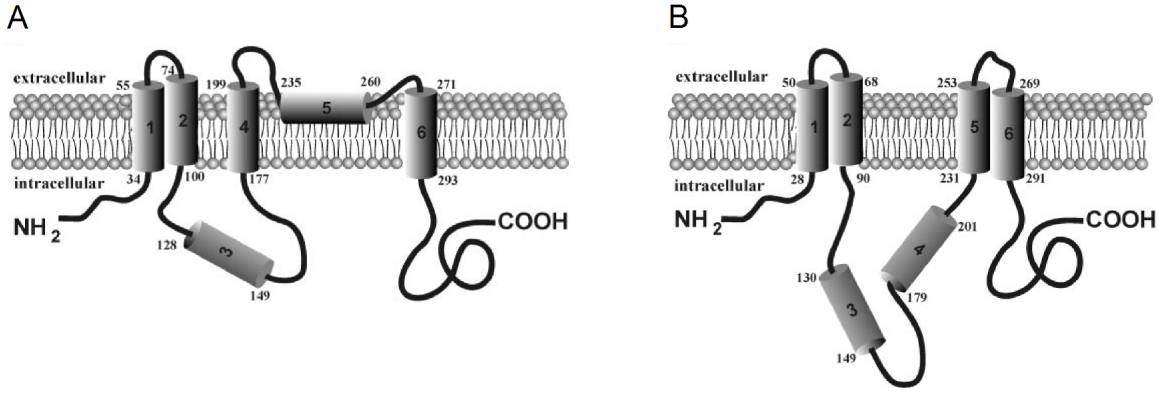

Fig. 2. Membrane topology models of bestrophin 1. A) Bestrophin 1 model suggested by Tsunenari *et al.* (139). Four segments traverse the membrane (TMDs1, 2, 4 and 6) with TMD5 as a re-entrant loop and TMD3 facing the cytosol. B) Bestrophin 1 model suggested by Milenkovic *et al.* (81). Four segments traverse the membrane (TMDs1, 2, 5 and 6) but differ from the previous one in that TMDs 3 and 4 are thought to form relatively hydrophobic cytosolic loops. Both models locate the N and C termini on the cytosolic side.

Since many ion channels are oligomers, it is reasonable to assume that also bestrophins are oligomeric. According to Sun *et al*. (130), bestrophins form tetramers and pentamers when expressed heterologously in human embryonic kidney (HEK) cells. In particular, best1 could exist as a homomeric tetramer or pentamer and also associate with human bestrophin 2 (hbest2), thereby raising the possibility that they could also co-assemble in heteromeric structures. However, the hydrodynamic studies of Stanton *et al*. (126) concluded that native bestrophin 1 isolated from porcine retinal pigment epithelial (RPE) cells only forms dimers (126). In order to find the reason of this discrepancy, they over-expressed pig bestrophin 1 (pbest1) in HEK293 cells and found that a considerable portion of the protein was aggregated. Based on that, these authors proposed that the tetrameric/pentameric model presented by Sun and colleagues was the result of a protein over-expression artifact. Although both studies present quite dissimilar membrane protein stoichiometry evidence, they agree that bestrophins oligomerize. A speculative rearrangement of bestrophins is discussed later in chapter 4.

Many studies have addressed the elucidation of the bestrophin pore structure. In this line, mouse bestrophin 2 (mbest2) has been analyzed most exhaustively (102;104;107). Like for best1, the TMD2 has been identified as the most plausible domain involved in pore formation of mbest2. TMD2 is one of the most highly conserved domains of bestrophins and mutations at 10 different positions of best1 are associated with human diseases (48). By mutagenesis and cysteine accessibility experiments, the group of Hartzell proved that TMD2 of mbest2 is critical for ion selectivity of the pore (102). However, it seems unlikely that the TMD2 forms the pore by itself, because mutation of residues in other parts of the protein also affect channel function (102). Other transmembrane domains like TMD5 and TMD6 are also highly conserved and are therefore possible pore-forming candidates. In addition to the similarities between hbest1 and mbest2, there are some structure-function differences which might indicate that pore architecture is different between bestrophins. The anionic selectivity of mbest2, the only bestrophin thoroughly examined, is identical to that described for CaCCs, having a lyotropic permeability sequence of $SCN^- > I^- > Br^- > Cl^- > F^-$. Like for many Cl^- channels, for wild type mbest2 the highly permeant anion SCN^- is poorly conductive, suggesting that it resides longer in the pore during transit through the channel than Cl^- does. This is further supported by the fact that, at low concentrations, SCN^- blocks Cl^- currents recorded from bestrophin channels (104). In general, the mutations carried out in TMD2 of mbest2 produce smaller but similar effect in terms of permeability. This brings to mind the poorly specialized pore of many other Cl^- channels; for example CLC-1 in which mutations of many amino acids in one TMD alter anionic permeability with only a modest overall effect (30;48).

Evidence that bestrophin forms a Ca^{2+}-activated Cl^- channel

To understand why bestrophin was initially proposed to form Cl^- channels it is worth examining the preliminary observation linking mutations in the hbest1 gene and the appearance of BVMD. RPE cells absorb lactate and lipofuscin, transport fluid and maintain the volume and composition of the subretinal space (127). Unlike most secretory epithelia, RPE polarity is inverted, i.e., the Na^+/K^+-ATPase and Na^+-K^+-$2Cl^-$ are located luminally, while Cl^- channels are located in the basolateral membrane (Fig. 3A). Epithelial transport across the RPE is guaranteed by Na^+-K^+-$2Cl^-$ cotransporters that use the energy of Na^+ gradients to move Cl^- into the cell and basolaterally secrete it down its electrochemical gradient via CaCCs, CFTR, and probably CLC-2 (35;127). When light stimulates the photoreceptors, a so-called light peak (LP) substance, presumably ATP or glutamate, is released and targets the P2Y receptors on the apical membrane of RPE cells. This is followed by a PLC / IP_3-mediated rise in intracellular Ca^{2+} levels (96;113). Thus the apical membrane, which is dominated by K^+ conductances, hyperpolarizes within seconds thereby generating the c-wave component of the electroretinogram (ERG; Fig. 3B). Subsequent depolarization of the basolateral membrane by activation of basolateral Cl^- channels causes a LP within minutes (127) (Fig. 3B). The fact that bestrophin 1 localizes to the basolateral membrane (75) and because the LP is reduced in patients with BVMD carrying mutations in best1, led to the assumption that bestrophin forms the Ca^{2+}-activated Cl^- channel in the basolateral membrane of RPE cells (47).

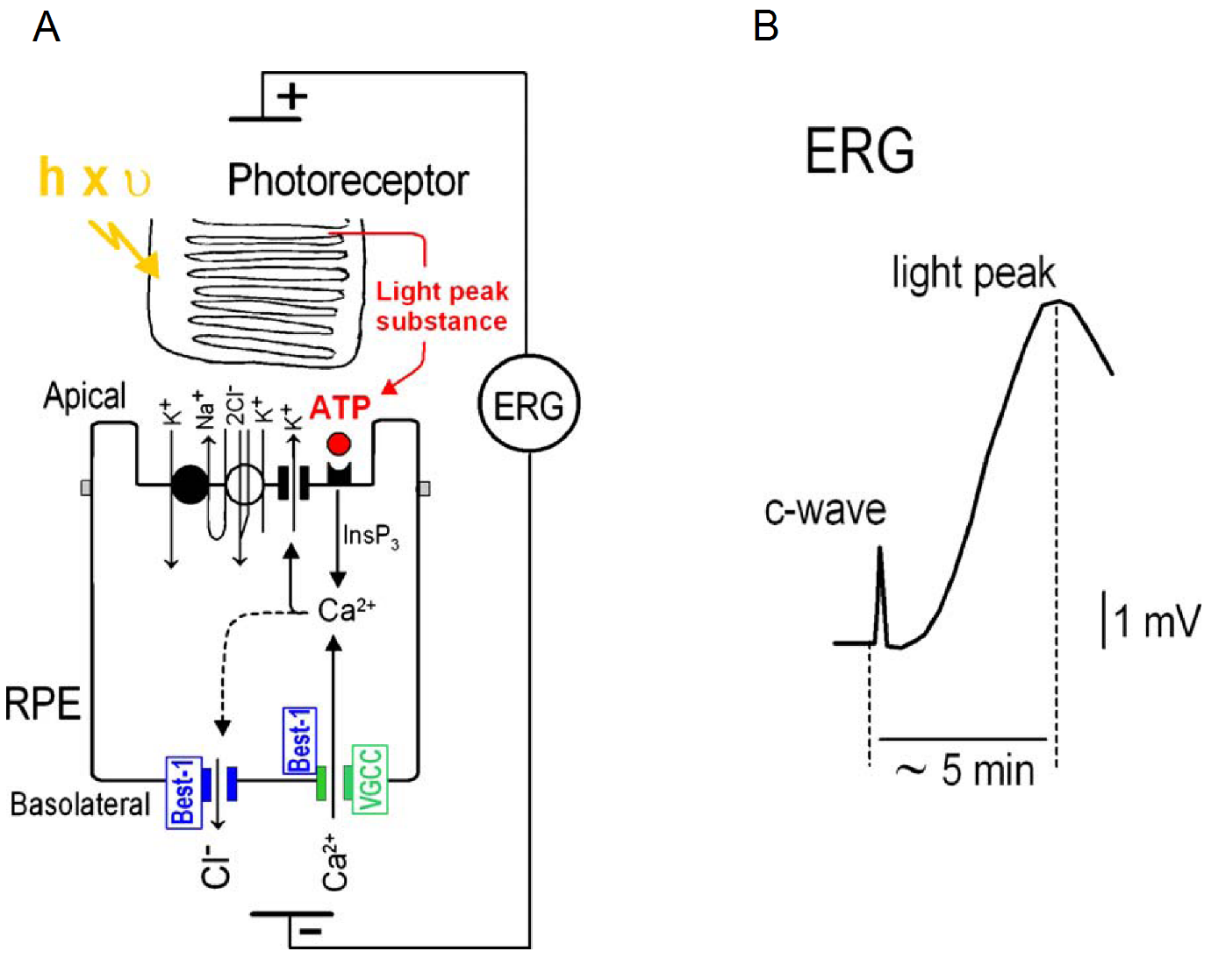

Fig. 3. Function of bestrophin in RPE cells. A) Upon light exposure, photoreceptors release a so-called light peak substance, which is likely to be ATP. Binding of ATP to purinergic receptors leads to increase in IP_3 and activation of Ca^{2+} influx through voltage-gated Ca^{2+} channels (VGCCs). best1 may be the Cl^- channel activated by Ca^{2+} or may function as a regulator of VGCCs. B) Fast activation (filled line) of K^+ channels contributes to the c-wave in the electroretinogram (ERG), while the light peak is thought to be due to delayed activation (dashed line) of basolateral Cl^- channels.

Moreover, the laboratories of Nathans and Hartzell have identified novel Cl^- currents using heterologous expression of hbest1 and other bestrophins in HEK293 cells (110;130). However, identification of Cl^- channels by heterologous expression has the disadvantage of often interfering with endogenous Cl^- channels, i.e. they may be upregulated by the overexpressed protein in such a way that it is difficult to discriminate native currents from those heterologously overexpressed. Nevertheless, the fact that overexpressing bestrophins in different cell lines produces similar types of currents minimizes the concern over upregulation of endogenous channels and therefore supports the idea that they are indeed Cl^- channels. Bestrophins are activated by cytosolic Ca^{2+} in the sub-micromolar range although this has not been shown for all bestrophins. Members of the bestrophin family like hbest1, *Xenopus* bestrophin 2 (xbest2), mbest2 and hbest4 have an apparent K_d for

activation by Ca^{2+} of about 200 nM (104;110;138;139). Tsunenari *et al*. (138) demonstrated hbest4 currents in excised membrane patches in the absence of substrates for phosphorylation, therefore suggesting a direct activation by Ca^{2+}. Likewise, endogenous *Drosophila* bestrophins (dbest) are also directly activated by Ca^{2+}, although their activation is enhanced in the presence of ATP, as shown in excised membrane patches (16). Besides the direct activation of CaCCs by Ca^{2+}, indirect activation via the Ca^{2+}-binding protein calmodulin, through phosphorylation or other enzymatic process are also feasible. In particular, hbest1 isolated from RPE cells interacts physically and functionally with the serine/threonine-protein phosphatase 2 (PP2A) indicating that phophorylation may play a role in regulation of hbest1 (76). Further evidence that bestrophins are regulated by phosphorylation in human pulmonary adenocarcinoma (Calu-3) cells comes from nitric oxide induced basolateral Cl^- currents via cGMP-dependent phosphorylation (26). The assumption is based on the fact that these cells express hbest1 and have decreased DIDS-inhibited Cl^- currents upon RNAi for hbest1. Interestingly, in some bestrophins such as hbest3, mbest3 and mbest2 an autoinhibitory domain localized at the C-terminus seems to play an important role for their regulation (103).

As discussed above, the generic lyotropic anion selectivity of bestrophins resembles that of classical CaCCs. Contrary to native CaCCs, hbest1 and mbest2 exhibit voltage and time-independent kinetics and linear i/v relationships. Point mutations in hbest1 and mbest2 confer outward rectification, voltage sensitivity and kinetics befitting CaCCs (48). Another evidence supporting the idea that bestrophins resemble classical CaCCs is brought about by single channel analysis demonstrating a 2 pS conductance for dbest1 channels as previously reported for native CaCCs (50;100). In addition, best1 and hbest3 transcripts have been found by RT-PCR in mouse salivary glands which exhibit large I_{ClCa} (63). Further evidence for best1 as a component of native I_{ClCa} is provided by experiments where best1-RNAi reduces endogenous CaCCs in airways and colonic epithelial cells and *Drosophila* S2 cells (11;16;26). This issue will be discussed in detail in chapters 2 and 3.

What is the evidence that bestrophin is a Ca^{2+} channel regulator?

Despite all the evidence that support bestrophins as the molecular counterpart of CaCCs, uncertainty is provoked by the studies of Marmorstein and Strauss, who were the first groups to introduce the idea that best1 is not a Cl^- channel but rather a channel regulator (77;115). They demonstrated that transient overexpression of hbest1 in RPE-J cell line can influence the kinetics of endogenous L-type Ca^{2+} channels along with a shift to the left for the voltage-dependence of Ca^{2+} activation closer to the resting potential. They also showed that voltage-

gated Ca^{2+} (Ca_v) channels play a role in generating the light peak as nimodipine, a Ca_v channel blocker, diminished its amplitude. The light peak is also reduced in mice lacking the α1.3 channel subunit and in *lethargic* mice which have a functional mutation in Ca_v-β4 subunit (77;148). Additional information supporting that mbest1 is involved in Ca^{2+} channel regulation was provided by experiments in which a greater Ca^{2+} response upon ATP-stimulation in RPE cells is observed in mbest1 knockout mice (best1-/-), while I_{ClCa} was indistinguishable between best1+/+ (wild type) and best1-/- mice. According to these observations, it has been proposed that mbest1 is not required to generate the LP but rather that its expression antagonizes it, possibly by inhibiting an increase in $[Ca^{2+}]_i$ in response to stimuli and by modulating Ca_v kinetics (115). This conclusion is further supported by the fact that some patients with hbest1 mutations demonstrate normal light peaks in their electro-oculograms (48). In accordance, a deficient Ca^{2+}-activated Cl^- transport in RPE cells may not be related to mutation in best1 and the changes observed for the LP might only be an epiphenomenon of the disease, and thus irrelevant to macular degeneration.

Other physiological roles of bestrophins

Recently, Pifferi *et al*. proposed that mbest2 is involved in the I_{ClCa} generated in olfactory cells (98). They found a correlation between the expression of mbest2 in olfactory sensory neurons (OSN) and the appearance of endogenous I_{ClCa}. To depict the complexity of the scenario, another group using a mbest2 knockout/lac-Z knocking model, demonstrated that indeed mbest2 is little or not present in nasal tissues (6). This study actually reveals that these mice have no significant olfactory deficit compared to wild type littermates. Indeed, they show that mbest2 protein is only expressed in the eye, in the nonpigmented epithelium and in the colonic epithelium. According to this study, the lack of mbest2 seems to have an impact in generating the intraocular pressure, presumably by regulating formation of aqueous humor (6).

Other reports proposed that bestrophin 1 and 2 could also play an important role in cell volume regulation. When mbest2 and hbest1 were expressed heterologously in HEK293-, HeLa- and ARPE-19 cells, a Ca^{2+}-dependent Cl^- current sensitive to volume changes appeared (31). Increasing the extracellular osmolarity caused cell shrinkage and a considerable reduction of the bestrophin current. Along this line, addition of a hypertonic solution to freshly isolated RPE cells also induces shrinkage and reduction of the endogenous Cl^- current. Thus, bestrophin 1 could contribute to the native volume sensitive Cl^- conductance of RPE cells, therefore facilitating the large volume changes to which RPE cells are exposed during phagocytosis of shed photoreceptor discs (31).

Furthermore, the group of Hartzell recently demonstrated that bestrophins are highly permeable not only to Cl^- but also to HCO_3^- (108). Heterologous expression of hbest1-disease-causing mutations abolished both Cl^- and HCO_3^- currents. This finding represents a new avenue in the understanding of the molecular basis of human Best disease due to the importance of HCO_3^- in regulating the intracellular pH and maintenance of fluid and ion transport across RPE. Finally, bestrophins seem to play a role in generating the Ca^{2+}-dependent Cl^- current in a variety of epithelia. As discussed in chapters 2 and 3, suppression of bestrophin 1 or 2 by RNAi in airway and colonic epithelial cells reduces the endogenous I_{ClCa}. Apart from these functions, a newly identified role for cell proliferation has been established for bestrophins. Expression of bestrophins determines the proliferative properties and is strongly correlated to epithelial-to-mesenchymal transition of the dedifferentiating epithelium (2).

Thesis outline

The relevance of CaCCs in regulating cell physiology is unquestionable. Clarifying the molecular identity of CaCCs is a major task in understanding the role of these channels in normal physiology, as well as in disease. The aim of the present thesis is to elucidate the cellular functions of the putative Ca^{2+}-activated bestrophin Cl^- channel in epithelia. The different cellular roles of bestrophins described here may offer novel therapeutic opportunities for the treatment of related diseases.

The first part (chapter 2 (11)) will focus on bestrophin 1 as the molecular entity of CaCC in epithelial tissues (26;27;36). Expression of bestrophin 1 had been described exclusively in basolateral membranes of RPE cells, where it presumably forms the Ca^{2+}-activated Cl^- channel. Epithelial cells express I_{ClCa} of unknown identity. It was therefore examined whether this protein would also account for the molecular counterpart of CaCC in other epithelia.

CaCCs are crucial in regulating the airway surface liquid and hence guaranteeing a proper mucociliary clearance. Thus, the second part (chapter 3 (10)) deals with the relevance of both best1 and best2 for the ATP-induced Ca^{2+}-dependent Cl^- transport in mouse airways. The hypothesis that best1 enables Ca^{2+}-dependent Cl^- conductance in epithelia was challenged using a mbest1 knockout (vmd2-/-) mouse model. Moreover, it was essential to examine to what extent the lack of best1 function would be compensated by the presence of other bestrophins. Because bestrophin 1 has also been described to regulate voltage gated Ca^{2+} channels, we investigate the involvement of this protein in controlling intracellular Ca^{2+} signaling triggered by hormonal stimulation.

In the third part of this thesis (chapter 4 (82)) the molecular and functional assembly was studied, as well as the purinergic activation of bestrophin paralogs. Although different bestrophins are present in a variety of epithelia, their structural arrangement is unresolved. Since many ion channels oligomerize, it was considered whether bestrophins are also oligomeric. Moreover, the cellular localization of human bestrophins was examined in HEK293 cells heterologously expressing bestrophins.

The fourth and last part of this thesis (chapter 5 (123)) reveals a novel physiological function of bestrophins for cell proliferation. Here, the relationship between best1 expression and ATP-dependent Cl^- currents and cell proliferation is examined.

Chapter 2

Bestrophin 1 enables Ca^{2+} activated Cl^- conductance in epithelia

Abstract

Epithelial cells express calcium activated Cl^- channels of unknown molecular identity. These Cl^- channels play a central role in diseases such as secretory diarrhea, polycystic kidney disease and cystic fibrosis. The family of bestrophins has been suggested to form calcium activated Cl^- channels. Here we demonstrate molecular and functional expression of bestrophin 1 (best1) in airways, colon and kidney of mouse and human. Endogenous calcium activated whole cell Cl^- currents coincide with endogenous expression of the Vmd2 gene product best1 in murine and human epithelial cells, whereas calcium activated Cl^- currents are absent in epithelial tissues, lacking best1 expression. Blocking expression of best1 with short interfering RNA (RNAi) or applying a best1 antibody to the patch pipette suppressed ATP induced whole cell Cl^- currents. Calcium dependent Cl^- currents were activated by ATP in HEK293 cells expressing best1. Thus best1 may form the Ca^{2+} activated Cl^- current, or it may be a component of a Cl^- channel complex in epithelial tissues.

Introduction

Ca^{2+} activated Cl^- channels (CaCC) are present in almost every cell type examined. Although this type of channel has been studied extensively, the molecular identity of CaCC in epithelial tissues remains a mystery (52;87). The channels are of small conductance; show outward rectification at moderate increase of intracellular Ca^{2+}, and have an anion selectivity of $I^- > Cl^-$ (46;65). Both direct activation of the channel by increase in intracellular Ca^{2+} and indirect activation through Ca^{2+} dependent phosphorylation by calmodulin kinase II (CaMKII) have been described (87;147). Small conductance Ca^{2+} activated Cl^- channels in excised membrane patches of human pancreatic CFPAC cells have been shown to be regulated by Ca^{2+}, CaMKII and inositol 3,4,5,6- tetrakisphosphate (50). CaCC is inhibited by compounds like 4,4'-diisothiocyanatostilbene-2,2'-disulfonic acid (DIDS) and niflumic acid (NFA), although these pharmacological tools lack of specificity (28).

Molecular candidates for CaCC have been proposed in the past. A family of Ca^{2+} activated Cl^- channels (CLCA) has been identified (20;94). These proteins are not only involved in chloride conductance and epithelial secretion, but also in cell-cell adhesion, apoptosis and cell cycle control. However, detailed structure function analysis is still missing and these proteins have a surprisingly low Ca^{2+} sensitivity (46;52). Thus CLCA could be part of a higher Cl^- channel complex (70). The CLC-3 channel has been shown to be regulated by CaMKII (51). However, CLC-3 is a cytosolic Cl^- channel, located in endosomes, and CLC-3 knockout animals apparently do not lack of Ca^{2+} activated Cl^- channels (52).

Previous studies demonstrated that bestrophin 1, the product of the vitelliform macular dystrophy (Vmd2) gene, is able to form Ca^{2+} activated Cl^- channels (130). Mutations in the Vmd2 gene cause early-onset autosomal dominant macular dystrophy of the retina, the so called Best disease (97). Previous studies detected this channel in the basolateral membrane of the retinal pigment epithelium (RPE) (75), where it controls the light-peak amplitude in the electro-oculogram. Expression of best1 was reported to be limited to the RPE, although it has also been detected in cultured airway epithelial cells (27;126). For the first time we will provide evidence that endogenously expressed best1 causes Ca^{2+} activated Cl^- conductance in epithelial tissues.

Material and Methods

Ussing chamber recordings

Animal studies were conducted according to the German laws on protection of animals. Mice (C57BL/6, Charles Rivers, Germany) were sacrificed under CO_2 narcosis by cervical dislocation. Tissues were put immediately into an ice cold buffer solution of the following composition (mmol/l): NaCl 145, KCl 3.8, D-glucose 5, MgCl2 1, HEPES 5, Ca-gluconate 1.3, pH 7.4. After mounting into a perfused micro Ussing chamber, apical and basolateral surfaces of the epithelium were perfused continuously with buffer solution at a rate of 5 - 10 ml/min (chamber volume 2 ml). All experiments were carried out at 37 °C under open circuit conditions. Transepithelial resistance (R_{te}) was determined by applying short (1 s) current pulses (I = 0.5 µA) and the corresponding changes in V_{te} (V_{te}) and basal V_{te} were recorded continuously. Values for the transepithelial voltage (V_{te}) were referred to the serosal side of the epithelium. The equivalent short-circuit current (I_{sc}) was calculated according to Ohm's law from V_{te} and R_{te} ($I_{sc} = V_{te} / R_{te}$).

Patch clamp

Cell culture dishes were mounted on the stage of an inverted microscope (IM35, Zeiss) and kept at 37 °C. The bath was perfused continuously with Ringer solution at about 10 ml/min. Patch-clamp experiments were performed in the fast whole-cell configuration. Patch pipettes had an input resistance of 2–4 MΩ, when filled with a solution containing (mM) KCl 30, K-gluconate 95, NaH_2PO_4 1.2, Na_2HPO_4 4.8, EGTA 1, Ca-gluconate 0.758, $MgCl_2$ 1.034, D-glucose 5, ATP 3. pH was 7.2, the Ca^{2+} activity was 0.1 µM. The access conductance was measured continuously and was 60 – 140 nS. Currents (voltage clamp) and voltages (current clamp) were recorded using a patch-clamp amplifier (EPC 7, List Medical Electronics, Darmstadt, Germany), the LH1600 interface and PULSE software (HEKA, Lambrecht, Germany) as well as Chart software (AD-Instruments, Spechbach, Germany). Data were stored continuously on a computer hard disc and were analyzed using PULSE software. In regular intervals, membrane voltages (V_c) were clamped in steps of 10 mV from -50 to +50 mV relative to resting potential. Membrane conductance G_m was calculated from the measured current (I) and V_c values according to Ohm's law.

mRNA expression of bestrophins in tissues and cultured cells

Total RNA was isolated from freshly isolated tissues and cell lines studied using NucleoSpin RNA II columns (Macherey-Nagel, Düren, Germany). After reverse transcription of total RNA (M-MLV Reverse Transcriptase, Promega, Mannheim, Germany), RT-PCR was used to detect expression of mRNAs for bestrophins. The oligonucleotide primers were designed for the mRNA of each gene product (name, gene, accession number: sense and antisense

primer, size of PCR product): hbest1, VMD2, NM_004183: 5´-CTGCTCTGCTACTACATCATC-3´, 5´-GTGTCCACACTGAGTACGC-3´, 552 bp; hbest2, VMD2L1, NM_017682: 5´-GTTCTACATGGCGCTGAGTG-3´, 5´-CATAGTGAAAGAGCATTCCAC-3´, 560 bp; hbest3, VMD2L3, NM_152439: 5´-CAGGAGTCCAAAAACGTTAC-3´, 5´- CCTTCATTCCGGGCTTTAG-3´, 433 bp; hbest4 , VMD2L2, NM_153274: 5´- CATGTCCCAGGAAGAGAGG´, 5´-GGTCCTCATCCCAGTACTG-3´, 584 bp; mbest1 , Vmd2, NM_011913: 5´-ACACAACACATTCTGGGTGC-3´, 5´- TTCAGAAACTGCTTCCCGATC-3´, 246 bp; mbest2, Vmd2l1, NM_145388: 5´- GAGCTGTTATGTTTCCTGGG-3´, 5´-GTAGCAACTTTAGGGCACTG-3´, 529 bp; mbest4 , Vmd2l3, NM_001007583: 5´-CAACCTGACGTCCCTGCTC-3´, 5´- CTTCTTCATCTTGGGCAAAC-3´, 607 bp. Oligonucleotide primers for both hβ-actin, ACTB, NM_001101 and mβ-actin, Actb NM_007393 were designed: 5´- CAACGGCTCCGGCATGTG-3´, 5´-GTGGTGGTGAAGCTGTAGC-3´, 576 bp. PCR reactions were performed at 94˚C for 2 min, 35 cycles at 94˚C for 30 sec, annealing temperature 60°C for 30 sec and 72˚C for 1 min. PCR products were visualized by loading on agarose gels and were verified by sequencing.

Downregulation of VMD2 expression by StealthTM RNAi

Duplexes of 25-nucleotide of RNAi were designed and synthesized by Invitrogen (Paisley, UK). The sense strand of the RNAi used to silence the VMD2 gene was 5´-UGUCCCUGUUGGCUGUGGAUGAGAU-3´, corresponding to position 1038 of the VMD2 mRNA relative to the start codon. A scrambled sequence RNAi ds-oligomer, not homologous to any known gene (BLOCK-IT™ Fluorescent Oligo) served as control. Transfection of HT_{29}, T_{84} and 16HBE cells was carried out one day after seeding (Lipofectamine™2000, Invitrogen, Germany) in Opti-MEM 1. After 24 to 48 h, cells were used for patch clamping and protein isolation.

Expression of human best1 in HEK-293 cells

pRK5 vector carrying cDNA for human best1 was kindly provided by Dr. Hugh Cahill, (John Hopkins University, Baltimore, MD, USA). The plasmid was co-transfected (Lipofectamine™2000) in Opti-MEM into HEK-293 cells, together with pEGFP-1 (Clontech, Palo alto, USA) at a ratio of 10:1. One day after transfection the cells were replated on 4 cm^2 glass coverslips. Transfected cells were identified by EGFP fluorescence and used for patch clamp experiments within 3 days.

Antibodies

Affinity purified polyclonal antiserum were produced in rabbits immunized with the peptide carrying either the mouse best1 (sequence aesypyrdeagtkpvlye) or the human best1 (sequence KDHMDPYWALENRDEAHS) coupled to keyhole limpet hemocyanin (Davids Biotechnologie, Regensburg, Germany).

Immunohistochemistry

Tissues were fixed for 2h with 4% paraformaldehyde in 0.1 M cacodylate buffer pH 7.4. Tracheas and colon were dehydrated and embedded in paraffin. Paraffin-embedded tissues were cut at 4 µm on a rotary microtome (Leica Mikrotom RM 2165, Wetzlar, Germany). Sections were de-waxed and re-hydrated. In tracheal sections endogenous peroxides activity was eliminated by incubation in methanol with 3% H_2O_2 for 20 min. Sections were incubated overnight at 4°C with rabbit anti- mouse bestrophin-1 antibodies diluted 1:10000 in Tris buffer containing Triton X-100 (0.8%) and goat serum to prevent non-specific binding. Subsequently, sections were incubated with horseradish peroxidase linked goat anti-rabbit secondary antibodies (Amersham Pharmacia Biotech, Freiburg, Germany) and ABC technique was used to visualize the labelling with 3,3-diaminobenzidine. The avidin biotin peroxidase complex (ABC) involves application of a biotin-labeled secondary antibody followed by the addition of avidin-biotin-peroxidase complex (38). Sections were counterstained with Mayer´s hematoxylin.

Detection of mbest1 and hbest1 protein by Western blot

Protein was isolated from mouse nose, trachea and kidney epithelium, and cultured cells using a buffer, which contains 150mmol NaCl, 50mmol Tris, 100mmol DTT, 1% NP-40, and 1% protease inhibitor cocktail (Sigma, Taufkirchen, Germany). Equal amounts of total protein (20 µg) were separated by a 7% sodium dodecyl sulphate (SDS) polyacrylamide gel and transferred to a PVDF membrane (Amersham Bioscience, Freiburg, Germany) which was blocked with 3% nonfat dried milk in PBS-Tween 20 (0.1%) buffer for 1h at RT. The membrane was incubated with rabbit anti-mouse or rabbit anti-human best1 antibodies (1:5000) over night at 4°C. Proteins were visualized using a goat anti-rabbit IgG horseradish peroxide (HRP) conjugated secondary antibody (1:30000, Acris Antibodies, Hiddenhausen, Germany) and ECL Advance Western Blotting Detection Kit (Amersham Bioscience, Freiburg, Germany). Signal detection was done by Fluor-S™ MultiImager system (Bio-Rad Laboratories, Hercules, USA).

Cell culture

9HTE and 16HBE-14o cells (bronchial epithelium; kindly provided by Prof. D. Gruenert, CPMRI, San Francisco, USA), Calu-3 cells (pulmonary adenocarcinoma), H441 cells (human

lung papillary adenocarcinoma; kindly provided by Dr. S. Wilson, University of Dundee, UK), HT_{29} cells (colorectal carcinoma epithelial), T_{84} cells (colorectal carcinoma) and M1 cells (mouse collecting duct cells; kindly provided by C. Korbmacher (Physiologisches Institut, Universität Erlangen, Germany)) were grown in Dulbecco's modified Eagle's (DMEM)/Ham's F-12 medium (1:1). HEK-293 cells (embryonic kidney; kindly provided by Dr. Ralph Witzgall (Institute of Anatomy, University of Regensburg, Germany)) and 9HTE / 16HBE cells were grown in DMEM and MEM respectively. H441 cells were grown in RPMI. All media were supplemented with 100 units/ml penicillin, 100 µg/ml streptomycin (Pen/Strep) and 10% fetal calf serum (FCS). Cells were incubated in 5% CO_2 at 37ºC. Media were substituted with 2 mM glutamine (Calu-3, H441, $T_{84,}$ and 9HTE), 20mg/ml galactose (HT_{29}), 10mM HEPES (Calu-3) and 10µg/ml insulin, 5.5µg/ml transferrin, 6.7µg/ml selenium and 0.1µM dexamethasone (H441 and M1). Cells were seeded on bovine plasma fibronectin (Invitrogen, Karlsruhe, Germany) and bovine dermal collagen (Cellon, Luxembourg) coated plastic dishes or glass cover slips.

Materials and statistical analysis

All compounds used were of highest available grade of purity from Sigma (Taufkirchen, Germany) or Merck (Darmstadt, Germany). All cell culture reagents were from GIBCO/Invitrogen (Karlsruhe, Germany). Student's t-test (for paired or unpaired samples as appropriate) and analysis of variance (ANOVA) was used for statistical analysis. $P<0.05$ was accepted as significant.

Results

Ca^{2+} activated Cl^- secretion in mouse airways

In mouse trachea, stimulation of luminal purinergic P2Y receptors by ATP (100 µM) increased intracellular Ca^{2+} and stimulated Cl^- secretion (64;73). ATP induced a negative voltage deflection in Ussing chamber experiments, and activated a short circuit current (I_{sc}) (Fig. 1). Application of inhibitors of Ca^{2+} activated Cl^- channels, DIDS (100 µM) or niflumic acid (NFA; 10 µM) inhibited ATP induced transport in the trachea (Fig. 1A,B). Activation of Cl^- secretion was suppressed by the Ca^{2+} chelator BAPTA (10 µM) or by depletion of intracellular ER Ca^{2+} stores with CPA (10 µM) (Fig. 1C,D).

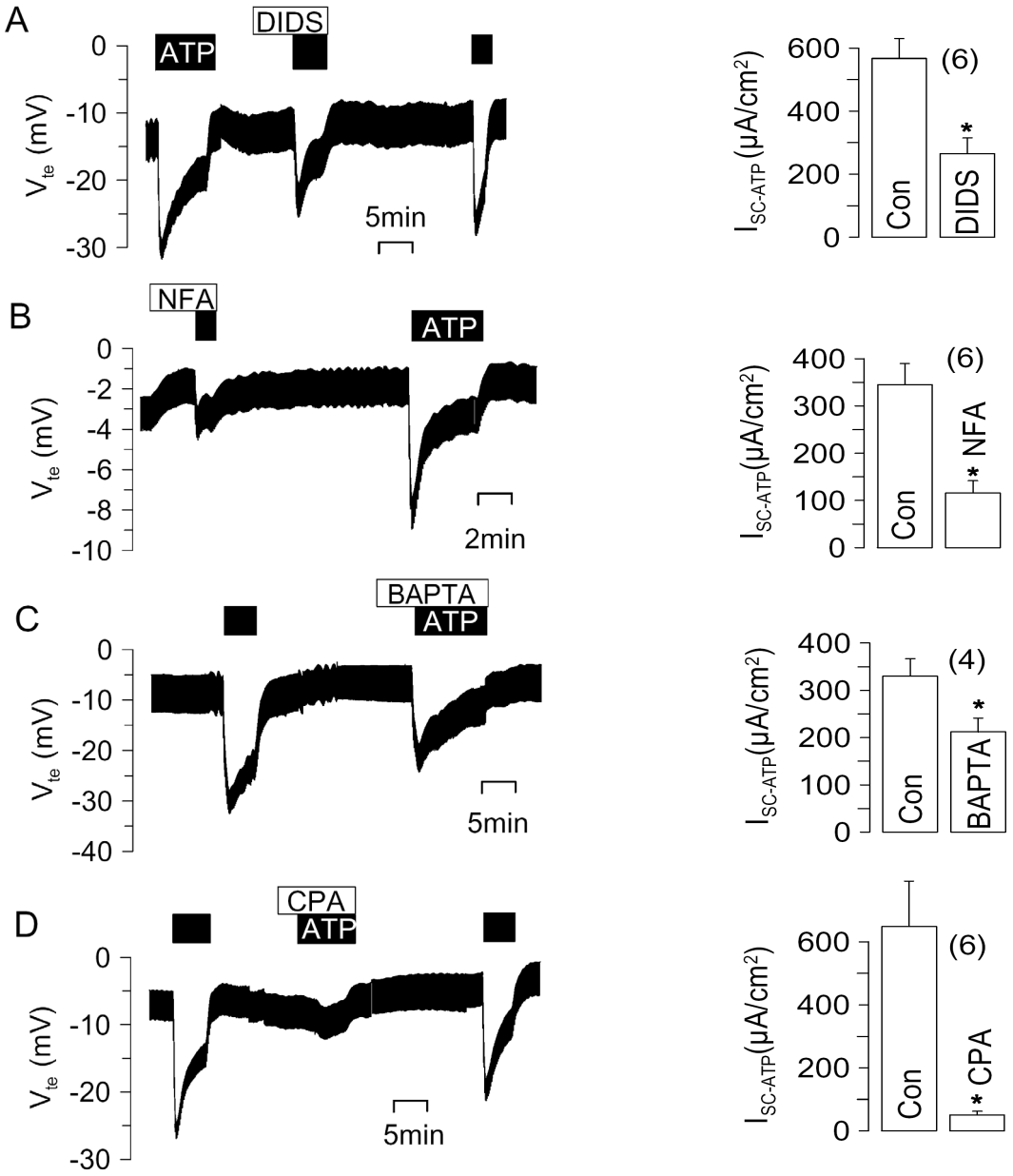

Fig. 1. Ca^{2+} activated Cl^- secretion in mouse trachea. Ussing chamber recordings of transepithelial voltage (V_{te}). A,B) ATP (100 µM) induced a negative voltage deflection and a short circuit current due to activation of CaCC in mouse trachea, which is inhibited by DIDS (100 µM) or NFA (10 µM). C,D) Activation of Cl^- secretion can be suppressed by the Ca^{2+} chelator BAPTA (10 µM) or by depletion of intracellular ER Ca^{2+} stores with CPA (10 µM). * indicates significant difference when compared to control (paired Student´s t-test). (number of experiments).

Ca^{2+} activated Cl^- channels have been found in primary murine nasal cell cultures and in CF nasal epithelium, but not in the normal murine nasal tissue (40-42). We occasionally detected a small Cl^- secretory response upon ATP stimulation which, however, was insignificant (Fig. 2A,B). mRNA analysis demonstrated the presence of all three mouse bestrophins 1, 2 and 4, in both trachea and nose (Fig. 2C). However, Western blot analysis detected best1 protein only in the trachea, but not in the nasal epithelium (Fig. 2D). Expression of best1 was further

demonstrated by immunohistochemistry, using rabbit IgG conjugated to horseradish peroxidase. Best1 was detected in tracheal epithelium at lower and higher magnification, while control stains without primary antibody were negative (Fig. 2E,F). Thus expression of best1 correlates with the appearance of Ca^{2+} activated Cl^- currents in mouse trachea.

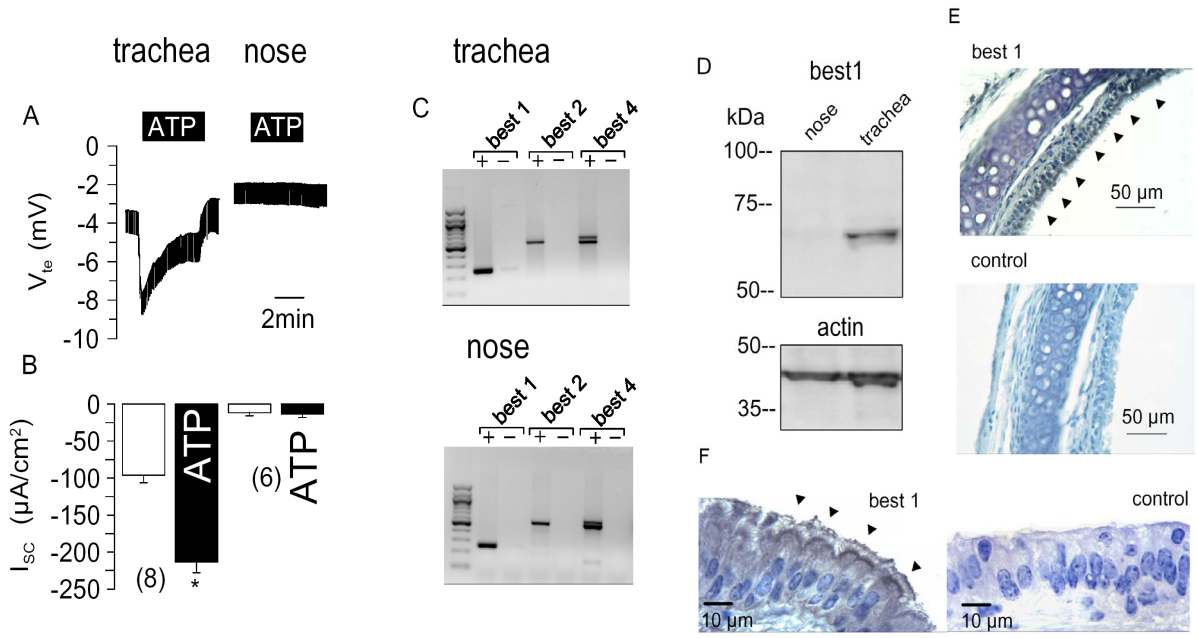

Fig. 2. Expression of best1 in mouse trachea but not in the nose. Ussing chamber recordings of transepithelial voltage (V_{te}). A,B) ATP (100 μM) induced a negative voltage deflection and a short circuit current due to activation of CaCC in mouse trachea but not nasal epithelium. C) RT-PCR analysis of mRNA (+/- reverse transcriptase) isolated from mouse tracheal and nasal epithelium. mRNA of all three mouse isoforms of bestrophin are expressed in both trachea and nose. D) Expression of best1 protein could only be detected in trachea but not nasal epithelium. The actin band is shown to indicate equal loading. E,F) Detection of best1 expression in the tracheal epithelium at two magnifications, using horseradish peroxidase. Arrowheads indicate expression on the apical side of the tracheal epithelium. Controls were obtained without primary antibody. * indicates significant difference when compared to control (paired Student´s *t*-test). (number of experiments).

Expression of endogenous best1 induces CaCC in airway cells

We examined CaCC in different human airway epithelial cell lines. In patch clamp experiments with human bronchial epithelial cells (16HBE), a whole cell Cl^- current was activated by 100 μM ATP, which was inhibited by 100 μM DIDS (Fig. 3). Expression of best1 protein in 16HBE cells was verified by Western blotting (data not shown). We suppressed expression of best1 in 16HBE cells by incubation with best1-RNAi. Successful suppression was verified by semi-quantitative RT-PCR, best1 immunocyto-chemistry, and Western blotting (Fig. 3E). ATP induced whole cell conductances were significantly reduced in RNAi

treated cells, when compared to control cells or cells transfected with scrambled RNA (Fig. 3D).

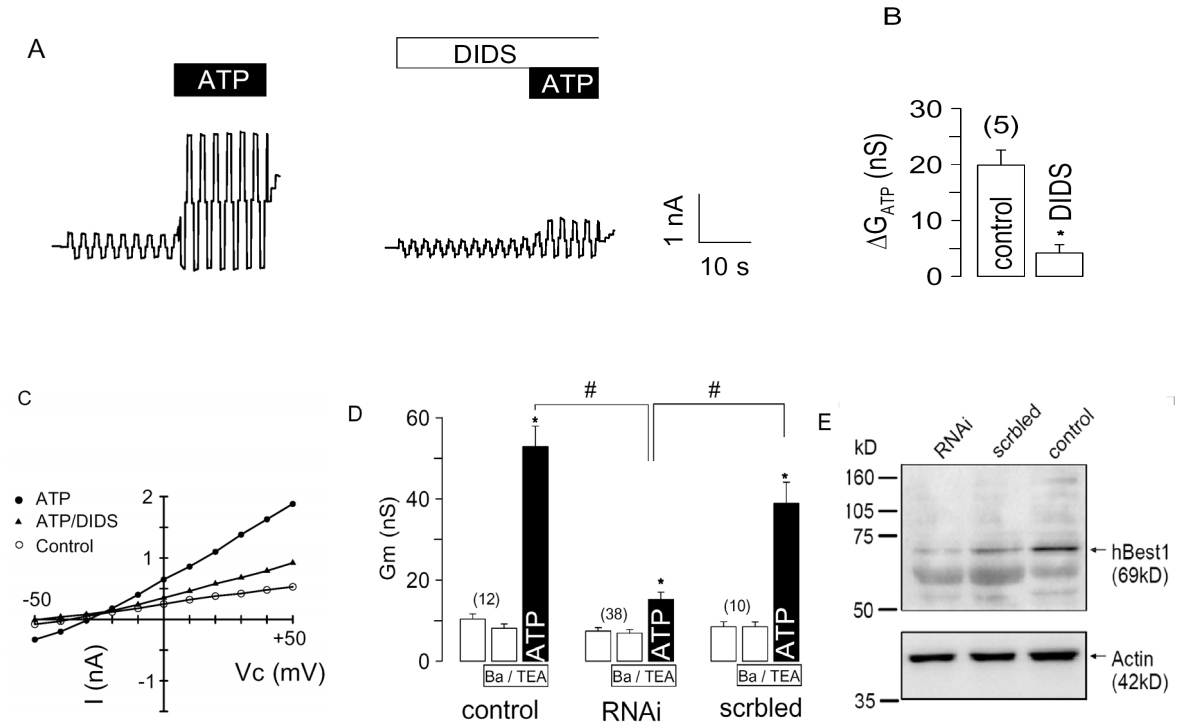

Fig. 3. Ca^{2+} activated Cl^- channels in human airway epithelial cells. A) Stimulation of human airway epithelial cells (16HBE) with 100 µM ATP activates a Cl^- current in a whole cell patch clamp experiment. Activation was inhibited by 100 µM DIDS. B) Summary of experiments as shown in A). C) i/v relationship of the whole cell currents before and after exposure to ATP and ATP/DIDS. D) Summary of the experiments in which 16HBE cells were incubated with best1-RNAi to knockdown best1 expression. Transfection with scrambled RNA (scrbled) served as control. Experiments were performed in the presence of the K^+ channel blockers Ba^{2+} (5 mM) and TEA^+ (10 mM) in order to exclude K^+ conductances. E) Western blot of hbest1 and actin in RNAi treated and control cells. * indicates significant difference when compared to control (paired Student´s *t*-test). # indicates significant difference when compared to RNAi (unpaired Student´s *t*-test). (number of experiments).

Ca^{2+} activated whole cell conductances were compared in four different human airway epithelial cell lines, grown on glass coverslips (Fig. 4). Because both Cl^- and K^+ currents may be activated by increase in intracellular Ca^{2+}, we stimulated the cells in the presence of the K^+ channel blockers Ba^{2+} (5 mM) and TEA^+ (10 mM). RT-PCR analysis of the 4 human bestrophin isoforms demonstrated expression of best1 in 16HBE and Calu-3 cells, but not in the cell lines H441 and 9HTE (Fig. 4). Accordingly, ATP activated Cl^- currents were only found in 16HBE and Calu-3 cells, but not in H441 or 9HTE cells. This further suggests that expression of endogenous best1 allows for Ca^{2+} activated Cl^- currents in airway epithelial cells.

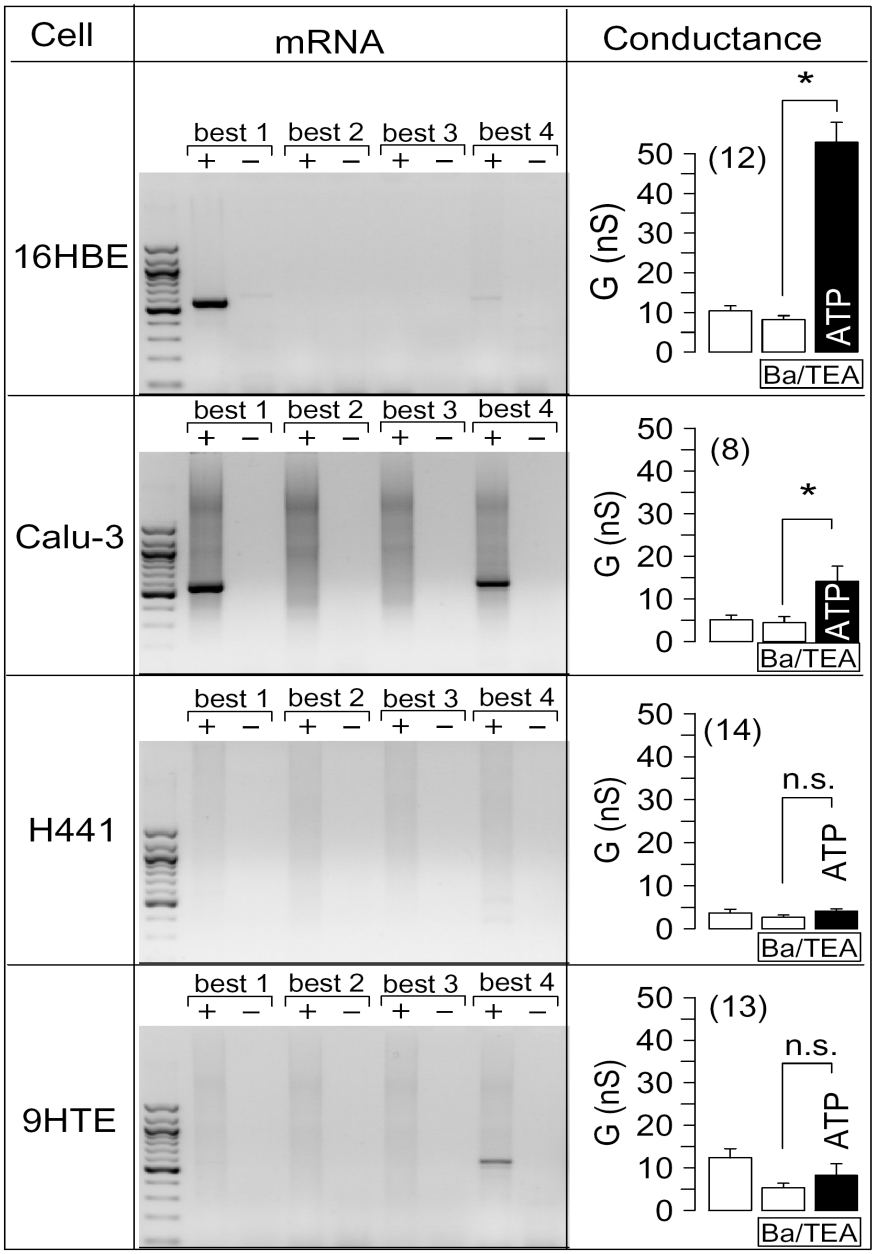

Fig. 4. Expression of bestrophins in different human airway epithelial cell lines. RT-PCR analysis (+/- reverse transcriptase) of the 4 human isoforms of bestrophin (best1 - 4) in 4 different human airway epithelial cell lines (left). Whole cell conductances measured before and after stimulation of airway epithelial cells by 100 µM ATP in the presence of the K^+ channel blockers Ba^{2+} (5 mM) and TEA^+ (10 mM) (right). ATP activates a whole cell current only in respiratory cell lines which express best1. * indicates significant difference when compared to control (paired Student´s *t*-test). n.s. indicates no significant changes upon ATP stimulation. (number of experiments).

Expression of best1 in colonic epithelial cells

We also detected expression of best1 along with best4 in the human colonic cancer cell line HT_{29} (Fig. 5A). These cells activate a Ca^{2+} dependent Cl^- conductance upon stimulation with ATP (Fig. 5B). Similar results, e.g. expression of best1 mRNA and protein along with Ca^{2+} activated Cl^- currents were obtained in the colonic cancer cell line T_{84} (data not shown). We

suppressed expression of best1 in HT_{29} cells by best1-RNAi. Best1 knockdown was 61- 78 %, according to densitometric analysis of Western blots (Fig. 5D). Incubation of the cells with scrambled unrelated RNA showed no effects. Whole cell patch clamp analysis demonstrated largely reduced Ca^{2+} (ATP-) activated whole cell currents in RNAi treated cells, when compared to control cells or cells transfected with scrambled RNA. Out of 23 RNAi incubated cells, none showed a current similar in size as control cells (Fig. 5C,E).

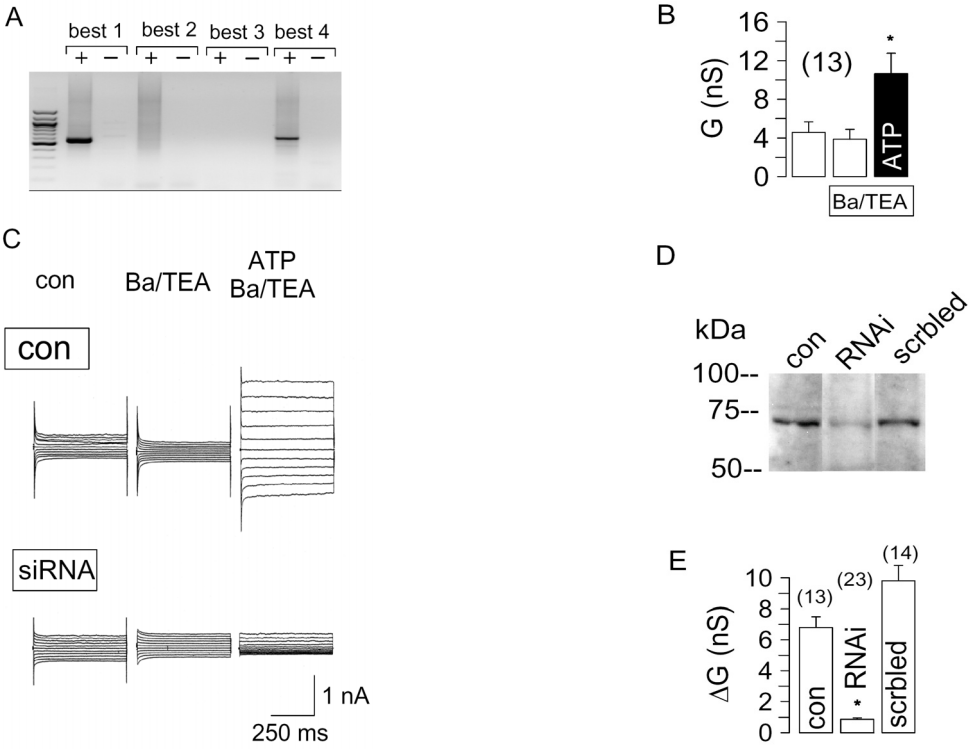

Fig. 5. Expression of best1 in HT_{29} colonic epithelial cells. A) RT-PCR analysis (+/- reverse transcriptase) of the 4 human isoforms of bestrophin (best1 - 4) in HT_{29} cells. B) Summary of ATP induced whole cell Cl^- conductances in HT_{29} cells. C) Activation of whole cell currents in HT_{29} cells by ATP (100 µM) under control conditions and after incubation of the cells with best1-RNAi. D) Western blot analysis of best1 expression in HT_{29} cells grown under control conditions, after incubation with RNAi or after incubation with scrambled (scrbled) RNA. E) Summary of the whole cell conductances activated in HT_{29} cells grown under control conditions, after incubation with RNAi or after incubation with scrambled (scrbled) RNA. * indicates significant difference when compared to control (paired Student´s *t*-test). (number of experiments).

We further examined expression of best1 in the native mouse colonic epithelium. To that end we isolated proximal and distal colonic epithelium and determined ion transport activated by carbachol stimulation of basolateral M3 receptors (CCH; 100 µM). In the proximal colon, CCH induced a fast and negative voltage deflection, due to activation of a transient Cl^- secretion. In contrast, stimulation of the distal colon activated a delayed luminal K^+ secretion (Fig. 6A,B). Expression of both best1 mRNA and protein was more prominent in isolated colonic crypts of the proximal colon (data not shown). Immunohistochemistry clearly detected

best1 expression in mouse proximal colon, whereas only a few cells stained positive for best1 in the distal colonic epithelium (Fig. 6C). Taken together these results suggest that best1 also participates in Ca^{2+} dependent Cl^- secretion in the proximal colonic epithelium.

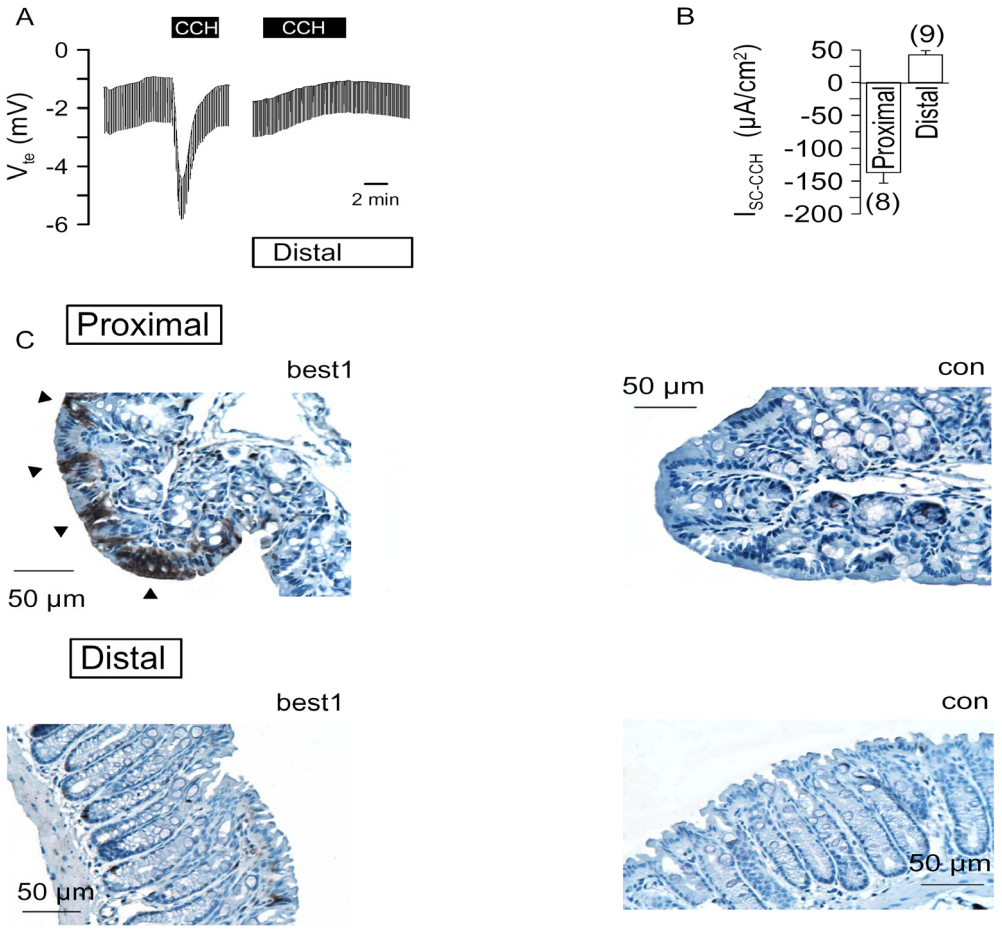

Fig. 6. Expression of best1 in proximal and distal mouse colon. A) Ussing chamber recordings of the transepithelial voltage (V_{te}) in proximal and distal colonic epithelium. Basolateral carbachol (CCH, 100 µM) induced a negative voltage deflection by activation of CaCC in the proximal colon, but caused a lumen positive voltage deflection in the distal colon, due to activation of K^+ secretion. B) Summary of the CCH induced I_{sc} in proximal and distal colonic epithelium. C) Detection of best1 expression in the proximal and distal colonic epithelium. Arrowheads indicate expression on the apical side of the proximal colonic epithelium. Controls were obtained without primary antibody. * indicates significant difference when compared to control (paired Student´s *t*-test). (number of experiments).

Expression of best1 in renal epithelial cells

In mouse collecting duct cells, ATP activated a whole cell conductance, which was inhibited by 100 µM DIDS, but not by 5 mM Ba^{2+} (Fig. 7A). The corresponding i/v curves were linear (Fig. 7B), probably due to high intracellular Ca^{2+} levels induced by purinergic stimulation (data not shown). We added an anti mouse best1 antibody (1:500) to the patch pipette filling solution, which binds to the C-terminal end of best. Inclusion of this antibody significantly reduced the whole cell conductance activated by 100 µM ATP (Fig. 7C, D). M1 cells express mRNA for the two isoforms best1 and best2 (Fig. 7E). Expression of best1 protein was

detected in lysates from M1 cells and mouse kidney (Fig. 7F). In mouse kidneys, immunohistochemistry detected expression of best1 throughout medulla and cortex, with strongest expression in the region of the papilla. However, not all cells within a tubular segment expressed best1, and thus a rather spotted staining was obtained. Fig. 7G shows co-staining of the cytoskeleton (red) and best1 (green). In agreement with this result, Ca^{2+} activated Cl^- channels have been found in cells from almost all renal tubular segments (46).

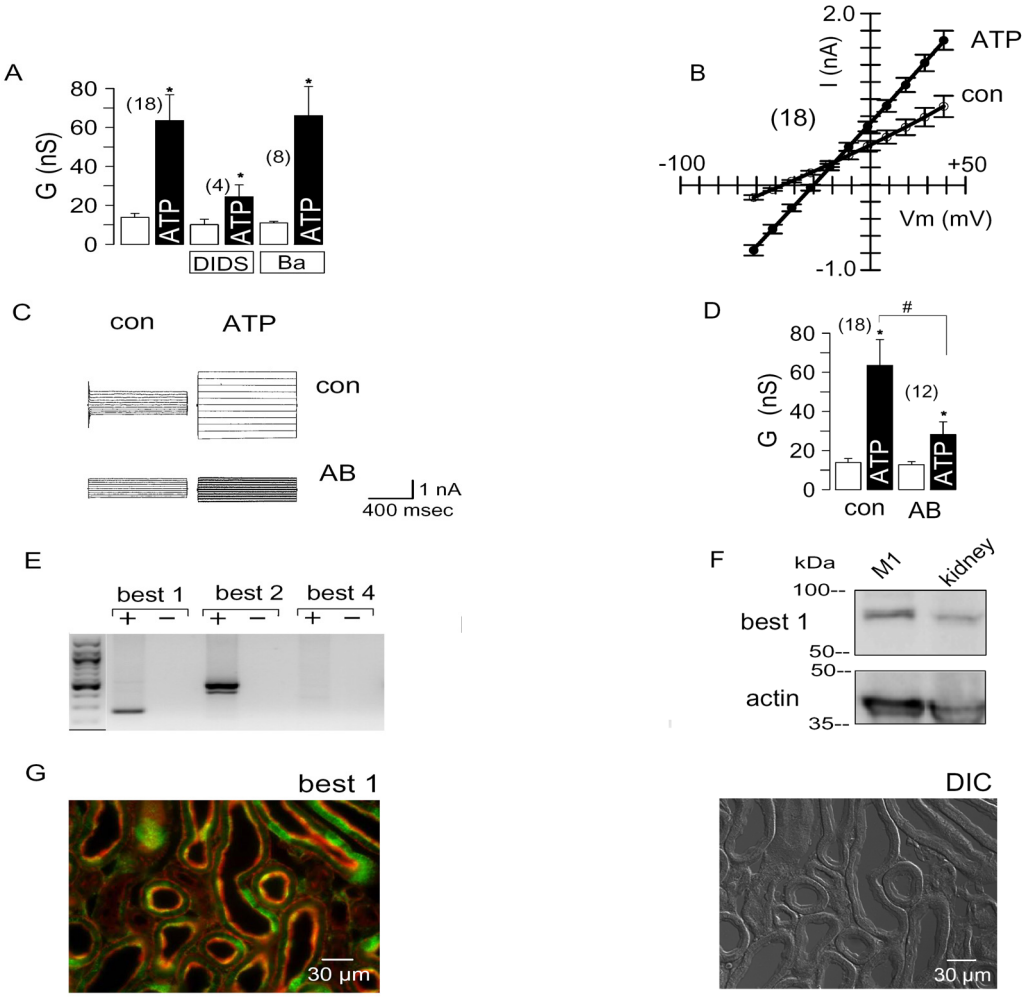

Fig. 7. Expression of best1 in cultured kidney epithelial cells and mouse kidney. A) Summary of the ATP (100 µM) induced whole cell Cl^- conductances in M1 cells and inhibition by DIDS (100 µM) but not by barium (Ba, 5 mM). B) Summary i/v curves of the whole cell currents measured before and after stimulation with ATP. C) Activation of whole cell currents by ATP in M1 cells with control solution in the patch pipette (con) or after adding a best1 antibody (AB) to the patch pipette filling solution. D) Summary of the experiments as shown in (C). E) RT-PCR analysis (+/- reverse transcriptase) of the 3 mouse isoforms of bestrophin in mouse kidney. F) Expression of best1 protein in M1 cells and kidney. The actin band is shown to indicate loading of the gel. G) Co-staining of the cytoskeleton (Alexa Fluor 647 phalloidin; red) and best1 (Alexa Fluor 546; green) in mouse kidney (left). Differential interference contrast (DIC) image of the kidney slice (right). * indicates significant difference when compared to control (paired Student´s *t*-test). # indicates significant difference when compared to the absence of the antibody (unpaired Student´s *t*-test). (number of experiments).

Expression of hbest1 induces CaCC in HEK293 cells

To further confirm a role of best1 as Ca^{2+} activated Cl^- channel, we expressed human best1 in HEK293 cells. Expression was verified by Western blot analysis and immunocytochemistry (data not shown). HEK293 cells coexpressing best1 and enhanced green fluorescent protein (EGFP), activated a whole cell conductance upon stimulation with 100 µM ATP. This was not observed in HEK cells expressing only EGFP (Fig. 8A, B). Coexpressing cells demonstrated an enhanced baseline conductance and a reduced membrane voltage, probably due to enhanced baseline Cl^- conductance. Membrane voltage was further depolarized and the whole cell conductance was inhibited by reducing bath Cl^- concentration to 30 mM (Fig. 8B, C). The ATP activated whole cell conductance was inhibited by 100 µM DIDS (Fig. 8D). Taken together, these results strongly suggest that Ca^{2+} dependent Cl^- currents in epithelial cells from airways, colon and kidney are due to expression of best1.

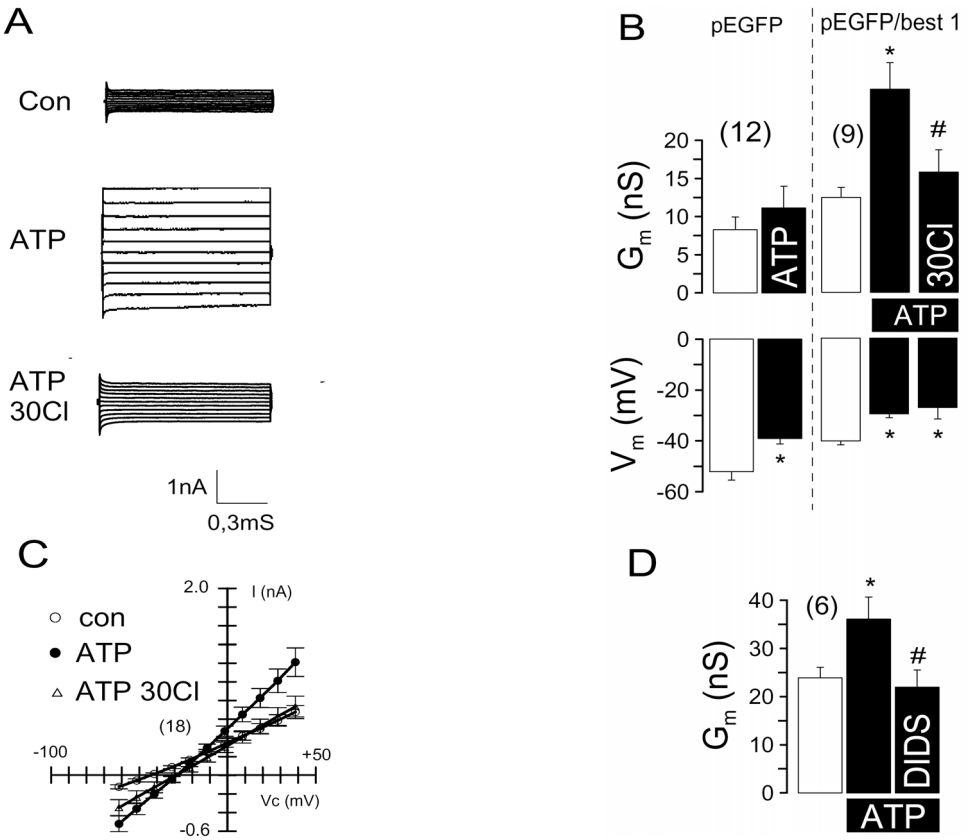

Fig. 8. Activation of CaCC in HEK293 cells after overexpression of hbest1. A) Activation of whole cell currents by ATP (100 µM) in HEK293 cells coexpressing EGFP and human best1. Lowering the bath Cl^- concentration to 30 mM reduced ATP activated whole cell conductance. B) Summary of the experiments as shown in (A). HEK293 cells expressing only EGFP do not activate a whole cell conductance. C) Summary i/v curves of the whole cell currents measured before and after stimulation with ATP. D) Summary of the effects of DIDS (100 µM) on ATP induced Cl^- conductance in HEK293 cells. * indicates significant difference when compared to control (paired Student´s *t*-test). # indicates significant difference when compared to ATP. (number of experiments).

Discussion

CaCC in epithelial tissues

Ca^{2+} activated Cl^- channels are fundamental for fluid secretion in acini of exocrine tissues, such as lachrymal, parotid, mandibular and pancreatic glands (39). In airways and in the colonic epithelium, electrolyte secretion is dominated by cystic fibrosis transmembrane conductance regulator (CFTR) Cl^- channels (57). Apart from CFTR, Cl^- secretion is activated through stimulation of CaCC, present in the apical membrane of airways and other organs. Previous studies showed that i) application of the Ca^{2+} ionophore ionomycin also activates Cl^- secretion, ii) in the presence of low (1 µM) extracellular Ca^{2+}, activation of Cl^- secretion is very transient, iii) after inhibition of phospholipase C, purinergic Cl^- secretion is reduced, and iv) DIDS inhibits Ca^{2+} activated Cl^- secretion in mouse airways (64). These and other experiments (73) strongly suggest that secretion occurs through Ca^{2+} dependent activation of Cl^- channels. ORCC channels are unlikely candidates, since Ca^{2+} activates small conductance Cl^- channels in HT_{29} and 16HBE cells (56;59).

Both CFTR and CaCC control airway surface liquid, which is essential for mucociliary clearance (135). Purinergic activation of CaCC in the airways resembles an important therapeutic principle for cystic fibrosis (61;67). Cl^- secretion in mouse airways is dominated by CaCC, which explains why CFTR knockout animals do not develop a CF lung disease (40). Interestingly, a functional relationship exists between CaCC and CFTR (62;143), and Ca^{2+} mediated Cl^- secretion is enhanced in CF airways (73). Thus, Ca^{2+} activated Cl^- secretion is found in CF but not normal murine nasal epithelium (40). After pre-stimulation of CFTR, CaCC was also activated in normal nasal epithelium. However, this is probably due to activation of basolateral K^+ channels, rather than activation of luminal CaCC (17). Although transcripts for best1 were detected in the nasal epithelium, no significant levels of best protein were found. This is probably not explained by mRNA instability since no AU rich elements could be detected.

In the human colonic epithelium of older infants and adults, CaCC mediated Cl^- secretion is less important. Thus no Cl^- secretion is found in the absence of functional CFTR, e.g. in the colonic epithelium of cystic fibrosis patients (12;72;74). Younger infants, however, may express CaCC in the colonic epithelium and be therefore susceptible for virus induced diarrhea. In fact, age dependent diarrhea was induced in mice by the rotavirus toxin NSP4 in a previous study (7). NSP4 increases intracellular Ca^{2+} and activates Cl^- secretion in newborn mouse pups (24). In the present study, we detected Ca^{2+} activated Cl^- secretion in the proximal but not distal colon. Accordingly, best1 was well detected in the proximal, but not in the distal colon. The role of CaCC in the kidney is controversial (69;117). However, in

studies with primary and permanent cultures of proximal and distal tubules, thick ascending limb and collecting ducts, CaCC was identified (9;13;71;109). Also in the present experiments with M1 collecting duct cells, CaCC was detected. Thus renal epithelial cells may retain the ability to induce Ca^{2+} activated Cl^- transport.

Bestrophin: a Cl^- channel or a regulator of Ca^{2+} signaling?

Sulfhydryl scanning enabled structure-function analysis and demonstrated that bestrophins form bona fide Cl^- channels (104;139). Direct activation of best4 by Ca^{2+} was demonstrated in excised membrane patches (138). Nevertheless, it has been proposed that best1 is a regulator of voltage gated L-type Ca^{2+} channels, rather than a Ca^{2+} regulated Cl^- channel (77;115). Purinergic increase of $[Ca^{2+}]_i$ was augmented in RPE cells of vmd2-/- mice. In this study $[Ca^{2+}]_i$ increase was remarkably slow. This is in sharp contrast to Ca^{2+} responses observed in the epithelial tissues used here: $[Ca^{2+}]_i$ increase occurs within less than a second and is typically 4 to 10 fold (data not shown). Moreover, ATP induced Ca^{2+} increase is due to Ca^{2+} release from intracellular stores (peak), and Ca^{2+} influx, probably through TRP-related Ca^{2+} channels (plateau) (89). Preliminary unpublished measurements show only insignificant changes in Ca^{2+} signaling upon manipulation of best1 expression.

Best1 mediates Ca^{2+} activated Cl^- secretion in epithelial tissues

The present data show endogenous expression of best1 in mouse and human epithelial cells from airways, colon and kidney. Best1 expression was clearly correlated with the appearance of CaCC. Rectification of the Cl^- currents varied between the different cell lines. I/V curves were almost linear for M1 and HEK293, but were rectifying for 16HBE cells. Rectification depends on the level of $[Ca^{2+}]_i$ and disappears at high ($>$ 1 µM) concentrations (5;29;65;109). ATP increased $[Ca^{2+}]_i$ to values above 1 µM in M1 cells, but to values below 1 µM in 16HBE cells (data not shown), which may explain the variability. In HT_{29} and 16HBE cells, suppression of best1 by RNAi inhibited CaCC. These results clearly indicate that best1 is necessary for Ca^{2+} activated Cl^- secretion. However, they do not rule out the possibility that best1 is a regulator of a still unidentified Ca^{2+} activated Cl^- channel, or that it is part of a Cl^- channel complex. Only a fraction of best1 appears to be localized in the plasma membrane, while most is found in the cytosol, probably bound to vesicular membranes. (126;139). The spotted expression of best1 in some tissues suggests that CaCC is not equally present within the epithelium. Thus expression may depend on additional factors, which should be subject of subsequent studies.

Chapter 3

Bestrophin 1 and 2 are components of the Ca^{2+} activated Cl^- conductance in mouse airways

Abstract

Ca^{2+} activated Cl^- transport is found in airways and other organs and is abnormal in cystic fibrosis, polycystic kidney disease and infectious diarrhea. The molecular identity of Ca^{2+} activated Cl^- channels (CaCC) in the airways is still obscure. Bestrophin proteins were described to form CaCC and to regulate voltage gated Ca^{2+} channels. The present Ussing chamber recordings on tracheas of bestrophin 1 knockout (vmd2-/-) mice indicate a reduced Cl^- secretion when activated by low concentrations (0.1 – 1 µM) of the purinergic agonist ATP. Both paralogs best1 and best2 are present in the tracheal epithelium from vmd2+/+ mice, while vmd2-/- mice have no best1 and, in addition, a reduced expression of best2. Whole cell patch clamp analysis of primary airway epithelial cells from vmd2-/- tracheas demonstrated 50% reduction in Ca^{2+}, i.e. ATP activated Cl^- currents. Additional mbest2 knockdown in vmd2-/- cells by short interfering RNA further suppressed ATP induced Cl^- currents down to 20 % of that observed in vmd2+/+ respiratory cells. In vmd2+/+ cells suppression of both mbest1 and mbest2 reduced CaCC. Direct activation of CaCC by increase of intracellular Ca^{2+} was also reduced in whole cell recordings of vmd2-/- cells. These results clearly suggest a role of bestrophin 1 and 2 for Ca^{2+} dependent Cl^- secretion in the airways.

Introduction

Airway epithelia secrete electrolyte upon stimulation by secretagogues, which activate Cl^- channels through an increase in intracellular Ca^{2+} or cAMP. cAMP activated cystic fibrosis transmembrane conductance regulator (CFTR) Cl^- channels are well established and their channel properties and regulation have been described in detail. Detailed information is also available for ligand-gated channels (GABA/glycine receptors) or the CLC chloride channel family (52). In contrast, the molecular counterpart of the Ca^{2+}-activated Cl^-channel is still a matter of controversy (87). The previously identified CLCA proteins have not been unanimously accepted as Ca^{2+} activated Cl^- channels (70). The genes hTTHY2 and hTTYH3 encode Ca^{2+} -activated maxi-Cl^- channels (Tweety) and are unlikely to form epithelial small conductance Ca^{2+} activated Cl^- channels (132). The group of Nathans and coworkers proposed that a family of proteins known to play a central role for a dominant form of macular dystrophy (Best disease) of the retina, comprises a new class of Ca^{2+} activated Cl^- channels (130). A series of subsequent papers described the properties of bestrophin paralogs, which were in good agreement with those found for native Ca^{2+} activated Cl^- currents (11;63;104;107;110;139).

Although bestrophin 1 was also reported to be a regulator of voltage gated L-type Ca^{2+} channels (77;115), whole cell recordings from cells heterologously expressing the four bestrophin paralogs clearly pointed out to their function as Ca^{2+} dependent Cl^- channels (reviewed in (48)). Mutations in both human best1 and mouse best2 altered anion conductance and permeability and changed their sensitivity to cysteine-reactive reagents (48). Moreover best2 is a molecular component of the Ca^{2+} activated Cl^- channel in mouse olfactory sensory neurons (98). We reported previously a correlation between best1 expression and Cl^- currents activated through stimulation of purinergic P2Y receptors in human and mouse epithelial tissues (11). In the present study on wt (vmd2+/+) and best1 knockout (vmd2-/-) mice, we provide evidence that both best1 and best2 are necessary components of the ATP-induced Ca^{2+}-activated Cl^- secretion in mouse airways. Bestrophins are therefore important for regulation of the airway surface liquid ensuring an adequate mucociliary clearance (137).

Material and Methods

Mouse tracheal epithelial cells isolation

Best1-KO (vmd2-/-) mice (C57BL/6x129Sv) were a generous gift from MERCK Research Laboratories (770 Sumneytown Pike West Point, PA, USA). vmd2-/- and wild type (vmd2+/+)

counterparts with same genetic background were sacrificed and tracheas were put in ice-cold AECGM plus supplement that contained bovine pituitary extract 13 mg/ml, EGF 10 ng/ml, epinephrine 0.5 µg/ml, hydrocortisone 0.5 µg/ml, retinoic acid 0.1 ng/ml, transferrin 10 µg/ml, and triiodo-L-thyronine 6.7 ng/ml. Media were further supplemented with 100 units/ml penicillin, 100 µg/ml streptomycin, 3 µg/ml fungyzone, 50 µg/ml chloramphenicol, 0.1 mg/ml kanamycin and 10% fetal bovine serum (FBS). Tracheas were washed with media and opened longitudinally. About 5 tracheas were incubated in AECGM-SM containing 1.5 mg/ml pronase (Roche, Indianapolis, USA) for 18 h at 4ºC and the content was collected by centrifugation at 420 g for 10 min at 4ºC. Cells were resuspended in 200 µl/trachea in AECGM-SM (FBS free) containing 0.5 mg/ml crude pancreatic DNase I and 10 mg/ml Bovine serum albumin (BSA). The cells were then incubated on ice cold AECGM-SM for 5 min, centrifuged at 420 g for 5 min at 4ºC and resuspended in AECGM-SM with 10% FBS. Cells were seeded on bovine plasma fibronectin (Invitrogen, Karlsruhe, Germany) and bovine dermal collagen (Cellon, Luxembourg) coated plastic dishes and incubated for 3-4 h in 5% CO_2 at 37ºC to adhere fibroblasts. Experiments were performed within 3-4 days after seeding.

mRNA expression of bestrophins in primary cultured cells

Total RNA was isolated from freshly isolated mouse tracheal cells collected from a single mouse trachea using RNeasy Micro Kit columns (QIAGEN, Hilden, Germany). cDNA was obtained from reverse transcription of total RNA (M-MLV Reverse Transcriptase, Promega, Mannheim, Germany). RT-PCR was used to detect expression of mRNAs for bestrophins. The oligonucleotide primers were designed for the mRNA of each gene product (name, gene, accession number: sense and antisense primer, size of PCR product): mbest1 , vmd2, NM_011913: 5´- ACACAACACATTCTGGGTGC-3´, 5´- TTCAGAAACTGCTTCCCGATC-3´, 246 bp; mbest2, vmd2l1, NM_145388: 5´- GAGCTGTTATGTTTCCTGGG-3´, 5´- GTAGCAACTTTAGGGCACTG-3´, 529 bp; mbest3 , vmd2l3, NM_001007583: 5´- CAACCTGACGTCCCTGCTC-3´, 5´- CTTCTTCATCTTGGGCAAAC-3´, 607 bp. Oligonucleotide primers for mβ-actin, Actb NM_007393 were designed: 5´- CAACGGCTCCGGCATGTG-3´, 5´- GTGGTGGTGAAGCTGTAGC-3´, 576 bp. PCR reactions were performed at 94˚C for 2 min, 32 cycles at 94˚C for 30 sec, annealing temperature 60°C for 30 sec and 72˚C for 1 min. All PCR products were verified by sequencing.

Antibodies

Affinity purified polyclonal antisera were produced in rabbits immunized with the peptide carrying either the mouse best1 (sequence aesypyrdeagtkpvlye) or the mouse best2

(sequence RAPAPPWLPSPIGEEEE) coupled to keyhole limpet hemocyanin (Davids Biotechnologie, Regensburg, Germany).

Detection of mbest1 and mbest2 protein by Western blot

Protein was isolated from vmd2+/+ or vmd2-/- primary cultured cells collected out of 5 pooled mouse tracheas using a buffer containing (mmol/l): NaCl 150, Tris 50, DTT 100, 1% NP-40, and 1% protease inhibitor cocktail (Sigma, Taufkirchen, Germany). Western blotting was performed as described (11).

Ussing chamber recordings

Animal studies were conducted according to the German laws on protection of animals. Experiments were carried out under open circuit conditions, essentially as previously described (11).

Patch clamp

Primary cell culture dishes were mounted on the stage of an inverted microscope (IM35, Zeiss) and kept at 37 °C. The bath was perfused continuously with Ringer solution at about 10 ml/min. Patch-clamp experiments were performed in the fast whole-cell configuration. Patch pipettes resistances were 2–4 MΩ, when filled with a solution containing (mmol/l) KCl 30, K-gluconate 95, NaH_2PO_4 1.2, Na_2HPO_4 4.8, EGTA 1, Ca-gluconate 0.758, $MgCl_2$ 1.034, D-glucose 5, ATP 3. Ca^{2+} activity was 0.1 µM and pH 7.2. The access conductance was monitored continuously and was 40 – 140 nS. Currents (voltage clamp) and voltages (current clamp) were recorded using a patch-clamp amplifier (EPC 7, List Medical Electronics, Darmstadt, Germany), the LH1600 interface and PULSE software (HEKA, Lambrecht, Germany) as well as Chart software (AD-Instruments, Spechbach, Germany). Data were analyzed using PULSE software. Membrane voltages (V_c) were clamped in steps of 10 mV from -50 to +50 mV relative to resting potential. Membrane conductance G_m was calculated from the measured current (I) and V_c values according to Ohm's law.

Downregulation of vmd2 and vmd2L1 expression by StealthTM RNAi

Double stranded RNAi (25-nucleotide) were designed and synthesized by Invitrogen (Paisley, UK). RNAi sense strands used to silence vmd2 and vmd2L1 genes were respectively: 5´- CCCAUGGAACGUGACAUGUACUGGA -3´, and 5´-GGAGCUGAAUGUGUUUCGGAGCAAA-3´, corresponding to positions 1203 of the vmd2 and 682 of the vmd2l1 mRNA relative to the start codon. A scrambled sequence RNAi ds-oligomer, not homologous to any known gene (BLOCK-IT^{TM} Fluorescent Oligo) served as mock control. Transfection of mTEC cells was carried out one day after seeding

(Lipofectamine™2000, Invitrogen, Germany) in Opti-MEM. Cells were used for patch clamping and immunostaining within 48 h.

Expression of mouse best1 in primary airway cells from vmd2-/- animals

pcDNA3.1 vector carrying mbest1 cDNA were kindly provided by Dr. Criss Hartzell, (Emory University School of Medicine, Atlanta, GA, USA). The plasmid was transfected (Lipofectamine™2000) in Opti-MEM into vmd2-/- cells.

Immunocytochemistry

Tracheal tissues and primary cultured vmd2+/+ or vmd2-/- cells were immunostained with mbest1 or mbest2 antibody as described previously (11). Briefly, tissues and cells were respectively fixed for 2 h and 30 min with 4% paraformaldehyde in 0.1 M cacodylate buffer pH 7.4. Tracheas were dehydrated, embedded in paraffin and cut at 4 µm on a rotary microtome (Leica Mikrotom RM 2165, Wetzlar, Germany). Endogenous peroxidase activity was eliminated by incubation in methanol with 3% H_2O_2 for 20 min. Sections and cells were incubated overnight at 4°C with rabbit anti- mouse best1 or best2 antibody diluted 1:10000 and 1:250 respectively in Tris buffer containing Triton X-100 (0.8%) and goat serum. Sections and cells were incubated with horseradish peroxidase linked goat anti-rabbit secondary antibodies (Amersham Pharmacia Biotech, Freiburg, Germany) and ABC technique was used to visualize the labelling as described (38).

Materials

All compounds used were of highest available grade of purity from Sigma (Taufkirchen, Germany) or Merck (Darmstadt, Germany). All cell culture reagents were from GIBCO/Invitrogen (Karlsruhe, Germany) except Airway Epithelial Cell Growth Medium (AECGM) and SupplementMix that were from PROMOCell/Bioscience alive (Heidelberg, Germany).

Statistical analysis

Student's t-test (for paired or unpaired samples as appropriate) was used for statistical analysis of the data. $P<0.05$ was accepted as significant.

Results

Expression of bestrophins and Ca^{2+} activated Cl^- currents in mouse trachea

Expression of all three bestrophin paralogs was detected in tracheas of wt (vmd2+/+) mice by RT-PCR, Western blotting, and immunohistochemistry, whereas best1-KO (vmd2-/-) mice

lack of best1 expression (Fig. 1). Notably, best2-protein was expressed at much higher levels than best1-protein (Fig. 1B). Accordingly mRNA for best2 was about 100 times more abundant than that for best1 as detected by real-time PCR. However, the absence of best1 expression in tracheas of best1-KO animals was paralleled by reduced expression of best2-protein.

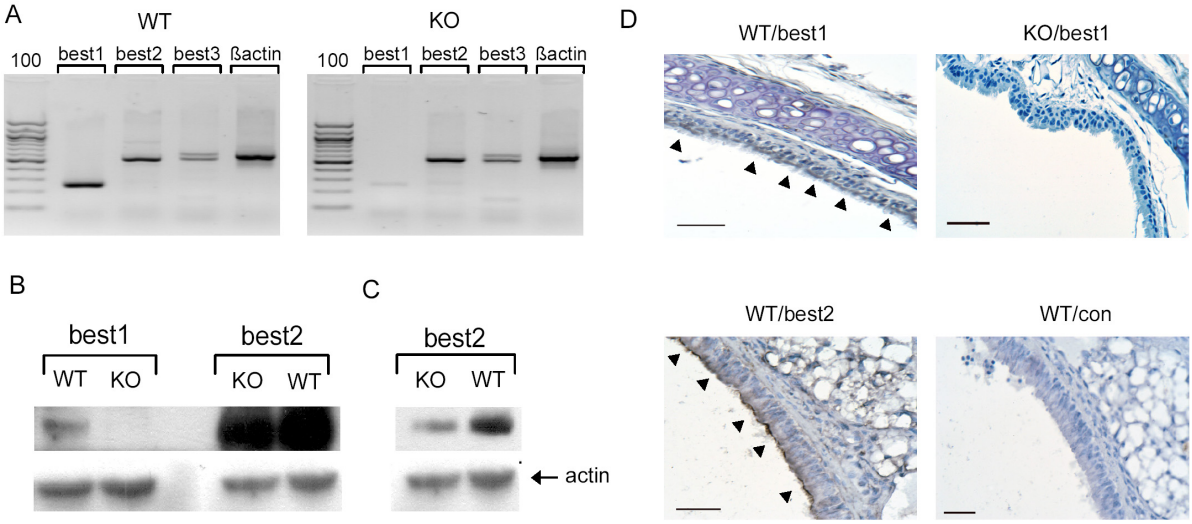

Fig. 1. Expression of bestrophins in tracheal epithelium. A) RT-PCR analysis of the 3 mouse isoforms of bestrophin (best1 - 3) in tracheas of wt (vmd2+/+) and best1-KO (vmd2-/-) mice. B) Expression of best1 and best2 protein in tracheal epithelial cells from wt (vmd2+/+) and best1-KO (vmd2-/-) mice. C) best2 protein in vmd2+/+ and vmd2-/- cells at lower exposure time demonstrates reduced expression of best2 in KO mice. D) Detection of best1 in wt but not in KO mice. Detection of best2 in airways of wt mice. Arrowheads indicate expression at the luminal side of the tracheal epithelium. Control for best2 was obtained without primary antibody and for best1 the primary antibody was added to vmd2-/- tissue. Scale bar 50µm.

The purinergic P2Y agonist ATP was used to activate Ca^{2+} dependent Cl^- secretion in Ussing chamber experiments. Luminal application of 1 µM ATP activated a transient short circuit current that was inhibited by the blocker of Ca^{2+} activated Cl^- channels, DIDS (200 µM). The peak response was reduced in best1-KO animals compared to wt mice (Fig. 2A,B). This subtle difference was only detectable at low ATP concentrations, but was masked at 10-100 µM ATP (Fig. 2C,D). Real time PCR analysis of the expression of relevant purinergic receptors indicated reduced expression of P2Y1, P2Y6, and A2B receptors in tracheas of best1-KO mice, however, expression of the most abundant receptor $P2Y_2$ was unchanged (Supplement 1). These results obtained in the intact tissue suggest a role of best1 for Ca^{2+} dependent Cl^- secretion in mouse airways.

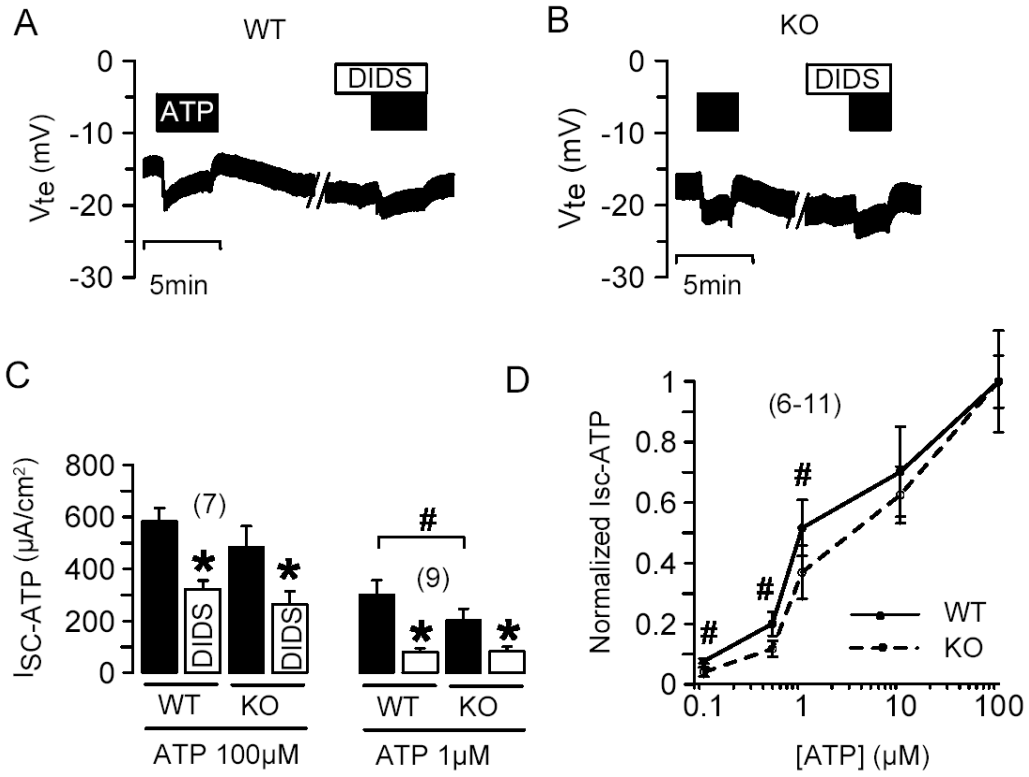

Fig. 2. Ca^{2+} activated Cl^- secretion in mouse trachea. Ussing chamber recordings of the transepithelial voltage (V_{te}) measured in mouse tracheas. Luminal application of 1 µM ATP induced a negative voltage deflection and a short circuit current in tracheas of wt (vmd2+/+) (A) and best1-KO (vmd2-/-) (B) mice. In both tissues the effect of ATP was partially inhibited by DIDS (100µM). C) Summary of the short circuit currents activated by 1 and 100 µM ATP and the effects of DIDS in both wt and best1-KO mice. D) Concentration- response curves for normalized short circuit currents (Isc_{ATP}) activated by ATP in vmd2+/+ and vmd2-/- mouse tracheas. # indicate significant difference between vmd2+/+ and vmd2-/- tracheas (unpaired Student´s *t*-test). * indicates significant effect of ATP and DIDS (paired Student´s *t*-test). (number of experiments).

Contribution of best1 and best2 to Ca^{2+}-activated Cl^- conductance in mouse airway cells

As Cl^- transport in intact tissues depends not only on the activity of Cl^- channels but also on other transport proteins we measured whole cell Cl^- conductances in primary short term cultures of mouse tracheal epithelial cells. A large Cl^- conductance was activated in wt (vmd2+/+) cells by maximal stimulation with ATP (100µM), and was inhibited by 200µM DIDS (Fig. 3A). In order to assess the individual contribution of best1 and best2 to Ca^{2+} activated Cl^- conductance, we used RNAi to silence individual bestrophins. It is shown that both best1-RNAi and best2-RNAi attenuated the ATP induced whole cell currents in mouse airway cells, while scrambled RNAi was without any effect (Fig.3A-C). Because of the low number of primary cells, we used immunocytochemistry to detect RNAi-silencing of best1 and best2 (Fig. 3D). Notably, most of the best1 and best2 protein is located in the cytosol, as reported

recently for other cell types (63). The corresponding i/v curves for the ATP activated whole cell current (Fig. 3E) were almost linear due to high $[Ca^{2+}]_i$ levels induced by 100 µM ATP (data not shown). The summary of the ATP-induced whole cell conductances indicated an approximate 50% inhibition for cells treated with either best1-RNAi or best2-RNAi (Fig. 3F).

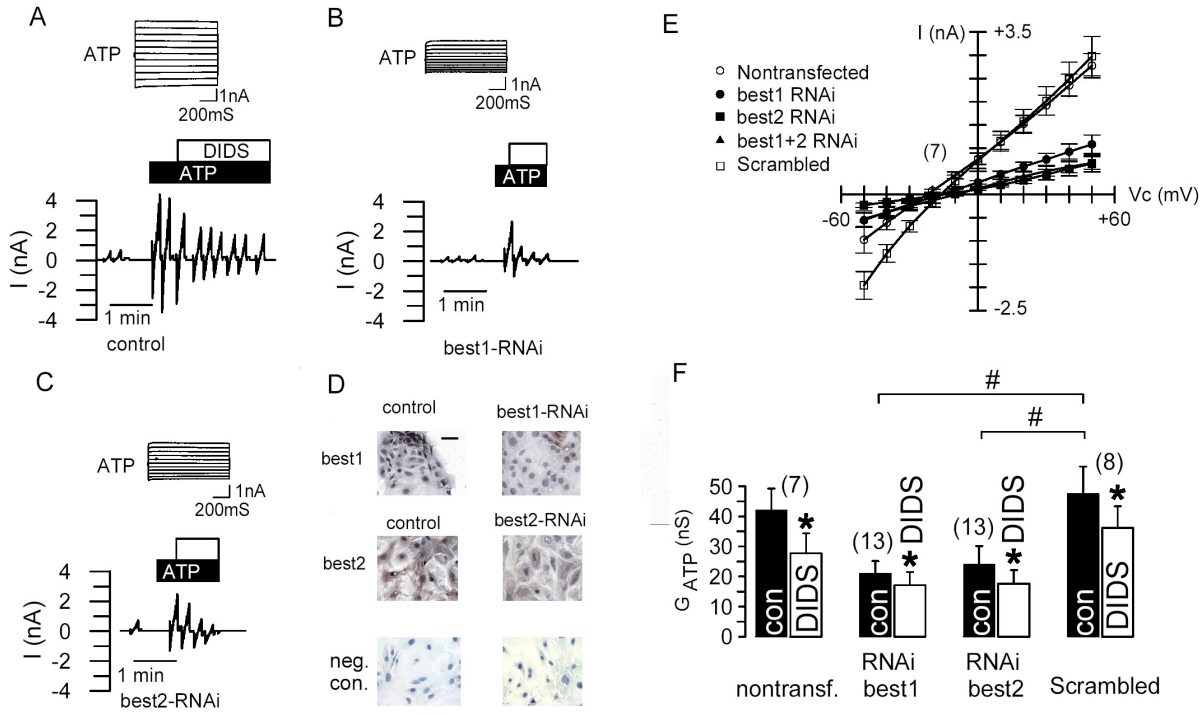

Fig. 3. Activation of endogenous CaCC in tracheal epithelial cells from vmd2+/+ mice. Activation of whole cell currents by ATP (100 µM) in primary tracheal epithelial cells from vmd2+/+ mice. Activation of whole cell currents in control cells (A), after incubation with best1-RNAi (B) or after incubation with best2-RNAi (C). D) Immunostaining of best1 and best2 in primary tracheal epithelial (control) cells and cells treated with best1-RNAi and best2-RNAi. Negative controls were obtained without primary antibody. E) Summary i/v curves for the ATP induced whole cell currents measured in control cells and in cells treated with best1-RNAi, best2-RNAi or scrambled RNAi, respectively. best1-RNAi. F) Summary of the ATP (100µM) induced whole cell Cl^- conductances in control cells and cells treated with best1-RNAi, best2-RNAi or scrambled RNAi, respectively. # indicate significant difference between cells treated with scrambled RNA or best1-RNAi and best2-RNAi, respectively (unpaired Student´s *t*-test). * indicates significant effect of DIDS (paired Student´s *t*-test). (number of experiments).

Moreover, when the Ca^{2+}-dependent Cl^- conductance was activated through muscarinic stimulation with carbachol (100 µM), attenuation of conductances was seen in cells treated with best1-RNAi or best2-RNAi, similar to that seen for ATP-dependent stimulation (Supplement 2).

Primary airway epithelial cells were also isolated form best1 KO (vmd2-/-) mice. ATP activated a whole cell Cl^- current in these cells that was partially blocked by DIDS (Fig. 4A). However, the Cl^- conductance activated by maximal stimulation with 100 µM ATP was attenuated to almost 50% of the conductance in wt cells (Fig. 4F). Knockdown of best2 by best2-RNAi further reduced the effect of ATP to about 20% of that observed in the wild type (Fig. 4B,F). In contrast, overexpression of mbest1 in cells from vmd2-/- animals enhanced the ATP conductance to nearly the same level found in wt (vmd2+/+) cells. The effects of best1-overexpression and best2-RNAi respectively, were verified by immunocytochemistry (Fig. 4E). Moreover, cholinergic Cl^- secretion by 100 µM carbachol was also significantly reduced in airway cells from vmd2-/- animals and was further attenuated after treatment with best2-RNAi (Supplement 2). These results further support the concept that both bestrophin 1 and 2 are essential for Ca^{2+} dependent Cl^- secretion in mouse airways.

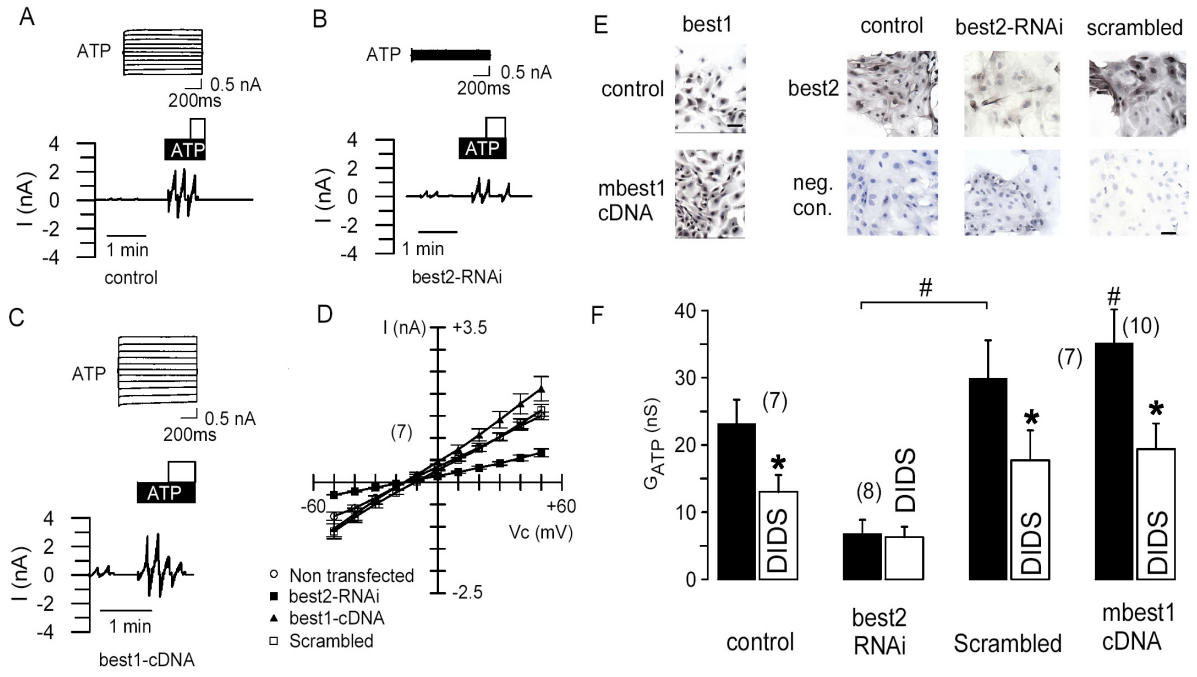

Fig. 4. Activation of endogenous CaCC in tracheal epithelial cells from vmd2-/- mice. Activation of whole cell currents by ATP (100 µM) in primary tracheal epithelial cells from vmd2-/- mice. Activation of whole cell currents in control cells (A), after incubation with best2-RNAi (B) or after overexpression of mbest1 (C). D) Summary i/v curves for the ATP induced whole cell currents measured in control cells and in cells treated with best2-RNAi or overexpressing mbest1. E) Immunostaining of best1 and best2 in primary tracheal epithelial (control) cells and cells treated with best2-RNAi or overexpressing mbest1. Negative controls were obtained without primary antibody. F) Summary of the ATP (100µM) induced whole cell Cl^- conductances in control cells and cells treated with best2-RNAi, scrambled RNAi, or overexpressing mbest1. # indicate significant difference between cells treated with scrambled RNA or best2-RNAi, respectively (unpaired Student´s *t*-test). * indicates significant effect of DIDS (paired Student´s *t*-test). (number of experiments).

Best1 may support Ca^{2+} signaling in airway epithelial cells

Stimulation by ATP leads to an initial release of Ca^{2+} from the endoplasmic reticulum through the phospholipase C / IP_3 pathway, which is followed by an extracellular Ca^{2+} influx through store-operated Ca^{2+} channels. We compared the time course of the whole cell Cl^- current activated by ATP and found that for vmd2+/+ cells (wt), an initial outwardly rectifying current (open squares) was followed by a linear current with a pronounced inward component (filled circles) (Fig. 5A). A linear i/v relationship of the Ca^{2+} activated Cl^- current suggests a high intracellular Ca^{2+} concentration in the close proximity of the Cl^- channel (65). When compared to wt cells, the i/v curve for the ATP activated Cl^- current in vmd2-/- cells (KO) was slightly more outwardly rectifying, and did not show a pronounced inward component (Fig 5B). This may indicate a lower intracellular Ca^{2+} concentration close to the Cl^- channel in vmd2-/- cells, and may therefore suggest a role of best1 for regulation of Ca^{2+} influx pathways, as suggested in earlier reports (77;115).

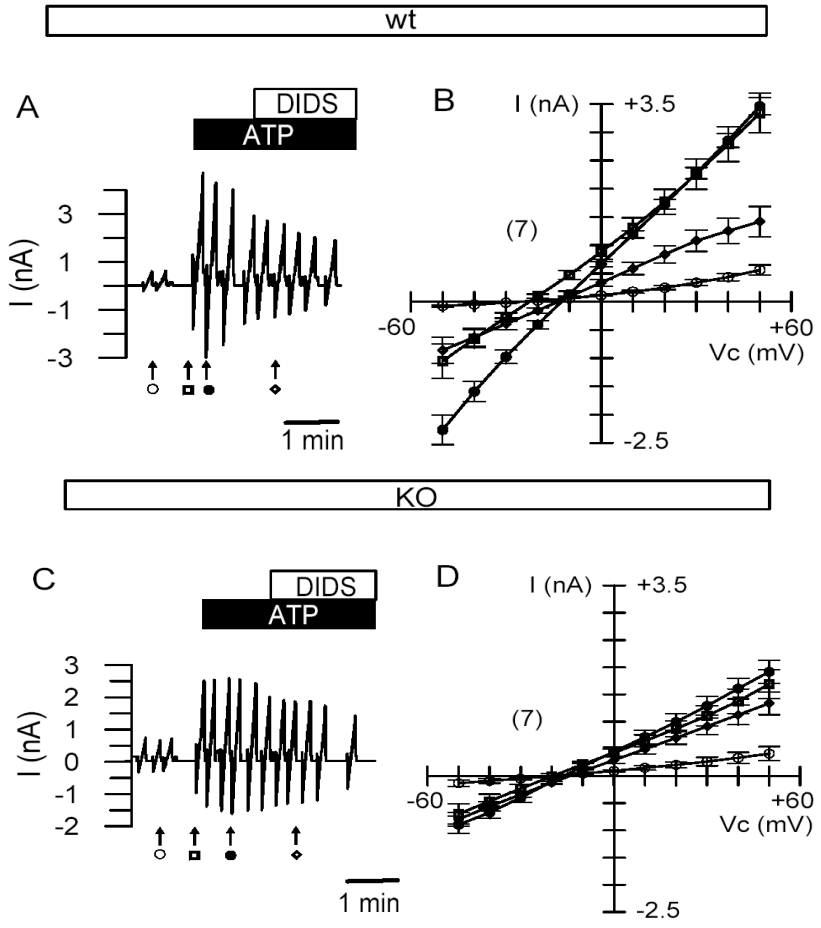

Fig. 5. Activation of Ca^{2+} dependent Cl^- currents in tracheal cells from vmd2+/+ (wt) mice and vmd2-/- (KO) mice. A) Activation of whole cell currents by 100 µM ATP and inhibition by DIDS. B) Current-voltage (i/v) relationships were obtained before stimulation (○), at the initial phase after stimulation with ATP (◘), 10s after initial activation (●), and after inhibition by DIDS (◊). (number of experiments).

These differences were not observed when Cl^- currents were activated directly by high intracellular Ca^{2+} concentrations (1 µM; open square) through the patch pipette filling solution in whole cell patch clamp experiments (Fig. 6). Here 1 µM Ca^{2+} activated linear Cl^- currents in both vmd2+/+ (wt) and vmd2-/- (KO) cells, while 0.1 µM Ca^{2+} activated an outwardly rectifying Cl^- current in both cell types (Fig. 6). However, the magnitude of the Cl^- current was reduced in vmd2-/- cells. Notably, higher Ca^{2+} concentrations (10 µM) induced a rundown of the Ca^{2+} activated Cl^- current, a phenomenon that has been described earlier (110). At any rate, the magnitude of the Cl^- current was reduced in vmd2-/- cells and thus bestrophins may have both functions that of a Ca^{2+} activated Cl^- channel and a regulator of Ca^{2+} channels.

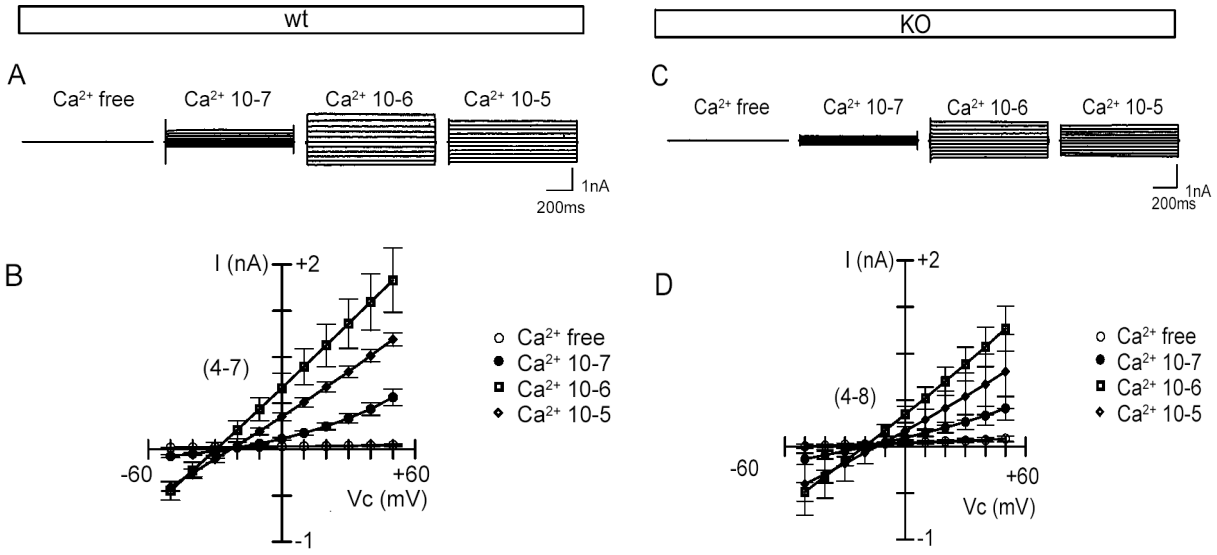

Fig. 6. Direct activation of Ca^{2+} dependent Cl^- currents by intracellular Ca^{2+} in tracheal cells from vmd2+/+ (wt) mice and vmd2-/- (KO) mice. Activation of whole cell currents in vmd2+/+ cells by different concentrations of intracellular Ca^{2+} (A) and corresponding current-voltage (i/v) relationships (B). Activation of whole cell currents in vmd2-/- cells by different concentrations of intracellular Ca^{2+} (C) and corresponding current-voltage (i/v) relationships (D). Note that Ca^{2+} concentrations higher than 1 µM have an inhibitory effect. (number of experiments).

Discussion

The present data reveal that both best1 and best2 are components of the endogenous Ca^{2+} activated Cl^- current in the mouse respiratory epithelium. Western blot analysis and immunohistochemistry revealed low expression levels for best1 in mouse trachea, which were substantially higher for best2. Negative stainings for best1 and missing detection of best1 in Western blots from in vmd2-/- tracheas, indicates the specificity of our best1 antibody. As best1 expression is low in mouse trachea, it is difficult to say whether the

protein is expressed in the luminal membrane or in a compartment close to the membrane. The situation is somewhat different for best2, which is expressed in mouse airways at much higher mRNA and protein levels. It appears to be localized within the luminal membrane. Membrane staining of best2 was also reported in cilia of mouse olfactory sensory neurons (98). Moreover, recently best2 was proposed to be the Ca^{2+} activated Cl^- channel in salivary glands (86).

We examined preferentially the role of best1 and best2 for purinergic stimulation of Cl^- secretion, since this pathway is most important for the mucociliary clearance of the airways particularly in mice, since they express only low levels of CFTR Cl^- channels (66). As $P2Y_2$ is the most abundant receptor, 85 % of the ATP stimulated Cl^- secretion is lost in $P2Y_2$ deficient mice (19). Since expression of $P2Y_2$ is unchanged in tracheas of vmd2-/- mice it is unlikely that the reduced Ca^{2+} activated Cl^- currents in airway cells of these animals is due to reduced expression of $P2Y_1$, $P2Y_6$ or A2B receptors (Supplement 2). Physiological ATP concentrations in the airway surface liquid probably never exceed 1 µM (91). At this concentration and below, a difference was found between wt and best1-KO animals even in Ussing chamber experiments. In the more quantitative whole cell patch clamp measurements on primary tracheal epithelial cells, the present data disclosed a remarkable difference in the magnitude and characteristic of the ATP activated Cl^- current between wt and best1-KO mice. The results support the previous finding that best1 enables Ca^{2+} dependent Cl^- secretion in mouse airways (11) and supply initial hints that best1 has a role for the Ca^{2+} regulation of the Cl^- channel. Since both Ca^{2+} signaling, i.e. regulation of Ca^{2+} influx and activation of Cl^- currents are intimately connected, it is difficult to examine both putative functions of best1 separately. Along this line it should be noted that compartmentalized Ca^{2+} signaling matters for channel regulation rather than cytosolic Ca^{2+} concentration (146). Subsequent research will need to focus on the putative role of bestrophins for spatio-temporal Ca^{2+} signaling and its role for regulation of Cl^- secretion.

The rather weak expression of best1 along with the fact that best1-KO animals have no obvious disease-phenotype asks for the importance of this protein. Although best2 is expressed more dominantly, both best1 and best2 clearly contribute to the Ca^{2+} activated, i.e. ATP-induced Cl^- conductance in mouse airways. Ongoing studies along with a previous report (130) show that both proteins interact with each other. Interestingly, the present results also show that expression of best2-protein is reduced in best1-KO animals, and also best3-mRNA expression detected by real-time PCR was found to be reduced in vmd2-/- animals (data not shown). This suggests some sort of co-regulation of bestrophin proteins and it will be interesting to study double-knockout animals in the near future (48). In this context it is

probably necessary to understand purinergic receptors, intracellular Ca^{2+} signals, the role of bestrophins and the Cl^- conductance as a functional unit.

Supplement material

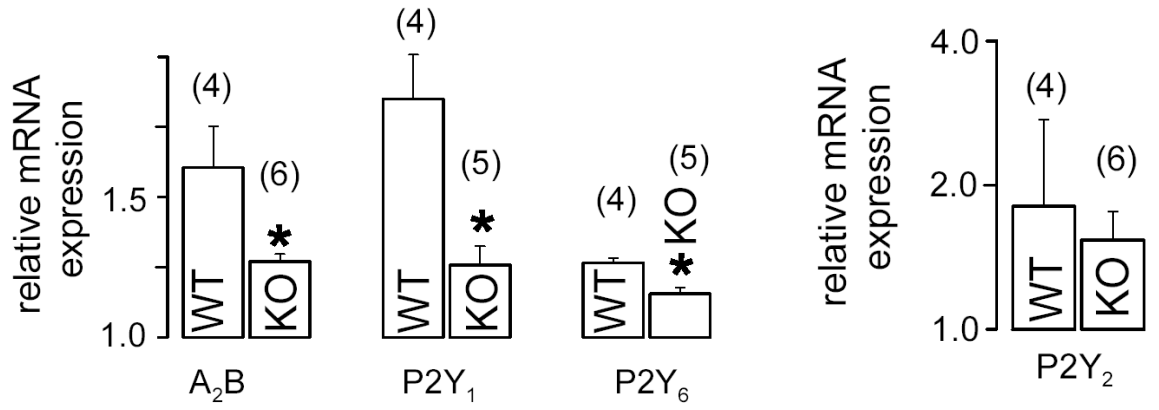

Supplement 1. Wt and KO relative mRNA expression. Relative expression of mRNA for purinergic receptor subtypes in wt (vmd2+/+) and KO (vmd2-/-) animals assessed by real-time PCR.

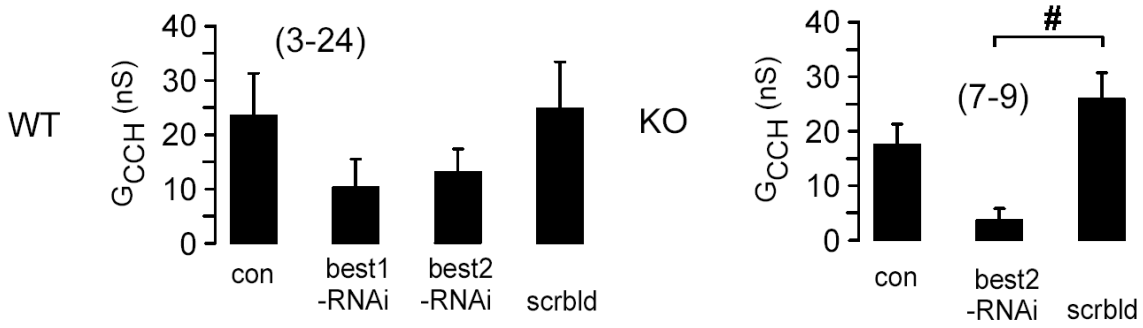

Supplement 2. Summary of the carbachol (CCH; 100 µM) activated whole cell Cl^- conductances of tracheal epithelial cells of wt (vmd2+/+) and KO (vmd2-/-) animals. Cells were examined as non-treated control cells and after treatment with best1-RNAi or best2-RNAi or scrambled RNAi.

Chapter 4

Functional assembly and purinergic activation of bestrophins

Abstract

Proteins of the bestrophin family produce Ca^{2+} activated Cl^- currents and may regulate voltage gated Ca^{2+} channels. Bestrophin 1 was first identified in the retinal pigment epithelium, but was later also found in other epithelial tissues such as testis, airways, and various epithelial cell lines, where it contributes to Ca^{2+} activated Cl^- transport. Four human paralogs (hbest1 - hbest4) exist and for some dimeric and heterotetrameric structures have been proposed. Here we demonstrate that hbest1 – hbest4 induce Cl^- conductances of very different amplitudes upon expression in HEK293 cells. They also respond differently to stimulation with the purinergic P2Y agonist ATP. Mutant forms of hbest1 that are known to cause autosomal dominant macular dystrophy (Best disease), did not produce a Cl^- current. Molecular and functional interaction and colocalization of bestrophins was detected in HEK293 cells overexpressing hbest1 and hbest2 or hbest4, and was also found in airway epithelial cells expressing endogenous bestrophins. Membrane expression was clearly detectable for hbest2 and hbest4, but was weak for hbest1. However, hbest1 appears necessary for ATP-induced Cl^- currents in both HEK293 and Calu-3 cells. Changes in ATP induced intracellular Ca^{2+} signaling were not observed upon expression of bestrophins. Since native epithelial tissues typically express several bestrophin paralogs, these proteins may exist as heterooligomeric structures.

Introduction

Ca^{2+} activated Cl^- channels (CaCC) are expressed in nearly all cell types (46). Ca^{2+} activated whole cell currents have been analyzed in many tissues but the molecular identity of CaCC in epithelial tissues is unclear (52;87). In most tissues CaCC have small single channel conductances and produce outwardly rectifying Cl^- currents at moderate intracellular Ca^{2+} levels. Activation of CaCC occurs through direct Ca^{2+} binding and Ca^{2+} dependent phosphorylation by calmodulin dependent kinase II (87;147). The channel is inactivated by inositol 3,4,5,6-tetrakisphosphate, which is a downstream metabolic product of the inositol trisphosphate (IP_3) pathway (50). Recently identified small-molecule inhibitors of CaCC may overcome the disadvantages of fairly nonspecific compounds such as 4,4'-diisothiocyanatostilbene-2,2'-disulfonic acid (DIDS) and niflumic acid (NFA), which have been used in the past to inhibit CaCC (22;28).

Previously suggested molecular candidates for CaCC produced conflicting data (20;94). CLCA proteins have been shown to produce a Ca^{2+} activated chloride conductance in epithelia, however they also function as cell adhesion proteins, promote apoptosis and may even control cell cycling. It is not unlikely that CLCA proteins are part of a higher Cl^- channel complex (70). CLC-3 was also suggested to form CaCC. Although CLC-3 is regulated by CaMKII, it appears to operate as an endosomal Cl^- channel. Moreover, the fact that CLC-3 knockout mice still produce Ca^{2+}-activated Cl^- currents makes it an unlikely candidate for CaCC (52)

In contrast, several reports support the role of bestrophin 1 (best1), the product of the vitelliform macular dystrophy (VMD2) gene, as a Ca^{2+} activated Cl^- channel (110;130;151). Mutations in the VMD2 gene cause early-onset autosomal dominant macular dystrophy of the retina, the so called Best disease (97). Initial studies detected this channel in the basolateral membrane of the retinal pigment epithelium (RPE) (75). Although early reports claimed exclusive expression of best1 in the RPE, later studies identified best1 in a number of epithelial tissues and in neuronal cells (1;11;27;48;126). Other studies arrived at the conclusion that best1 regulates voltage gated Ca^{2+} channels (77;115). Here we examined if human paralogs of bestrophin (hbest1-hbest4) enable secretagogue activation of Ca^{2+} activated Cl^- transport. We used ATP as a ligand for purinergic P2Y receptors. These receptors, in particular the subtype $P2Y_2$, are most important for activation of Ca^{2+} dependent Cl^- secretion in airways (11;19;85;119). In fact all bestrophins induced Cl^- conductances with different functional properties and are able to form heterooligomers. The data support the role of bestrophins for Ca^{2+} activated Cl^- transport in epithelial tissues (11).

Material and Methods

Cell culture, cDNAs, transfection

HEK-293 and Calu-3 cells were cultured as described elsewhere (11;16). Fisher rat thyroid cells were cultured in DMEM-F12 medium, supplemented with 10% FCS, 100.000 units/l penicillin, and 100 mg/l streptomycin. cDNA constructs of human bestrophin 1 to 4 (VMD2, VMD2L1, VMD2L3, VMD2L2) were kindly provided by Dr. J. Nathans (Johns Hopkins University, Baltimore, USA). Human bestrophin 1 and $P2Y_2$ receptors were His_6-tagged at the C-terminus. Human bestrophin 4 was Flag-tagged at the C-terminus by PCR, using primers 3´- GGGCCTTGTACGCTGTGC-5´ and 3`-ATTCCCGGGTCACTTATCGTCGTCATCCTTGTAATCGGGCTCCAGGGCCTCGTCC-5´.
Site specific mutations (D301E, R218C) were introduced into human bestrophin 1 using QuickChange™ (Stratagene, Heidelberg, Germany). The EYFP-I152L plasmid was kindly provided by Dr. A. Verkman (UCSF, San Francisco, USA). All cDNAs were verified by sequencing. They were transfected into HEK293 or FRT cells (lipofectamine, Invitrogen, Karlsruhe, Germany). All experiments were performed 48 hours after the transfection.

Western blotting and antibodies

Protein was isolated from HEK293 and Calu-3 cells and mouse colonic crypts in a buffer containing 150 mmol NaCl, 50 mmol Tris, 100 mmol DTT, 1% NP-40, and 1% protease inhibitor cocktail (Sigma, Taufkirchen, Germany). Equal amounts of total protein (20 µg) were separated by 7% SDS-PAGE and Western blots were performed as described previously (11). The peptides KDHMDPYWALENRDEAHS and PAPPWLPSPIGEEEE containing amino acids 568-585 and 492–506 of human bestrophin 1 and 2, respectively, were used to generate affinity-purified rabbit polyclonal antibodies (Davids Biotech, Regensburg, Germany). The hbest-4 antibody was from Abcam (Cambridge, UK).

Immunoprecipitation

Prior to addition of 1-5 µg of the primary antibody, lysates were pre-cleared with protein A/G agarose beads (Pierce, Rockford, USA). Pre-cleared protein lysates were incubated overnight at 4°C with primary antibodies, and the protein-antibody complex was immobilized by addition of 25 µl protein A/G agarose beads. The beads were washed three times in lysis buffer (1 % TX-100, 10 % glycerol, 1 x PBS pH 7.4), boiled in 1 x Laemmli sample buffer and proteins were analyzed by SDS-PAGE and immunoblotting.

Immunohistochemistry and confocal microscopy

Transfected HEK-293 cells were grown on glass cover slips and fixed for 10 min at room temperature with 4 % (w/v) para-formaldehyde. After washing, cells were permeabilized with blocking/permeabilization solution (10 % (v/v) goat serum, 0.5 % (v/v) triton X-100 in 1x PBS) for 30 min and labeled for 1 hour with primary (1:1000) and secondary antibodies (1:1000, conjugated with Alexa 488 and Alexa 594, Invitrogen). Nuclei were labeled with Hoe33342 (Aplichem, Darmstadt, Germany) at a final concentration of 0.1 µg/ml in 1x PBS. Cellular compartments were labelled with: (lysosomes) rat anti-mouse LAMP1 (ID4B; Developmental Hybridoma Bank, University of Iowa), (Golgi) mouse monoclonal anti-Golgi 58 kDa protein antibody (a generous gift of Dr. M. Amaral), (mitochondria) mouse monoclonal anti MTCO1 antibody (Abcam, Cambridge, UK), (endoplasmic reticulum) rabbit polyclonal anti-calreticulin antibody (a generous gift of Dr. Ralph Witzgall, Regensburg, Germany). Cells were mounted on a confocal matrix (Micro Tech Lab, Graz, Austria) and examined with an Axioskop (Zeiss, Göttingen, Germany) fluorescence microscope. Confocal images were quantitatively analyzed using an image software package. Pearson´s correlation coefficient (PCC) was employed to evaluate colocalization.

Measurement of the intracellular Ca^{2+} concentration and iodide quenching

HEK293 cells were loaded with 2 µM Fura-2 AM and intracellular Ca^{2+} concentrations were measured as described previously (123). YFP_{I152L} fluorescence was excited (wave length 500 nm) using a polychromatic illumination system for microscopic fluorescence measurements (VisiChrome, Germany) and light emission was measured at 535 ± 15 nm with a photomultiplier detector (SF, Zeiss). Quenching of YFP_{I152L} fluorescence by I^- influx was induced by replacing 20 mM extracellular Cl^- by I^-.

Ussing chamber and patch clamp

FRT cells grown on permeable supports (Millipore, Schwalbach, Germany) were mounted into a perfused micro Ussing chamber. Apical and basolateral surfaces of the epithelium were perfused continuously with Ringer solution at a rate of 5 - 10 ml/min (chamber volume 2 ml). All experiments were carried out at 37 °C under open circuit conditions (11). Transepithelial resistances (R_{te}) were determined by applying short (1 s) current pulses (I = 0.5 µA) and recording of corresponding changes in the transepithelial voltage (V_{te}). The equivalent short-circuit current (I_{sc}) was calculated according to Ohm's law from V_{te} and R_{te} ($I_{sc} = V_{te} / R_{te}$). For patch clamp experiments, cover slips were mounted on the stage of an inverted microscope (IM35, Zeiss, Göttingen, Germany), kept at 37 °C and perfused continuously with Ringer solution. Experiments were performed in fast and slow whole cell configurations as described previously (11).

Materials and statistical analysis

All compounds used were of highest available grade of purity and were from Sigma (Taufkirchen, Germany) or Merck (Darmstadt, Germany). All cell culture reagents were from Invitrogen. Student's t-test (for paired or unpaired samples as appropriate) and analysis of variance (ANOVA) was used for statistical analysis. P values < 0.05 were accepted as significant.

Results

Anion conductances induced by expression of bestrophins

Bestrophin paralogs were coexpressed individually together with YFP_{I152L} in HEK293 cells and anion conductances was assessed by iodide uptake, which induced quenching of YFP_{I152L} fluorescence (37). To that end 20 mM Cl^- was isotonically replaced by I^- in the absence or presence of 100 µM ATP, which was used as a purinergic receptor agonist to raise intracellular Ca^{2+} levels (11). HEK293 cells express only low levels of endogenous hbest1 and unrelated Cl^- channels (not shown). Therefore ATP only marginally increased quenching in control (YFP) cells (Fig. 1). Expression of both hbest2 and hbest4 enhanced baseline anion conductances in HEK293 cells, while expression of the disease causing mutant hbest1-R218C suppressed the baseline anion conductance (Fig. 1B). Similar was observed for another disease causing mutant, hbest1-D301E (n = 20, data not shown). ATP further enhanced anion conductances in cell expressing hbest1 and hbest3, but did not further increase the large baseline Cl^- conductance found in hbest2 and hbest4 expressing cells. Activation of hbest1 by ATP was not augmented by coexpression of $P2Y_2$-receptors (Supplement 3). Taken together, the human bestrophins 1 - 4 produce anion conductances that show remarkable differences in size and coupling to purinergic stimulation. The fact that hbest1 is necessary to induce ATP-activated Cl^- currents in HEK293 cells, fully complies with previous results obtained in native epithelial tissues (11).

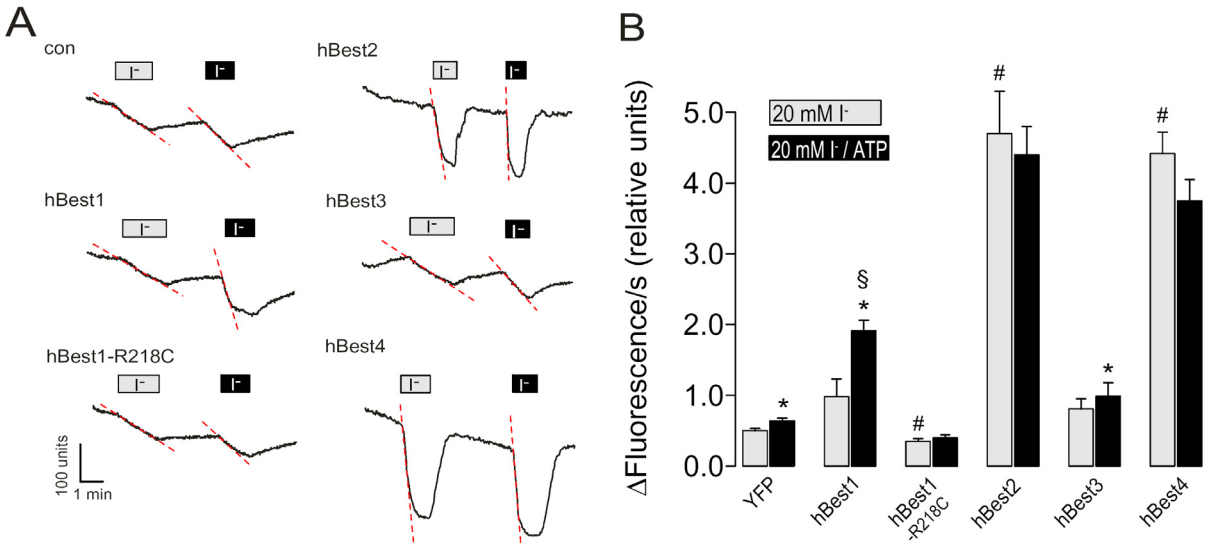

Fig. 1. Purinergic activation of bestrophins. A) Recordings of YFP_{I152L} fluorescence (arbitrary units) in hBest transfected HEK293 cells. Fluorescence quenching was induced by isotonic application of 20 mM I^- in the absence (grey box) or presence (black box) of 100 µM ATP. B) Summary of I^- induced fluorescence quenching in hbest expressing cells. * significant increase by ATP (paired Student´s t-test). # significant difference when compared to YFP (ANOVA). § significantly enhanced effect of ATP when compared to YFP. Number of experiments = 36 - 136.

To further confirm these results, bestrophins were examined in whole cell patch clamp experiments with HEK293 cells, before and after stimulation with ATP. Expression of both hbest1 and hbest3 induced ATP activated Cl^- currents, which were only of small amplitude in case of hbest3 (Fig. 2). As shown in the quenching experiments (Fig. 1), hbest2 and hbest4 induced a high baseline Cl^- conductance that was not further enhanced by ATP. Similar results were obtained when cells were exposed to the Ca^{2+} ionophore ionomycin (1 µM), or when experiments were performed in the slow whole cell configuration (Fig. 2E). Except for hbest4 expressing cells, which had a rather depolarized membrane voltage (Vm) due to large Cl^- currents, Vm of HEK293 cells was depolarized upon stimulation with ATP. Replacement of 140 mmol bath Cl^- by gluconate ($5Cl^-$) inhibited whole cell currents and shifted I/V curves to more depolarized clamp voltages after stimulation with ATP (hbest1) or in non-stimulated cells (hbest4) (Fig. 2C,D). Both Cl^- conductances induced by hbest1 and hbest4 were inhibited by 100 µM DIDS, similar to endogenous Ca^{2+} activated Cl^- conductances in epithelial cells (Fig. 2F).

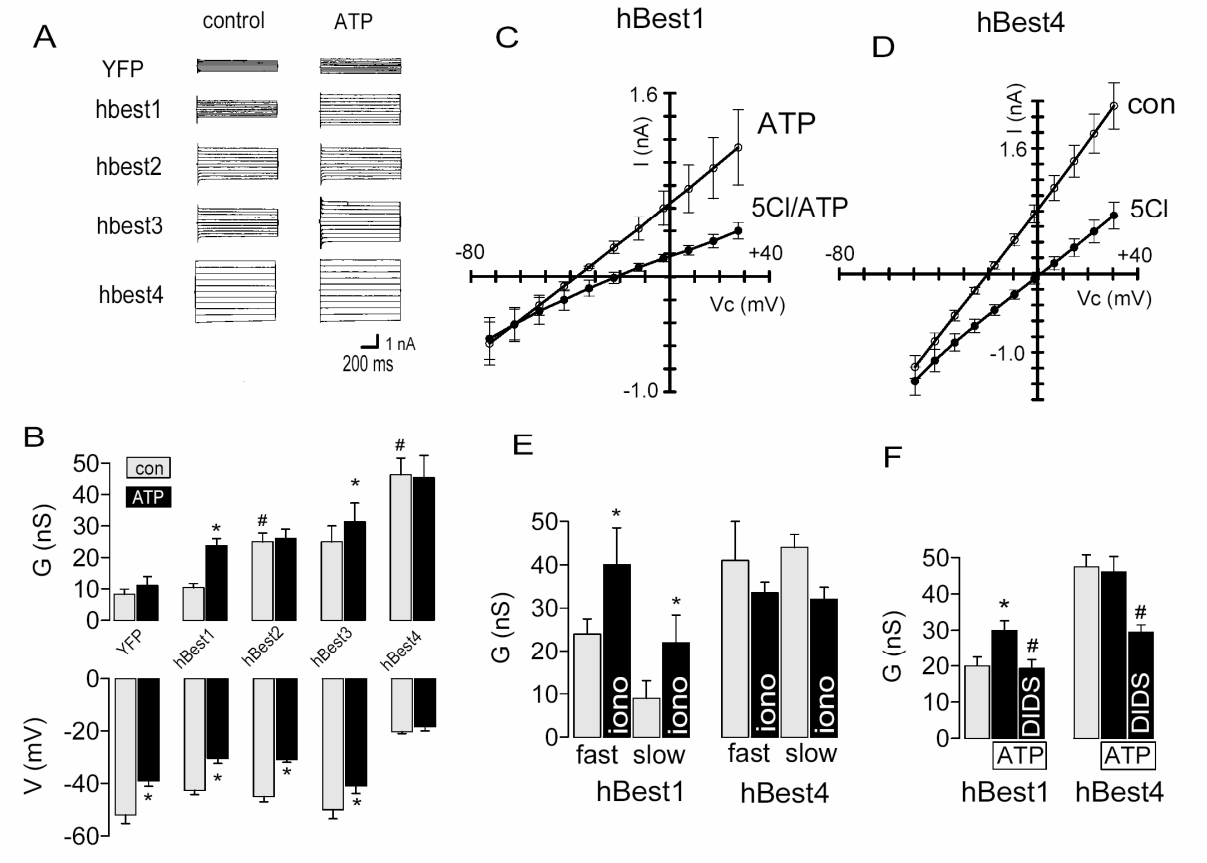

Fig. 2. Bestrophins induce whole cell Cl^- conductances. A) Whole cell currents in hbest expressing HEK293 cells before and after stimulation with ATP (100 µM) as measured by voltage clamping from -60 to +40 mV. B) Summary of the calculated whole cell conductances and membrane voltages measured in HEK293 cells. C) Summary I/V curve for hbest1 expressing HEK293 cells after stimulation with ATP and shift of the I/V curve by replacement of extracellular Cl^- by gluconate (5Cl). D) Summary I/V curve for hbest4 expressing HEK293 cells without ATP- stimulation and shift of the I/V curve by replacement of extracellular Cl^- by gluconate (5Cl). E) Summary of the whole cell conductances for hbest1 and hbest4 when cells were exposed to the Ca^{2+} ionophore ionomycin (1 µM) in the fast or slow whole cell configuration. F) Summary of the ATP (100 µM)-induced whole cell Cl^- conductances for hbest1 and hbest4 expressing HEK293 cells and inhibition by DIDS (100 µM). * significant increase by ATP (paired Student´s *t*-test). # significant difference when compared to YFP (ANOVA). § significantly enhanced effect of ATP when compared to YFP. Number of experiments = 9 - 44.

Functional interference of bestrophin paralogs

Single expression of either hbest2 or hbest4 induced a pronounced anion conductance that was, however, not further enhanced by stimulation with ATP. When coexpressed with hbest1 or hbest3, baseline anion conductances generated by hbest2 or hbest4 were significantly inhibited (Fig. 3). Thus bestrophin paralogs may interact with each other and probably form heterooligomers.

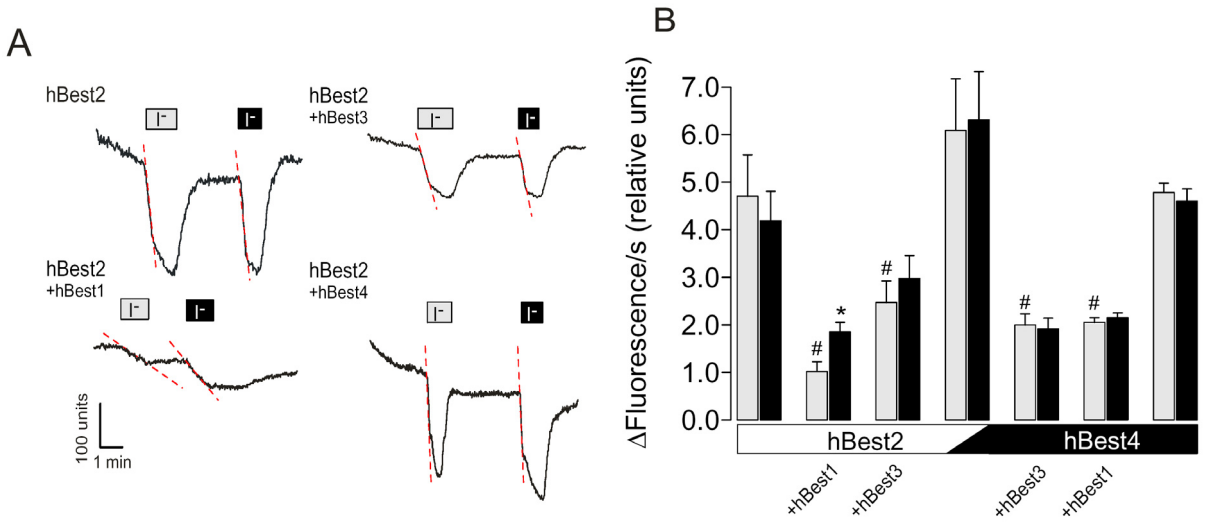

Fig. 3. Coexpression of human bestrophins. A) Recordings of YFP_{I152L} fluorescence (arbitrary units) in hbest2 transfected HEK293 cells coexpressing hbest1, hbest3 or hbest4. Fluorescence quenching was induced by isotonic application of 20 mM I^- in the absence (grey box) or presence (black box) of 100 µM ATP. B) Summary of I^- induced fluorescence quenching in HEK293 cells expressing hbest2 or hbest4 or coexpressing two different bestrophins. * significant increase by ATP (paired Student´s *t*-test). # significant difference when compared to YFP (ANOVA). § significantly enhanced effect of ATP when compared to YFP. Number of experiments = 19 - 39.

Inhibition of hbest2 and hbest4 Cl^- currents was also found by coexpression with disease-causing mutants such as hbest1-R18C or hbest1-D301E (Supplement 1). Interestingly coexpression with mouse best1 did not reduce iodide quenching by hbest4 (4.8 ± 0.29 vs. 3.8 ± 0.22; n = 39), suggesting poor oligomerization of human and mouse bestrophins.

Functional interference of bestrophins was also observed in patch clamp experiments. ATP (100 µM) induced whole cell conductances in hbest1-expressing HEK293 cells were reduced by coexpression with hbest2 or hbest4 (Fig. 4A). These results are further supported by experiments with Fisher rat thyroid (FRT) cells expressing human bestrophins. Filter grown FRT cells were permeabilized basolaterally with nystatin (50 µg/ml). A luminal Cl^- conductance was activated by ATP in FRT cells expressing hbest1, but not in cells coexpressing hbest2 or hbest4 (Fig. 4B). Thus bestrophin paralogs are functionally different and are likely to interact heterologously and probably in native cells (48;80).

It has been suggested that bestrophin 1 regulates voltage gated Ca^{2+} channels in RPE cells (77;115). Because bestrophins may induce Cl^- conductance by controlling intracellular Ca^{2+} levels, we examined potential effects of hbest1-hbest4 on intracellular Ca^{2+} signaling, induced by stimulation of purinergic receptors. As shown in the inset of Fig. 4C, 100 µM ATP

caused peak and plateau Ca^{2+} increase in YFP expressing (control) HEK293 cells. While the peak resembles Ca^{2+} release from the endoplasmic reticulum, the plateau is caused by Ca^{2+} influx through store operated Ca^{2+} channels. However, neither store release nor Ca^{2+} influx appeared to be affected by expression of bestrophins (Fig. 4C). Similar results were obtained for cells expressing mutant hbest1-D301E (data not shown). Thus human bestrophins don't appear to change receptor mediated Ca^{2+} signaling in HEK293 cells. Moreover, high baseline Cl^- conductances observed for hbest2 and hbest4 in non-stimulated HEK293 cells are not caused by an increase in basal cytosolic Ca^{2+} levels.

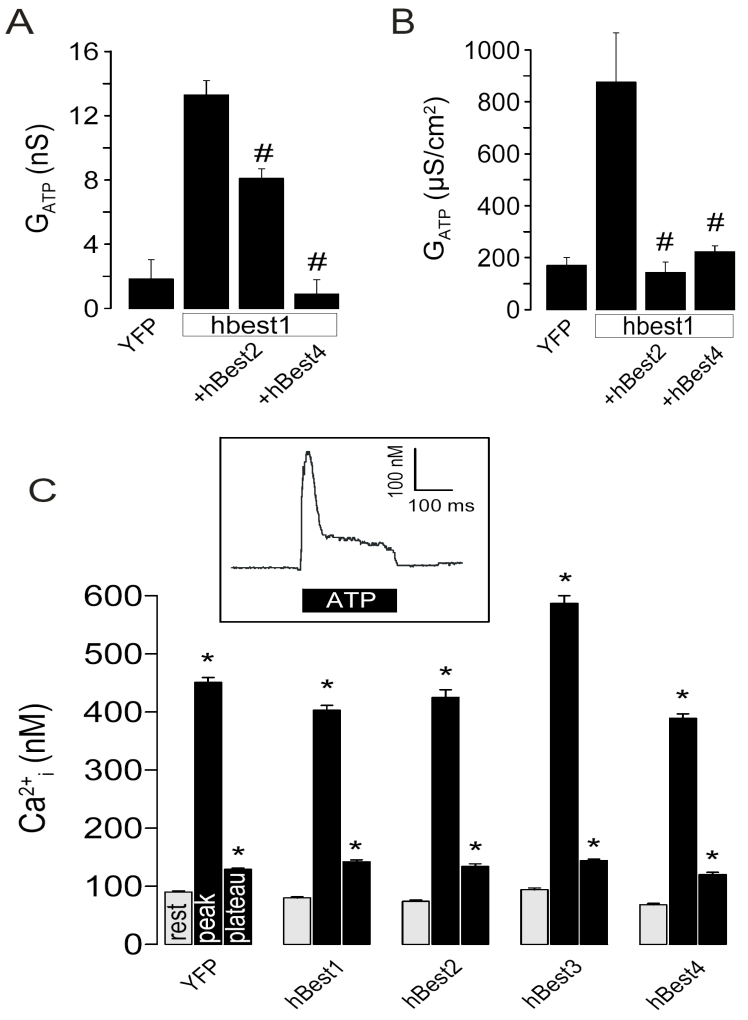

Fig. 4. Coexpression of bestrophins and effect on Ca^{2+} signalling. A) Summary of Ca^{2+}- (100 µM ATP) induced whole cell conductances in HEK293 cells expressing hbest1 or coexpressing two bestrophins (n = 10 – 44). B) Summary of ATP induced conductances in basolaterally permeabilized FRT-cell monolayers expressing hbest1 or coexpressing two bestrophins (n = 5 – 6). C) Intracellular Ca^{2+} concentrations ($[Ca^{2+}]_i$) in bestrophin- expressing HEK293 cells. $[Ca^{2+}]_i$ was determined under resting conditions (rest) and peak and plateau increase were observed after stimulation with ATP (insert) (n = 47 – 121). * significant effect of ATP when compared to resting Ca^{2+} (paired Student´s *t*-test).

Molecular interaction of bestrophins

We explored cellular colocalization of human bestrophins in HEK293 cells by cotransfection of His-tagged hbest1 together with hbest2 or Flag-tagged hbest4, using immunocytochemistry and confocal microscopy. Tagged bestrophins produced anion conductances and demonstrated functional interference similar to the non-tagged proteins (Supplement 1). Immunocytochemistry suggested cellular colocalization of hbest1/hbest2, hbest1/hbest4 and hbest2/hbest4 (Fig. 5A-C). Pearson´s co-localization coefficients were assessed using quantitative confocal microscopy. High coefficience was detected for hbest1/hbest2 (92 %), hbest1/hbest4 (93 %) and hbest2/hbest4 (93 %), In contrast hbest1 and $P2Y_2$ receptors colocalized only weakly (21 %), and therefore poor membrane expression was found for hbest1 (Fig. 5D). In contrast to hbest1, hbest2, hbest4 and mbest2 (Supplement 2) are clearly membrane localized.

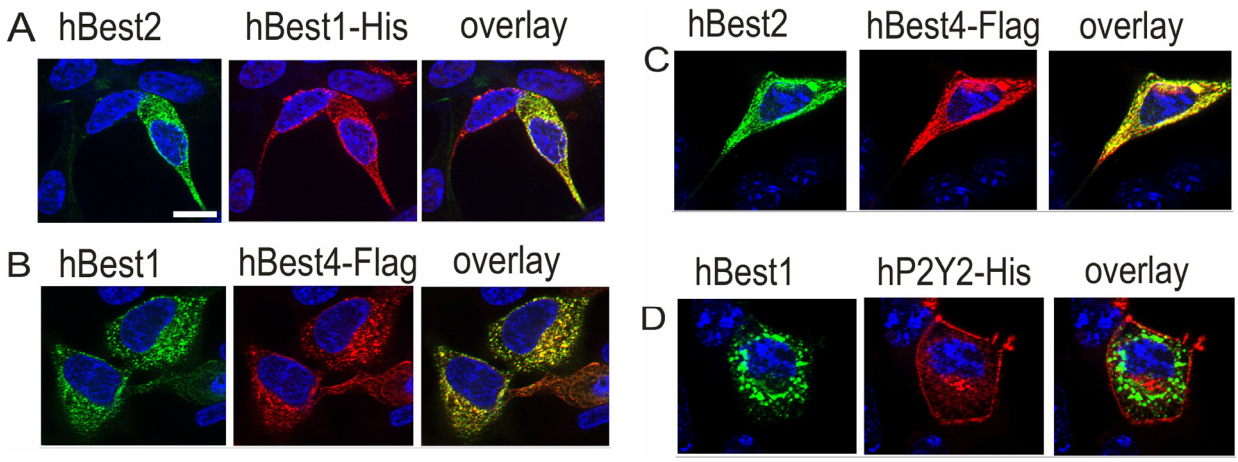

Fig. 5. hbest1/hbest2 and hbest1/hbest4 are colocalized. Using anti-hbest1, anti-hbest2, anti-His and anti-Flag antibodies, immunohistochemistry indicated a cellular colocalization of hbest1-His/hbest2 (A), hbest1/hbest4-Flag (B) and hbest2/hbest4-Flag (C), while hbest1 and coexpressed His-tagged $P2Y_2$ receptor did not colocalize (D). Bar indicates 20 µm. Experiments were performed at least in triplicates.

Different to recombinant hbest1 in HEK293 cells, endogenous best1 in porcine RPE is located close to or within the basolateral plasma membrane, as judged from confocal images (Fig. 6A). We examined whether hbest1 is localized in a particular intracellular compartment in HEK293 cells. We co-stained hbest1 and different intracellular compartments such as lysosomes, endoplasmic reticulum, Golgi or mitochondria. Confocal microscopy suggested localization of hbest1 in the ER but not in any of the other compartments (Fig. 6B).

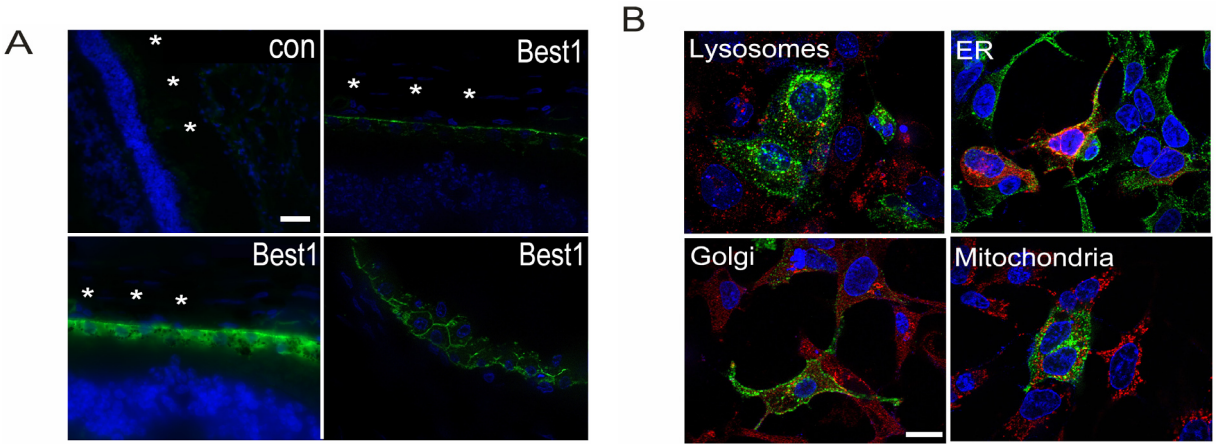

Fig. 6. Expression of hbest1 in native RPE and HEK293 cells. A) Immunohistochemistry of best1 expressed in native porcine retinal pigment epithelium (left lower). Asterisks indicate basal (choroidal) compartment. Con indicates control staining using preimmune serum (left upper). Right upper and right lower confocal images (ApoTome) suggest basolateral membrane expression of best1 in porcine RPE cells. B) Immunohistochemistry of hbest1 expressed in HEK293 cells. Co-staining of intracellular membrane compartments suggests that some of the expressed hbest1 is localized in the endoplasmic reticulum (yellow overlay). No colocalization is found with markers of lysosomes, Golgi-compartment or mitochondria (confocal images using ApoTome). Bar indicates 20 µm. Experiments were performed at least in triplicates.

Molecular interactions of hbest1 with hbest2 or hbest4 were further examined by coimmunoprecipitation. To that end we coexpressed His-tagged hbest1 and hbest2 in HEK293 cells. hbest2 (57 kDa) was immunoprecipitated using anti-hbest2 and coimmunoprecipitated His-tagged hbest1 (68 kDa) was detected by His- antibodies (Fig. 7A). Anti-hbest1 antibodies were used to immunoprecipitate hbest1, and coimmunoprecipitated hbest4-Flag (55 kDa) was detected by Flag- antibodies (Fig. 7B). In contrast His-tagged $P2Y_2$ receptors did not coimmunoprecipitate with hbest1 (Fig. 7C).

Moreover, we identified interaction of hbest1 and hbest4 in native Calu-3 airway epithelial cells by co-immunoprecipitating hbest1 and hbest4 (Fig. 7D). Calu-3 cells only express hbest1 and hbest4 (11) and show Ca^{2+} activated (100 µM ATP) Cl^- conductance, which is no longer detectable upon RNAi-knockdown of hbest1 (11) (Fig. 7E). In contrast, hbest1-RNAi treated Calu-3 cells have a higher baseline Cl^- conductance, similar to hbest-4 expressing HEK293 cells (Fig. 7F). Taken together these results and the fact that native epithelia such as the colonic epithelium (Fig. 7G) or renal and airway epithelial cells (11) coexpress several bestrophins, strongly suggests interaction of bestrophins in native epithelia. Co-assembly of bestrophins paralogs appears necessary to impart receptor mediated stimulation of Ca^{2+} activated Cl^- channels.

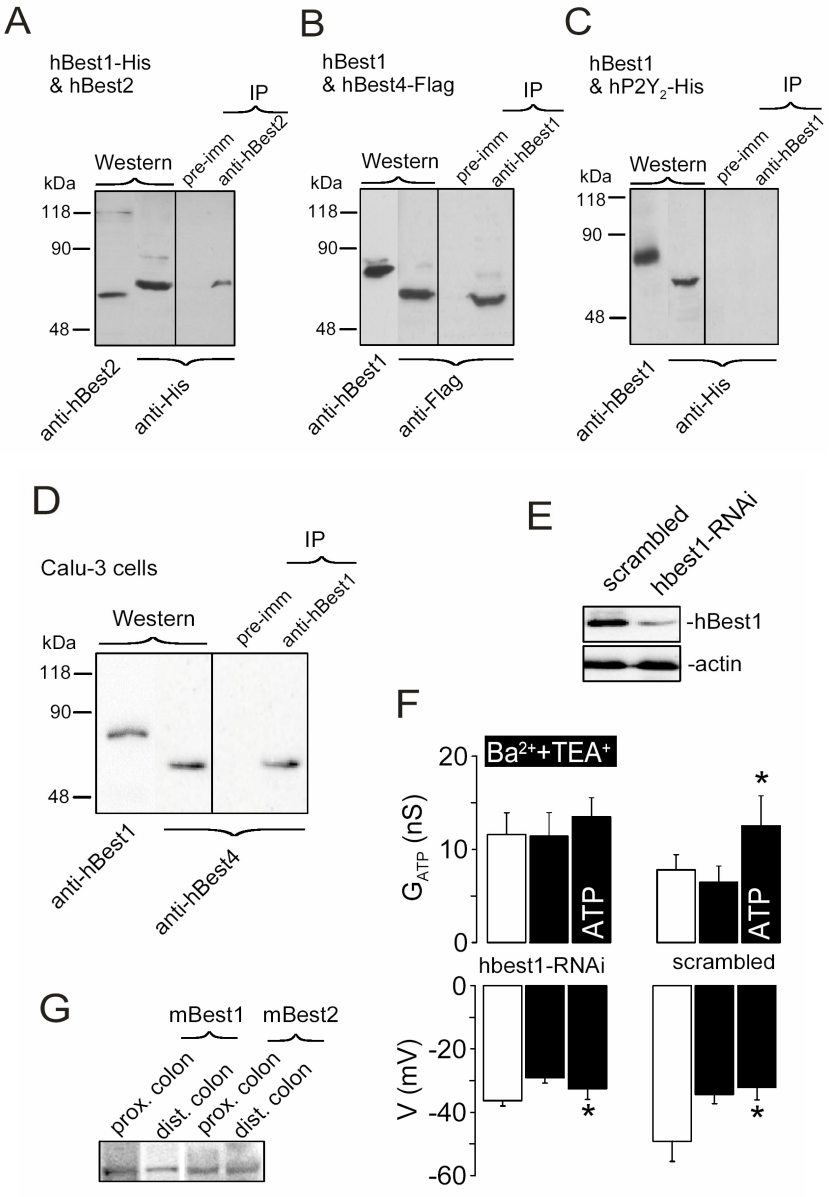

Fig. 7. Coimmunoprecipitation of hbest1/hbest2 and hbest1/hbest4. A) His-tagged hbest1 and hbest2 were coexpressed in HEK293 cells. Expression of hbest1 and hbest2 was detected by Western blot. hbest2 (57 kDa) was immunoprecipitated using anti-hbest2 and coimmunoprecipitated hbest1 (68 kDa) was detected by His- antibodies. B) Coexpression of hbest1 and Flag-tagged hbest4 was detected by Western blot. hbest1 (68 kDa) was immunoprecipitated using anti-hbest1 and coimmunoprecipitated hbest4 (55 kDa) was detected by Flag-antibodies. C) Coexpression of hbest1 and His-tagged hP2Y2 was detected by Western blot. hbest1 was immunoprecipitated using anti-hbest1 but did not coimmunoprecipitate $P2Y_2$. D) Coimmunoprecipitation of hbest1 and hbest4 coexpressed endogenously in Calu-3 human airway epithelial cells. E) Western blot of hbest1 indicating RNAi-knockdown of hbest1 in Calu-3 cells. F) Summary of the whole cell conductances and membrane voltages measured in Calu-3 cells treated with hbest1-RNAi or with scrambled RNA. G) Western blot of mbest1 and mbest2 indicating coexpression in mouse proximal and distal colon. Experiments were performed at least in triplicates.

Discussion

Bestrophins are functionally different

In a recent in silico analysis of the molecular evolution of bestrophins a significant functional divergence was found between bestrophin 4 and the other family members, as well as between bestrophin 2 and bestrophin 3 (80). Interestingly, both best1 and best3 have extended C-terminal amino acid sequences, when compared to best2 and best4. Stimulation by ATP activated a Cl^- conductance in HEK293 cells expressing hbest1. A much smaller but still detectable Cl^- conductance was found in hbest3 expressing cells, which is in good agreement with previous studies identifying a short inhibitory motif in the C-terminus of mbest4 (hbest3) (103;111). In contrast the human paralogs hbest2 and hbest4, which have shorter C-termini and therefore probably lack of inhibitory motifs, produced large Cl^- conductances in HEK293 cells even in the absence of ATP or ionomycin. This suggests that the C-termini of hbest1 and hbest3 have regulatory functions that enable receptor mediated activation of Ca^{2+} dependent Cl^- conductance. Since native epithelia always express several bestrophin paralogs (11) and because interaction is also observed for endogenous bestrophins, they may function as heterooligomers in native epithelia.

Bestrophins - a component of Ca^{2+}-activated Cl^- channels

Evidence was provided by several laboratories that bestrophins form Ca^{2+}-activated Cl^- channels and that disease causing mutations in hbest-1 impair chloride channel function (107;110;130;138;139;151). In a previous study we showed that best-1 is a component of endogenous Ca^{2+}-activated Cl^- currents in mouse airways and a number of epithelial cell lines (11). The Hartzell team was able to suppress endogenous CaCC by best-1-RNAi in *Drosophila* S2 cells (16;27). Single channel analysis demonstrated the expected small single channel conductance of 2 pS for best-1 channels (16). Moreover best2 was identified as a molecular component of the Ca^{2+}-activated Cl^- channel in mouse olfactory cells (98). In contrast, Rosenthal and coworkers found that bestrophin 1 modulates voltage gated Ca^{2+} channels in RPE cells by shifting their voltage-dependence closer to the resting potential (115). Surprisingly the Marmorstein lab reported an augmented ATP induced Ca^{2+} increase in RPE cells from best1 (vmd2-/-) knockout mice when compared to wt animals. Ca^{2+} activated Cl^- currents were indistinguishable between wt and $vmd2^{-/-}$ mice, although subtle differences in the whole cell currents were found with low intracellular Ca^{2+} (77).

As Hartzell and coworkers pointed out in a recent review article, both functions of best1 as a Cl^- channel and as a regulator of Ca^{2+} channels are not mutually exclusive (48). Although the present results do not supply a direct answer to the question whether bestrophins are Cl^-

channels or channel regulators, they imply that hbest1 is a component of the Ca^{2+} activated Cl^- conductance activated by ATP. However, no effects on intracellular Ca^{2+} signaling could be detected.

HEK293 cells express low levels of proteins important for intracellular Ca^{2+} signaling such as STIM and Orai/CRACM (122;152). This may explain why the magnitude of ATP induced Cl^- conductance was relatively small compared to that found for endogenous bestrophins (11). However, it may also be due to weak membrane expression of hbest1 in HEK293 cells (63). Tsunenari and coworkers found that most hbest1 protein expressed in HEK293 cells accumulates in cytosolic vesicles (139).

Ca^{2+}-activated Cl^- channels – a complex of proteins?

We present evidence for functional and molecular interaction of hbest1 and hbest2 or hbest4, respectively. According to the present results, hbest1 and hbest3 regulate the large Cl^- conductance caused by hbest2 and hbest4. A previous study by Sun et al. also suggested that hbest1 and hbest2 heterooligomerize, thereby allowing for combinatorial channel diversity (130). Such a protein assembly, together with additional auxiliary proteins may be necessary for proper membrane expression and activation by intracellular Ca^{2+}. However, purinergic regulation of Ca^{2+} activated Cl^- channels may not be tightly coupled to intracellular Ca^{2+} activity (129). The group by Hopfer found that calcium is not required for purinergic Cl^- secretion in colonic carcinoma cells (43). In our hand, the Ca^{2+} ionophore ionomycin had only weak effects on Ca^{2+} dependent Cl^- secretion in airway epithelial cells, although cytosolic Ca^{2+} was raised to maximal levels. Moreover, Ca^{2+} chelating agents such as BAPTA-AM only partially inhibited Ca^{2+} activated Cl^- currents in mouse tracheas (11). This supports the concept that Cl^- channel activity is not tightly linked to intracellular Ca^{2+} levels. However, we also found that emptying of intracellular Ca^{2+} stores by cyclopiazonic acid completely eliminates purinergic Cl^- secretion (11). This suggests that local Ca^{2+} increase in a confined compartment is relevant of activation of Cl^- channels, rather than a global rise in cytosolic Ca^{2+}. In fact Wong and Ko nicely demonstrated that Cl^- secretion mediated by purinergic P2Y receptors in polarized epithelial cells occurs via membrane-restricted Ca^{2+} signaling (146). It may be therefore important to determine the role of bestrophin-heterooligomers for localized Ca^{2+} signaling and purinergic activation of Cl^- transport.

Supplement material

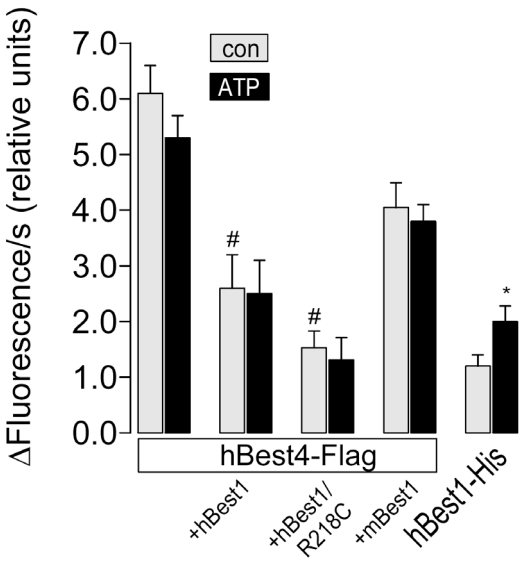

Supplement 1. Expression of Flag-tagged hbest4 and His-tagged hbest1 in HEK293 cells. Anion conductance was assessed by quenching of YFP fluorescence by isotonic application of 20 mM I^- before (grey bar) and after (black bar) application of 100 µM ATP. # significant decrease by coexpression with hbest1 (ANOVA). * significant increase by stimulation with 100 µM ATP (paired t-test). Number of experiments = 17 – 33

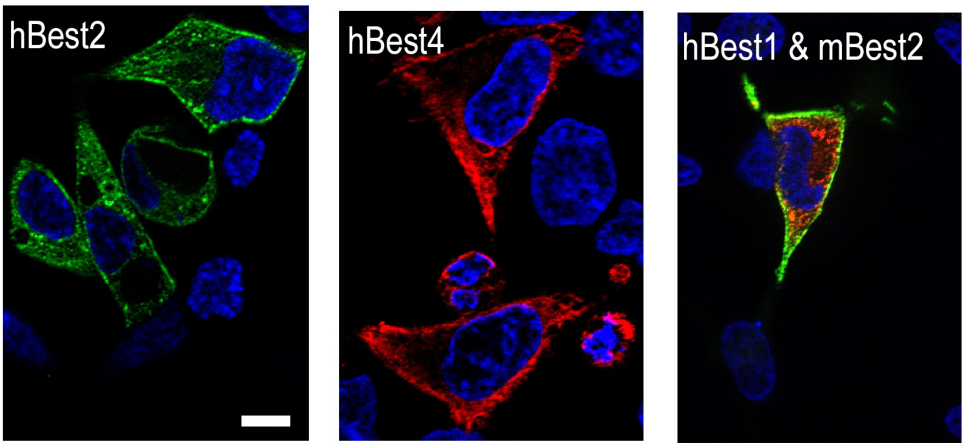

Supplement 2. Immunohistochemistry (confocal microscopy) of bestrophins expressed in HEK293 cells. Left: hbest2 (green).Middle: hbest4 (red). Right: hbest1 (red) & mbest2 (green).

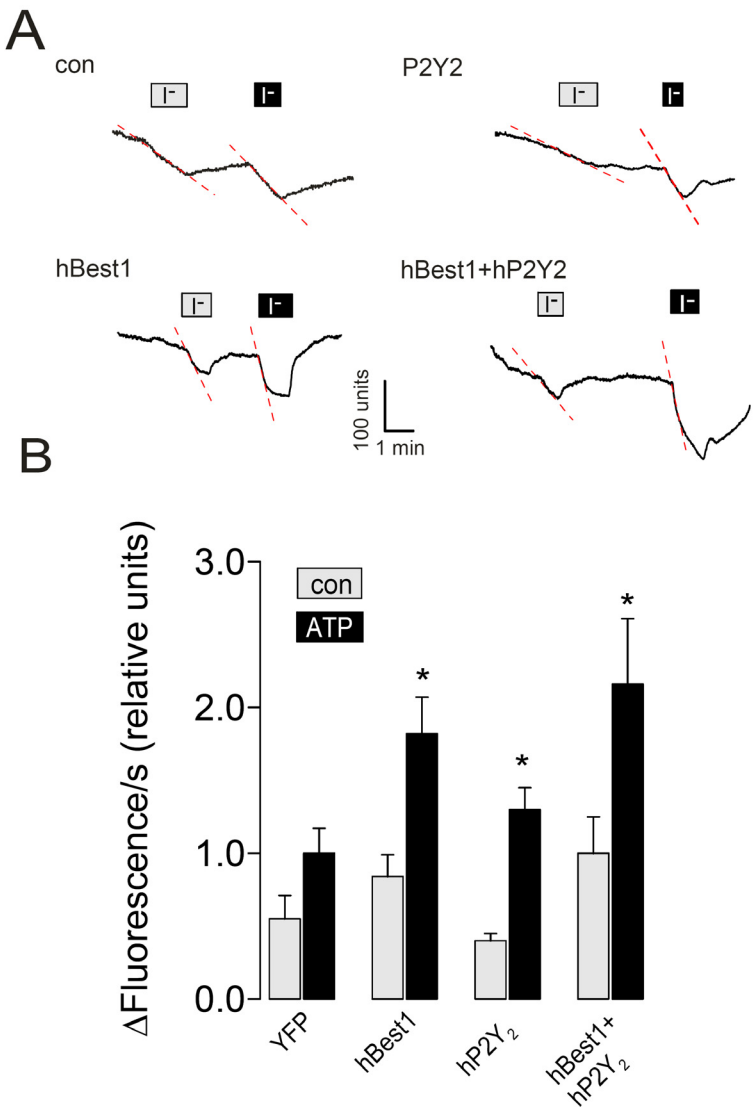

Supplement 3: Expression of hbest1, hP2Y2 or coexpression of both proteins in HEK293 cells. Anion conductance was assessed by quenching of YFP fluorescence by isotonic application of 20 mM I^- before (grey bar) and after (black bar) application of 100 µM ATP. * significant increase by ATP (paired Student´s t-test). Number of experiments = 12 - 27.

Chapter 5

Eag1 and Bestrophin 1 are upregulated in fast growing colonic cancer cells

Abstract

Ion channels like voltage gated ether á gogo (Eag1) K^+ channels or Ca^{2+} activated Cl^- channels have been shown to support cell proliferation. Bestrophin 1 (best1) has been proposed to form Ca^{2+} activated Cl^- channels in epithelial cells. Here we show that original T_{84} colonic carcinoma cells grow slow (T_{84}-slow) and express low amounts of Eag1 and best1, while spontaneously transformed T_{84} cells grow fast (T_{84}-fast) and express high levels of both proteins. Both Eag1 and best1 currents are upregulated in T_{84}-fast cells. Eag1 currents were cell cycle dependent, with upregulation during G1/S transition. T_{84}-slow but not T_{84}-fast formed tight monolayers when grown on permeable supports. RNAi inhibition of Eag1 and best1 reduced proliferation of T_{84}-fast cells, while overexpression of best1 turned T_{84}-slow into fast growing cells. Eag1 and best1 improve intracellular Ca^{2+} signaling and cell volume regulation. These results establish a novel role of bestrophins for cell proliferation.

Introduction

An increasing number of studies demonstrate proliferative effects of membrane ion channels (141). Voltage gated K^+ channels and other types of K^+ channels are expressed in numerous types of tumors, where they may serve as diagnostic and prognostic markers and potential drug targets (92;118;128). Eag1 channels are probably necessary for progression through the G_1 phase and G_0/G_1 transition of the cell cycle (145). A recent study demonstrates the hyperpolarizing effects of Eag1 and other Kv channels on the membrane voltage of T_{84} cells, which supports intracellular pH regulation and Ca^{2+} increase, necessary for proliferation (124).

Much less is known about the role of Ca^{2+} activated Cl^- channels for cell proliferation (58). This may be due to the ongoing controversy regarding the molecular nature of Ca^{2+} activated Cl^- channels (63). A family of putative Ca^{2+} activated Cl^- channels (CLCA) has been identified, which also controls cell-cell adhesion, apoptosis and cell cycle. However, their structure and biophysical properties are poorly understood (52;94). Recent studies defined bestrophin proteins as bona fide Ca^{2+} activated Cl^- channels. The Cl^- currents generated upon expression of bestrophin show many of the properties found for native Ca^{2+} activated Cl^- currents (104;130;139). However, bestrophins have also been proposed to function as regulators of voltage gated L-type Ca^{2+} channels (115). Our own ongoing work in epithelial cells supports both concepts in that bestrophins may form part of a Cl^- channel complex or may couple intracellular Ca^{2+} signals to Cl^- channels of unknown molecular identity (11).

In the present report we demonstrate that both voltage gated Eag1 K^+ channels and bestrophin (best1) Cl^- channels support proliferation of fast growing T_{84} colonic carcinoma cells. The fast growing T_{84} cell clone was obtained through a spontaneous transformation of slow-growing T_{84} cells. In contrast to slow growing T_{84} cells, transformed cells do not form polarized monolayers and show a remarkable upregulation of Eag1 and best1 expression. We demonstrate that both currents are in charge of enhanced cell proliferation.

Material and Methods

Cell culture and proliferation studies

Human colorectal carcinoma epithelial T_{84} cells (ATCC, Rockville, MD, USA) were grown in DMEM/Ham's F-12 medium (1:1) supplemented with 10% fetal bovine serum, 2 mM glutamine, 100 units/ml penicillin and 100 µg/ml streptomycin (Invitrogen, Karlsruhe,

Germany) at 5% CO_2/37ºC. Cells were seeded on fibronectin (Invitrogen)/collagen (Cellon, Luxembourg) coated glass cover slips or permeable supports (snap-well, Costar). Typically these cells grow slowly as polarized monolayers (T_{84}-slow). Due to spontaneous transformation, a T_{84} cell line was selected which grew remarkably faster (T_{84}-fast). For proliferation assays cells were plated at a density of 2000 cells/0.35 cm^2 and incubated 2 days later with either niflumic acid (0,01–100mM) or astemizole (0,5–5000nM). Cell proliferation was assessed by 5-bromo-2´-deoxyuridine (BrdU) incorporation using an ELISA kit (Roche, Penzberg, Germany) and cell counting. The cell number was assessed after fixation in 3.7% formaldehyde / 0.5% Triton X-100 for 30 minutes at room temperature and after staining with Mayers hemalaun (Merck, Darmstadt, Germany) for 5 minutes. Digitized microscopic images were taken (Fluovert FS, Leitz, Germany) and nuclei were counted using imaging software (TINA 2.09g). Toxicity of the blockers was assessed using Trypan Blue (Sigma). Each experiment was performed at least in triplicate.

Cell cycle, FACS analysis, Caspase assay, RT-PCR

Cells were synchronized into early G1 by 24h serum starvation. Incubation in thymidine (2 mM), (Sigma) halted the cells at G1/S transition. 36h treatment with demecolcine (0.05 µg/ml) (Sigma) synchronized into M phase. Synchronization was verified by FACS (COULTER EPICS® XL-MCL, Beckmann, Miami, USA) using propidium iodide staining of the DNA (Sigma). Apoptosis was analyzed after 8h and 24 h incubation with the protein kinase C inhibitor staurosporine (1 µM), (Sigma) and detection of cleaved caspase-3 in Western blots using rabbit anti-human caspase-3 antibody (1:1000, Cell Signaling Technology, Inc., Danvers, USA). For RT-PCR total RNA was isolated using NucleoSpin RNA II columns (Macherey-Nagel, Düren, Germany). 1 µg total RNA was reverse transcribed for 1 h at 37˚C using random primer and RT (M-MLV Reverse Transcriptase, Promega, Mannheim, Germany). For PCR the following primers were used: hEag1 (KCNH1, NM_002238): 5´-CGCATGAACTACCTGAAGACG-3´ (s), 5´-TCTGTGGATGGGGCGATGTTC-3´ (as), 560 bp. hbest1 (VMD2, NM_004183): 5´-CTGCTCTGCTACTACATCATC-3´ (s), 5´-GTGTCCACACTGAGTACGC-3´ (as), 552 bp. The conditions were: 94˚C / 2 min, 35 cycles of 94˚C / 30 sec, 58°C / 30 sec and 72˚C / 1 min. PCR products were visualized by loading on 2% agarose gels and verified by sequencing.

Downregulation of best1 and Eag1 expression by RNAi

Three different batches (A,B,C) of duplexes of 21-nucleotide RNAi with 3'-overhanging TT were purchased from Invitrogen (Karlsruhe, Germany). The sense strands of the RNAi used to silence the best1 gene were 5´- AAUUCCUGUCGACAAUCCA-GUUGGU -3´(A), 5´-AUCUCAUCCACA-GCCAACAGGGACA -3´(B), and 5´-

UAAAUAAAGCGGAUGAUGUAGUAGC -3´(C). RNAi sequences for Eag1 are shown in (124). Fluorophore labeled RNAi and exposure to the transfection reagent lipofectamine 2000, (Invitogen) served as controls. After 48 hrs cells were further processed in proliferation assays and for western blotting.

Detection of Eag1 and best1 by Western blotting

T_{84} cells were homogenized in lysis buffer (mmol/l: NaCl 150, Tris 50, DTT 100, 1% NP-40, and 1% protease inhibitor cocktail) (Sigma). Equal amounts of total protein (50 µg) were separated by 7% SDS-PAGE, transferred to Hybond-P (Amersham Biosiences, Freiburg, Germany) and incubated with either rabbit anti-hKv10.1 (Eag1) (Alomone labs, Jerusalem, Israel) or rabbit anti-hVMD-2 (best1) (11) antibodies. Proteins were visualized using goat anti-rabbit IgG conjugated to horseradish peroxidase (Acris Antibodies, Hiddenhausen, Germany) and ECL (Amersham). Signals were detected by an Fluor-STM MultiImager (Bio-Rad Laboratories, Hercules, USA).

Measurement of the intracellular Ca^{2+} concentration and cell volume

T_{84} cells were loaded with 2 µM Fura-2 AM (Molecular Probes, Eugene, USA) in Opti-MEM medium (GIBCO) with 2.5 mM probenecid (Sigma) for 1h at room temperature. Fluorescence was detected in cells perfused with ringer solution containing 2.5 mM probenecid (Sigma) at 37°C, using an inverted microscope IMT-2 (Olympus, Nürnberg, Germany) and a high speed polychromator system (VisiChrome, Puchheim, Germany). Fura-2 was excited at 340/380 nm and emission was recorded between 470 and 550 nm using a CCD camera (CoolSnap HQ, Visitron). $[Ca^{2+}]_i$ was calculated from the 340/380 nm fluorescence ratio (after background subtraction). The formula used to calculate $[Ca^{2+}]_i$ was $[Ca^{2+}]_i = K_d \times (R-R_{min})(R_{max}-R) \times (S_{f2}/S_{b2})$ where R is the observed fluorescence ratio. The values R_{max}, R_{min} (maximum and minimum ratios) and the constant S_{f2}/S_{b2} (fluorescence of free and Ca^{2+}-bound fura-2 at 380 nm) were calculated, using 2 µmol/l ionomycin (Calbiochem), 5 µmol/l nigericin, 10µmol/l monensin (Sigma) and 5 mmol/l EGTA to equilibrate intracellular and extracellular Ca^{2+} in intact fura-2-loaded cells. The dissociation constant for the fura-2-Ca^{2+} complex was taken as 224 nmol/l.

Patch clamping

Cell culture dishes were mounted on the stage of an inverted microscope (IM35, Zeiss, Germany), and perfused continuously (37°C) with Ringer solution. Patch-clamp experiments were performed in the fast and slow whole-cell configuration. Patch pipettes had an input resistance of 2–4 MΩ, when filled with a solution containing (mM) KCl 30, K-gluconate 95, NaH_2PO_4 1.2, Na_2HPO_4 4.8, EGTA 1, Ca-gluconate 0.758, $MgCl_2$ 1.034, D-glucose 5, ATP 3.

pH was adjusted to 7.2, the Ca^{2+} activity was 0.1 µM. The access conductance was monitored continuously and was 60–120 nS. Currents (voltage clamp) and voltages (current clamp) were recorded using an EPC7 amplifier (HEKA, Darmstadt, Germany), the LH1600 interface and PULSE software (HEKA) as well as Chart software (AD-Instruments, Spechbach, Germany). In intervals membrane voltages (V_c) were clamped in steps of 10 mV from -50 to +50 mV relative to resting potential. The membrane conductance G_m was calculated from the measured current (I) and V_c values according to Ohm's law.

Cell volume was measured directly by a Zeiss-Axiovert 200M/ApoTome using Axiovision software or was assessed by fluorescence measurements in calcein (2 µM; Molecular Probes, USA) loaded cells at an excitation of 500 nm and emission of 520-550 nm. The experiments were done in the presence of 2.5 mM probenecid. The control isotonic solution (290 mOsm) was prepared by adding 120 mM mannitol. The hypotonic (170 mOsm) and control isotonic solution contained 85 mM NaCl.

Materials and statistical analysis

All compounds used were of highest available grade of purity. Astemizole, niflumic acid (NFA), DIDS, tetrapentylammonium (TPeA), carbachol, and ATP were all from SIGMA (Taufkirchen, Germany). Student's t-test (for paired or unpaired samples as appropriate) and analysis of variance (ANOVA) was used for statistical analysis. $P<0.05$ was accepted as significant.

Results

Fast growing colonic carcinoma cells (T_{84}-fast) express Eag1 and best1

T_{84} cells typically grow in slowly expanding patches (T_{84}-slow). At passage number 73, the cell line spontaneously changed its growth pattern, i.e. the cells grew remarkably faster (T_{84}-fast) as single cells, non-polarized and above each other (Fig.1A,B). T_{84}-slow formed tight monolayers with a transepithelial resistance (R_{te}) of 2.2 $\pm$ 0.3 kΩcm^2 (n= 25), when grown on permeable supports, while T_{84}-fast did not (0.12 $\pm$ 0.07 kΩcm^2; n= 23). Thus, growth pattern or phenotype were not changed by the way the cells were grown. We examined apoptosis in both cell lines by Western blotting and analyzed uncleaved and cleaved caspase 3. Small amounts of cleaved caspase 3 were detected in T_{84}-slow but not in T_{84}-fast cells, after treatment with the PKC inhibitor staurosporin (1 µM) (Fig. 1C).

Semi-quantitative RT-PCR analysis was performed for voltage gated K^+ channels (Eag1) and putative Ca^{2+} activated Cl^- channels (best1), using ß-actin as an internal standard.

Densitometric analysis suggested transcript numbers for Eag1 and best1 that were at least 10 times higher in T_{84}-fast cells. Thus much higher protein expression was found for Eag1 and best1 in T_{84}-fast cells in Western blots (Fig. 1D). The membrane conductance properties were analyzed in T_{84}-slow and T_{84}-fast cells in whole cell patch clamp experiments and membrane voltages (Vm) were measured in the current clamp mode. T_{84}-slow cells (n = 8) were more hyperpolarized (-51.7 ± 5.6 mV) and had a lower baseline conductance (3.8 ± 0.7 nS) than T_{84}-fast cells (-36.6 ± 2.9 mV and 23.8 ± 2.9 nS, n = 8). The increased baseline conductance and depolarized Vm of T_{84}-fast cells was due to a higher activity of Cl^- channels, since replacement of extracellular Cl^- by gluconate (5Cl) shifted the I/V curve to more positive clamp voltages. This was not observed for T_{84}-slow cells (Fig. 1E).

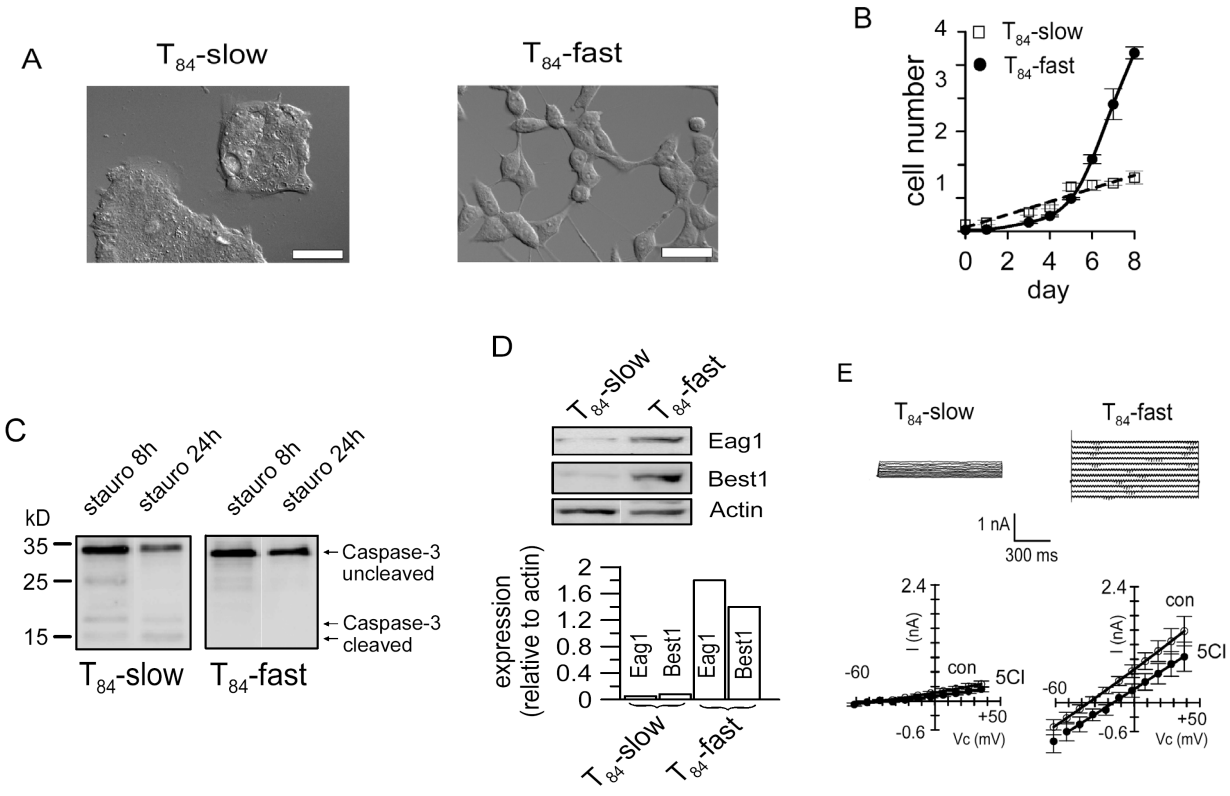

Fig. 1. Slow and fast growing T_{84} cells. A) Typical growth patterns of T_{84}-slow cells as obtained from ATCC, and spontaneously transformed T_{84}-fast cells. Bars indicate 50 µm. B) Proliferation curves for T_{84}-slow and T_{84}-fast cells, as obtained by cell counting (n = 4). C) Western blot for uncleaved and cleaved caspase-3 in T_{84}-slow and T_{84}-fast cells after 8 and 24 h incubation with 1 µM staurosporine (stauro). D) Western blot analysis of the expression of Eag1 and best1 in slow and fast growing T_{84} cells. Actin indicates equal loading of the gel. Bar graph indicates larger upregulation of ion channel expression in T_{84}-fast cells. E) Whole cell currents measured in slow and fast growing T_{84} cells under control conditions (upper panels). Corresponding current/voltage relationships (n = 8 for both cell types; lower panels). Replacement of extracellular Cl^- by gluconate (5Cl) shifted the i/v curve to more depolarized clamp voltages only in fast growing T_{84} cells, indicating the presence of a baseline Cl^- conductance. RT-PCR and Western blots were performed at least in triplicates.

Eag1 controls proliferation of fast but not of slow growing T_{84} cells

Eag1 has been demonstrated to support proliferation of several different cell types (93;124). We therefore examined if high expression levels of Eag1 correlate with increased proliferation of T_{84}-fast cells. To that end T_{84}-slow and T_{84}-fast cells were treated with three different batches (A-C) of siRNA for Eag1. Incubation of the cells with either fluorescence labeled scrambled oligos or lipid (transfection reagent) and non-treated cells served as controls. Measurement of BrdU incorporation clearly indicates inhibition of proliferation of T_{84}-fast cells after treatment with siRNA for Eag1 (Fig. 2A). siRNA treatment of T_{84}-slow cells did not affect cell proliferation, suggesting a proliferative function of Eag1 only in T_{84}-fast cells. Notably, Eag1 expression was significantly upregulated by re-addition of 10% FCS in serum starved cells (data not shown). Using the inhibitor astemizole (5 µM), we examined the contribution of Eag1 to whole cell currents measured in T_{84}-slow and T_{84}-fast cells. Astemizole inhibited whole cell currents in both cell types, however, the effect was more pronounced in T_{84}-fast cells and thus astemizole-sensitive whole cell currents were significantly larger in T_{84}-fast cells (Fig. 2B,C). The normalized conductance/voltage relationship for Eag1 (astemizole sensitive whole cell conductances) was not different for T_{84}-fast (solid line) and T_{84}-slow (dashed line) cells (Fig. 2D).

A previous report supplied evidence that hyperpolarizing Eag1 currents assist in the increase of intracellular Ca^{2+} ($[Ca^{2+}]_i$), when cells are stimulated with secretagogues (ATP, carbachol) or mitogens, and may thereby support proliferation. Both Ca^{2+} release from ER stores and Ca^{2+} influx through store operated Ca^{2+} channels depend on Kv channel function, as reported earlier (124). We compared increase in $[Ca^{2+}]_i$ in Fura-2 loaded T_{84}-slow and T_{84}-fast cells upon stimulation with ATP (100 µM). ATP binds to purinergic $P2Y_2$ receptors and thereby induces a peak and plateau $[Ca^{2+}]_i$ increase in both cell lines (Fig. 2E). The peak $[Ca^{2+}]_i$ increase was doubled in T_{84}-fast when compared with T_{84}-slow cells, which suggests a role of Eag1 for Ca^{2+} signaling in T_{84}-fast cells (Fig. 2E,F). Enhanced Ca^{2+} signaling is not due to an increased expression of the abundant purinergic receptor $P2Y_2$ in T_{84}-fast. In contrast, $P2Y_2$ expression was slightly higher in T_{84}-slow cells (Fig. 2G).

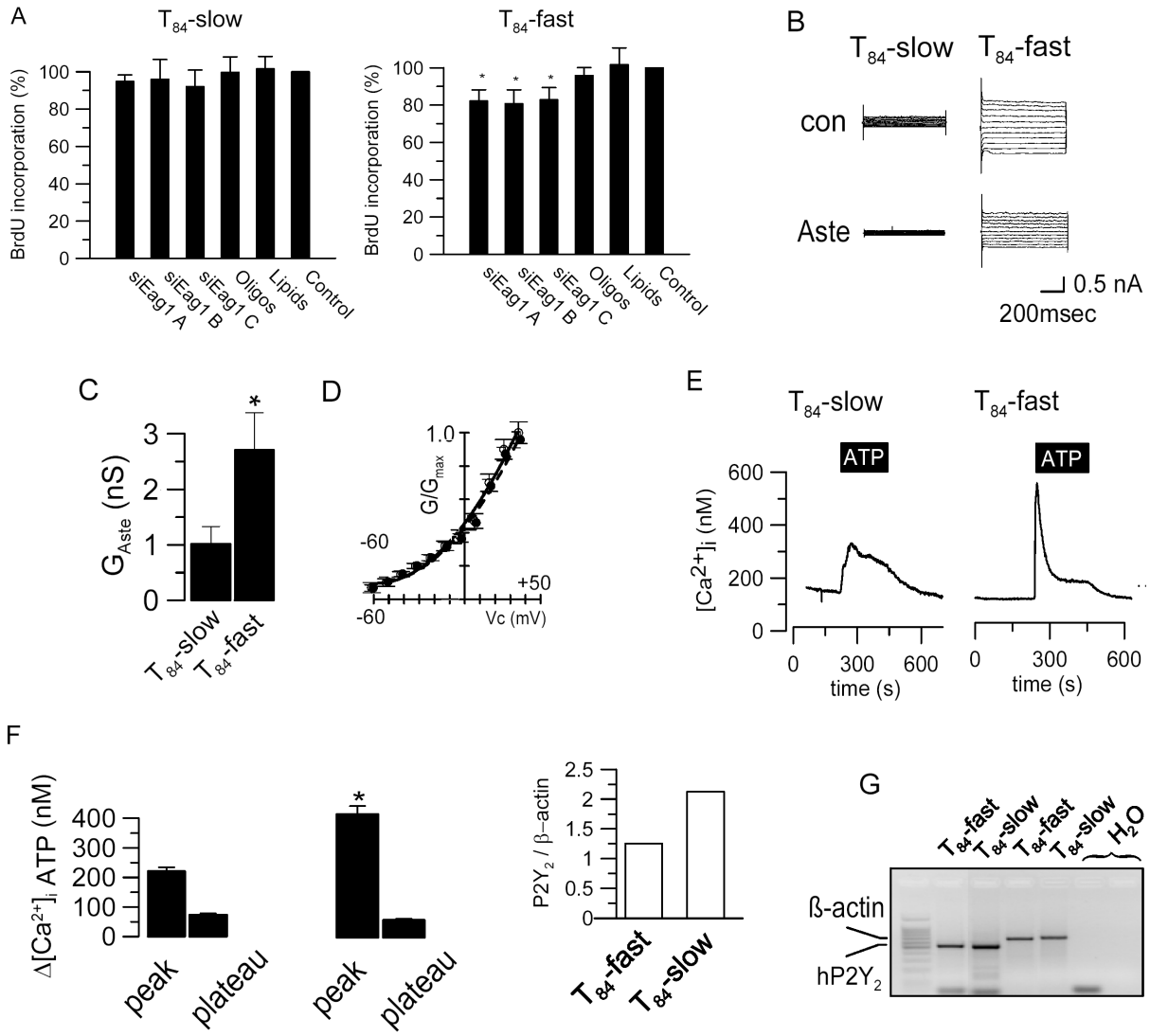

Fig. 2. Eag1 supports proliferation of fast growing T_{84} cells. A) Proliferation of slow and fast growing T_{84} cells as measured by BrdU incorporation. Cells were treated with three different batches (A-C) of siRNA for Eag1. Incubation of the cells with fluorescence labeled scrambled oligos (Oligos) or transfection reagent only (Lipid) and non-treated cells (Control) served as controls. Assays were performed at least in triplicates. * indicate significant inhibition of proliferation by RNAi in T_{84}-fast cells (ANOVA). B) Whole cell currents in T_{84}-slow and T_{84}-fast cells and effect of the Eag1 inhibitor astemizole (Aste; 5 µM). C) Summary of the calculated astemizole sensitive whole cell conductances (G_{Aste}) in T_{84}-slow (n = 8) and T_{84}-fast (n = 9) cells. G_{Aste} was significant in both cell lines and was enhanced in T_{84}-fast cells (unpaired t-test). D) Normalized conductance / voltage relationship for Eag1 (i.e. astemizole sensitive whole cell conductance) measured in T_{84}-fast (solid line) and T_{84}-slow (dashed line) cells. E) Increase of the intracellular Ca^{2+} concentration ($[Ca^{2+}]_i$) by stimulation with ATP (100 µM) in T_{84}-slow and T_{84}-fast cells. F) Summary of the ATP induced peak and plateau increase in $[Ca^{2+}]_i$ in slow (n = 59) and fast (n = 69) growing T_{84} cells. G) RT-PCR analysis of mRNA expression for $P2Y_2$ receptors (764 bp) in T_{84}-slow and T_{84}-fast cells. When compared to the internal ß-actin standard, expression of $P2Y_2$ receptors was slightly enhanced in T_{84}-slow. H_2O served as control. For PCR conditions c.f. Methods.* indicates significant difference in peak $[Ca^{2+}]_i$ increase in T_{84}-fast cells.

Eag1 activity in T_{84}-fast cells is cell cycle dependent

In other cell types Eag1-activity varies during the cell cycle (93). Therefore we examined cell cycle dependence of Eag1 in T_{84}-fast cells. Cells were synchronized in early G1 (eG1), G1/S or M phase (c.f. methods), and synchronization was verified by FACS analysis (Fig. 3A). We found that astemizole sensitive whole cell currents were augmented in cells synchronized in G1/S, when compared to eG1 or M phase (Fig. 3B). T_{84} cells also express other voltage gated K^+ channels such as Kv1.5 or Kv3.4, which are blocked by the inhibitor TPeA (124). However, in contrast to Eag1, TPeA sensitive whole cell currents were not cell cycle dependent (data not shown). We further compared the increase in $[Ca^{2+}]_i$ in T_{84}-fast cells synchronized in eG1 and G1/S phase. Both peak and plateau $[Ca^{2+}]_i$ increase were significantly enhanced in G1/S-cells. Moreover, the Eag1-blocker astemizole inhibited peak and plateau $[Ca^{2+}]_i$ increase in both cell cycle phases, but the effect of astemizole on plateau $[Ca^{2+}]_i$ was augmented in the G1/S phase (Fig. 3C). These results supply evidence for cell cycle regulated Eag1-currents in T_{84}-fast cells and cell cycle dependent effects of Eag1 on Ca^{2+} signaling.

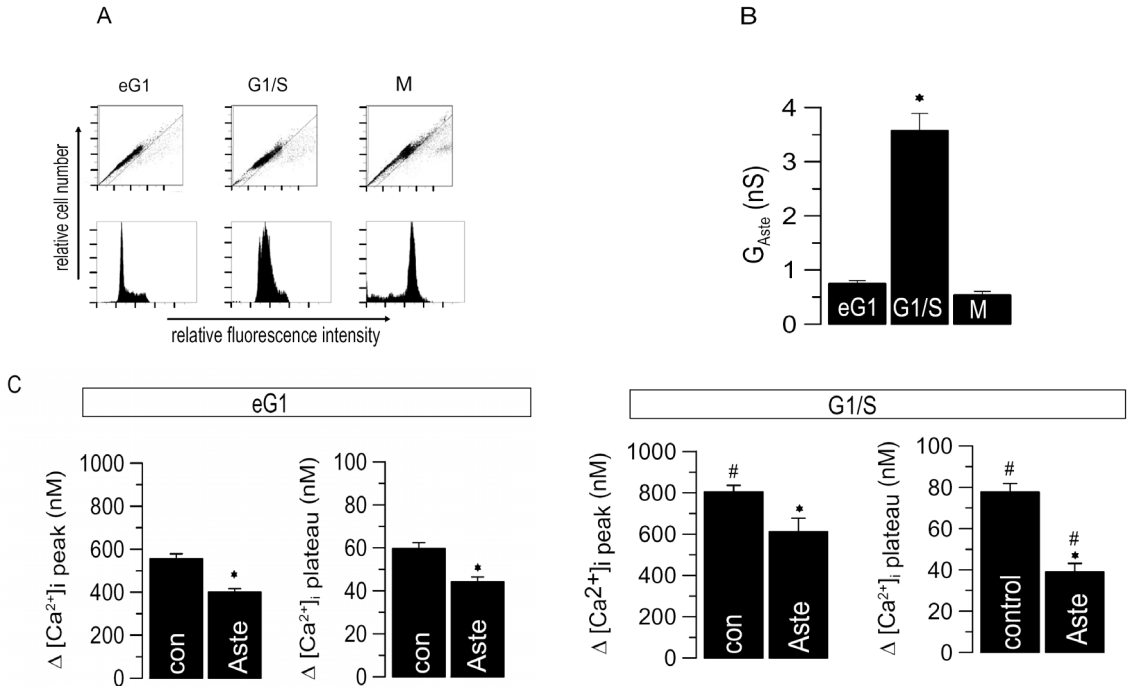

Fig. 3. Eag1 operates as a cell cycle regulated channel in fast growing T_{84} cells. A) FACS analysis of fast growing T_{84} cells synchronized in early G1 (eG1), G1/S transition and M phase (c.f. Methods). Experiments were performed at least in triplicates. B) Astemizole sensitive whole cell conductances (G_{Aste}) measured in T_{84}-fast cells synchronized in eG1 (n = 14), G1/S (n = 9) and M (n = 9) phase. G_{Aste} was significant during all cell cycle phases but was enhanced during G1/S (ANOVA). C) Summary of the peak and plateau $[Ca^{2+}]_i$ increase induced by CCH in T_{84}-fast cells, synchronized into eG1 and effects of 0.5 µM astemizole (Aste, n = 73) (left panel) or G1/S and effects of 0.5 µM astemizole (Aste, n = 64) (right panel). The effect of astemizole was significant in all series (paired t-test) and was enhanced for plateau $[Ca^{2+}]_i$ increase in G1/S when compared to eG1 (unpaired t-test).

Best1 controls proliferation of fast but not of slow growing T_{84} cells

Because T_{84}-fast cells show much higher expression of best1 when compared with T_{84}-slow cells (Fig. 4A), we examined the effect of this putative Ca^{2+} activated Cl^- channel on cell proliferation. T_{84}-slow and T_{84}-fast cells were treated with three different batches (A-C) of siRNA for best1, which reduced best1 levels in T_{84}-fast cells. Expression levels in T_{84}-slow cells were already very low, so that more protein was loaded on the gel, as indicated by the ß-actin signal (Fig. 4A,B). Incubation of the cells with either fluorescence labeled scrambled oligos or transfection reagent (lipid) and non-treated cells served as controls. Measurement of BrdU incorporation clearly indicates inhibition of proliferation of T_{84}-fast cells after treatment with siRNA for best1 (Fig. 4C). No effects of siRNA were seen in T_{84}-slow cells, suggesting a proliferative function of best1 only in T_{84}-fast cells.

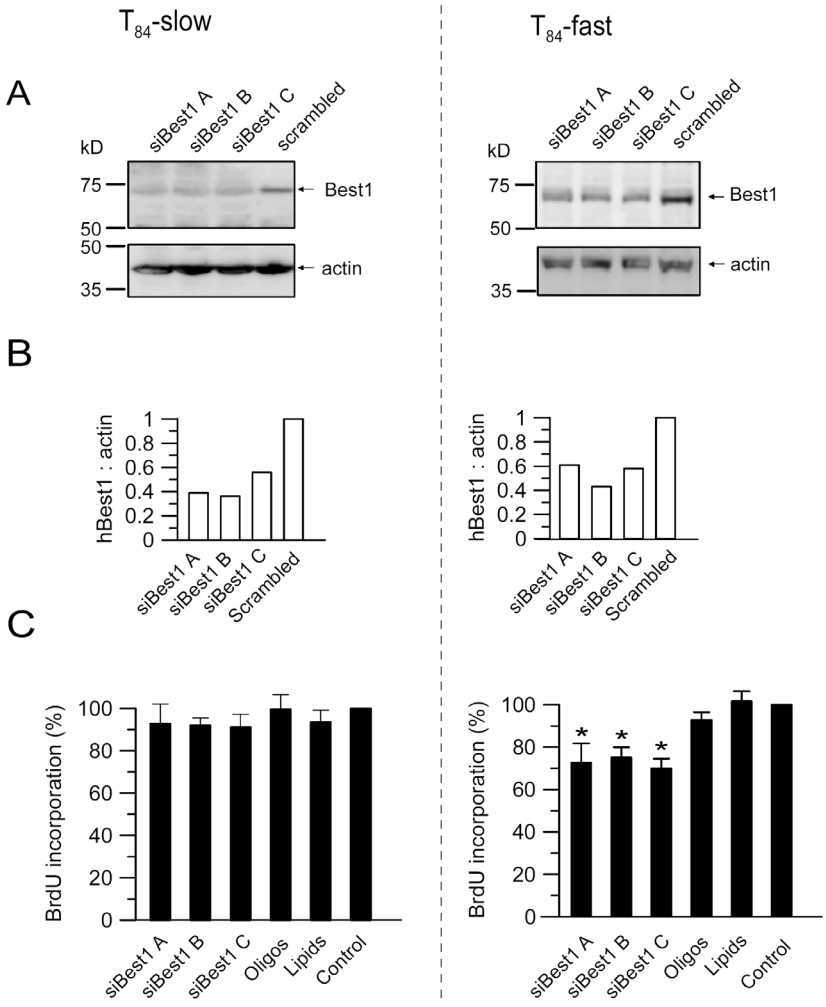

Fig. 4. Best1 supports proliferation of fast growing T_{84} cells. A) Western blot analysis of best1 in T_{84}-slow and T_{84}-fast cells treated with three different batches (A-C) of siRNA for best1. Incubation of the cells with fluorescence labeled scrambled oligos (Oligos) or non-treated cells (Control) served as controls. Actin indicates equal loading of the gels. B) Densitometric analysis of best1 expression and ratio between best1 and actin expression. C) Proliferation of slow and fast growing T_{84} cells as measured by BrdU incorporation. Assays were performed at least in triplicates. * indicate significant inhibition of proliferation by RNAi in T_{84}-fast cells (ANOVA).

In whole cell patch clamp experiments, the high baseline conductance found in T_{84}-fast cells could be partially inhibited by the blockers of Ca^{2+} activated Cl^- channels, NFA and DIDS (both 100 µM). Both inhibitors had no effect in T_{84}-slow cells (Fig. 5A). Stimulation with ATP (100 µM) to increase intracellular Ca^{2+} (Fig. 2D), activated a whole cell current in T_{84}-slow but not in T_{84}-fast cells (Fig. 5B). In T_{84}-slow cells, ATP activated primarily a K^+ conductance, as indicated by the hyperpolarizing effect of ATP on the membrane voltage (Fig. 5C). Little effects of ATP were seen in T_{84}-fast cells. Correspondingly, replacement of extracellular Cl^- by impermeable gluconate (5Cl) showed no effects in T_{84}-slow cells, but reduced the baseline conductance in T_{84}-fast cells (Fig. 5D). Taken together, these results suggest active best1 Cl^- channels in non-stimulated T_{84}-fast cells, which cause enhanced proliferation.

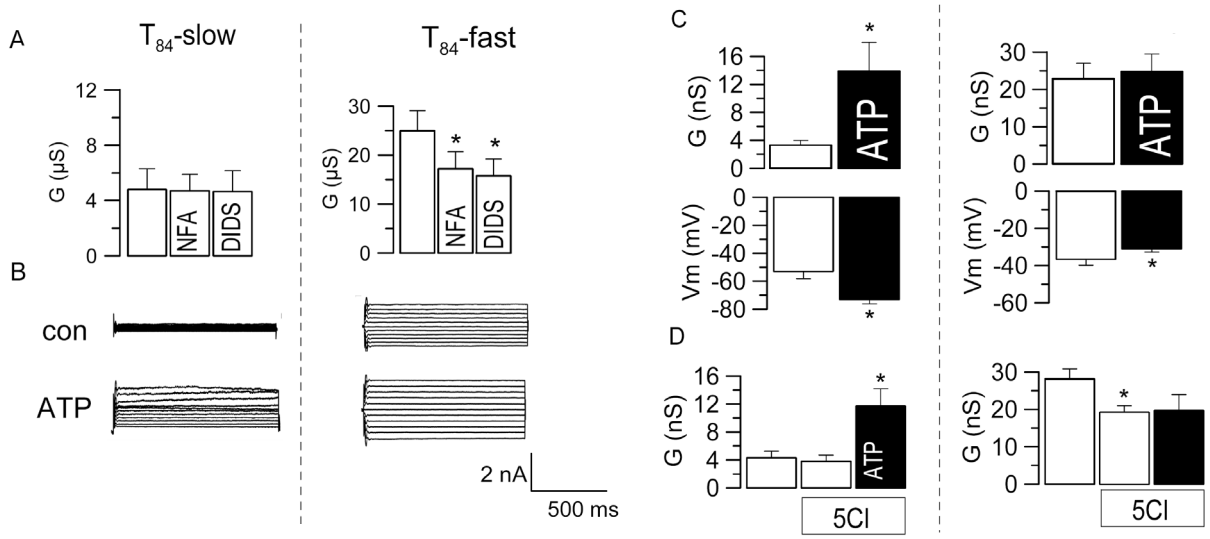

Fig. 5. T_{84}-fast but not T_{84}-slow cells have a Cl^- conductance. A) Summaries for the baseline whole cell conductances (G) and effects of the inhibitors of Ca^{2+}-activated Cl^- channels, niflumic acid (NFA; 10 µM) and DIDS (100 µM) in slow and fast growing T_{84} cells (n = 8 – 11). * indicate significant effects of NFA and DIDS (paired t-test). B) Whole cell currents measured in T_{84}-slow and T_{84}-fast cells. Stimulation of the cells with ATP (100 µM) activated a whole cell conductance only in T_{84}-slow but not in T_{84}-fast cells. C) Summaries for the whole cell conductances (upper panels) and membrane voltages (lower panels) measured in T_{84}-slow (n = 13) and T_{84}-fast (n = 14) cells, and effects of ATP (100 µM). * indicate significant effects on whole cell conductance and membrane voltages (paired t-test). D) Summaries for the whole cell conductances measured in T_{84}-slow (n = 9) and T_{84}-fast (n = 8) cells, and effect of replacement of extracellular Cl^- by gluconate ($5Cl^-$) and ATP (100 µM). * indicate significant activation of conductance by ATP in T_{84}-slow cells and significant inhibition by $5Cl^-$ (paired t-test).

Increased proliferation and Cl^- conductance in best1-transfected T_{84}-slow cells

To further demonstrate that best1 contributes to proliferation of T_{84} cells, we expressed human best1 in T_{84}-slow cells. As shown in Fig. 6A, transfection of 100 ng of exogenous best1 increased best1 expression in T_{84}-slow cells almost to the level found in T_{84}-slow cells. No change was seen in mock transfected cells. Notably, overexpression of best1 changed the growth pattern of T_{84}-slow cells towards that found for T_{84}-fast cells (Fig. 6B). Moreover, after expression of best1, a DIDS-sensitive whole cell current appeared in T_{84}-slow cells, which was not found in mock-transfected or parental cells (Fig. 6C). Measurement of the BrdU-incorporation indicated a significant increase in proliferation of best1-transfected T_{84}-slow cells, which was not observed for mock-transfected cells (Fig. 6D). In summary, both Eag1 K^+ channels and best1 Cl^- channels are upregulated in spontaneously transformed T_{84} cells, where they augment proliferation.

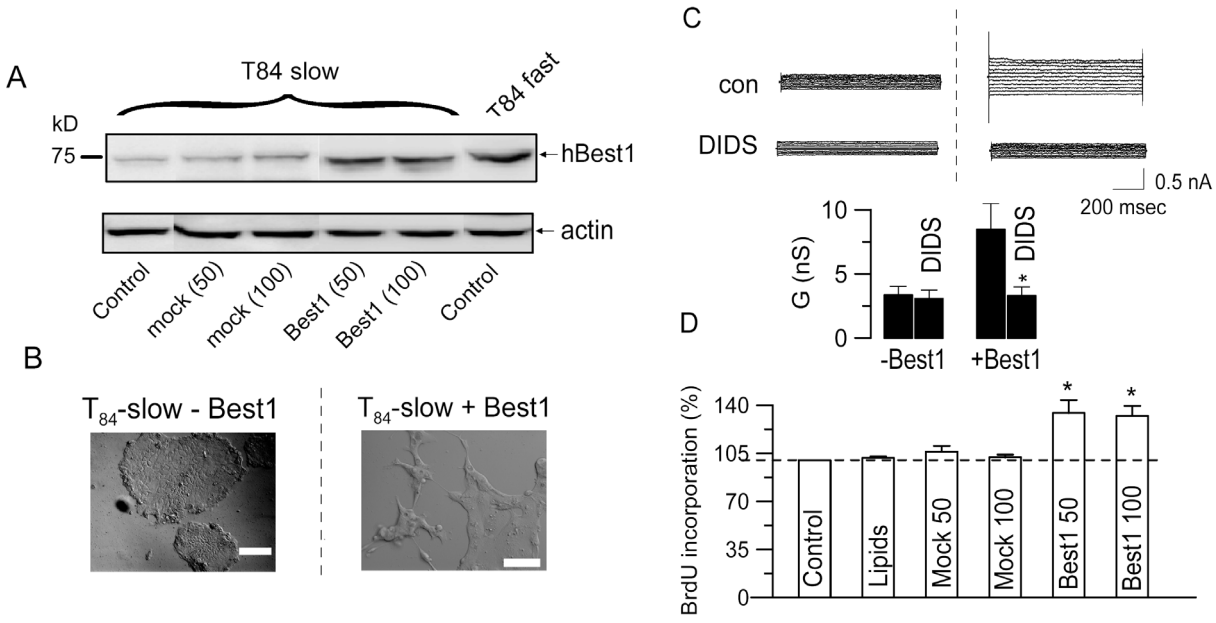

Fig. 6. Expression of best1 in T_{84}-slow cells enhances Cl^- currents and proliferation. A) Western blot analysis of human best1 expression in T_{84}-slow cells after transfection of 50 or 100 ng of best1 cDNA, or mock (50 and 100 ng) transfection, and comparison with the level of best1 expression in T_{84}-fast cells and non-transfected T_{84}-slow cells. Actin indicates equal loading of the gel. B) Growth pattern of mock transfected (- best1) and best1 transfected (+best1) T_{84}-slow cells. Bars indicate 50 µm. C) Upper panel: Whole cell currents measured in mock-transfected and best1-transfected T_{84}-slow cells and effect of DIDS (100 µM). Lower panel: Summaries of the whole cell conductances and effects of DIDS on mock transfected (n = 7) and best1 transfected (n = 7) T_{84}-fast cells. * indicates significant inhibition of whole cell conductance by DIDS (paired t-test). D) Proliferation of mock transfected (50 and 100 ng) and best1 transfected (50 and 100 ng) cells. Non-transfected cells (Control) and cells exposed the transfection reagent only (Lipids) served as controls. * indicate significant increase in proliferation (ANOVA).

Eag1 and best1 support intracellular Ca^{2+} signaling and volume regulation, respectively

Eag1 K^+ channels (and to some degree best1) have a clear impact on intracellular Ca^{2+} signaling. This was demonstrated by stimulation with ATP (100 µM), which increased intracellular peak (ER- Ca^{2+} release) and plateau (Ca^{2+} - influx through SOC) in T_{84}-fast cells. Treatment with siRNA for Eag1 significantly reduced peak and plateau Ca^{2+} increase (Fig. 7A). Volume measurements indicate stronger cell swelling and potent regulatory volume decrease (RVD) in T_{84}-fast, when compared to T_{84}-slow cells, as identified by direct volume measurements and indirect measurements of calcein fluorescence (Fig. 7B-E). T_{84}-fast cells treated with siRNA-best1 show reduced RVD (Fig. 7B). As both intracellular Ca^{2+} and cell volume control is essential for the mitotic cell cycle, these results may provide a mechanism for the proliferative role of Eag1 and best1.

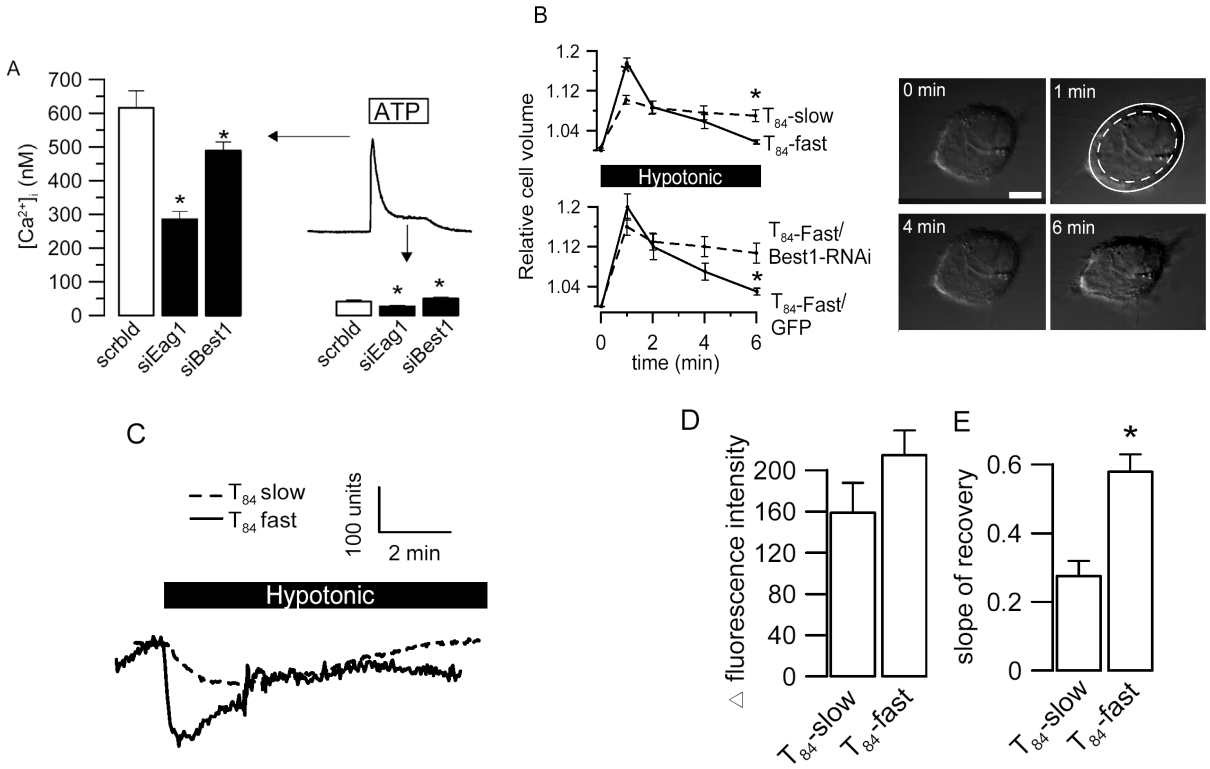

Fig. 7. Eag1 and best1 support intracellular Ca^{2+} signaling and volume regulation. A) Summary of intracellular peak (left) and plateau (right) Ca^{2+} increase in T_{84}-fast cells, upon stimulation with ATP (100 µM). Cells were treated with scrambled siRNA or siEag1 and sibest1, respectively (n = 24 – 57). B) Hypotonic (170 mosmol) cell swelling assessed by volume measurement in T_{84}-slow and T_{84}-fast cells (upper trace) and T_{84}-fast cells treated with siRNA-best1 or control transfection (GFP) (n = 5 each time point). C) Change in calcein fluorescence due to hypotonic cell swelling. D,E) Summaries for maximal change in fluorescence intensity and slope of recovery (from swelling) of T_{84}-slow and T_{84}-fast cells (n = 12). * indicate significant difference (paired t-test).

Discussion

Transformation of colonic epithelial cells increases proliferation and ion conductances

T_{84} colonic carcinoma cells are well established (23;60). They grow slowly in patches and form tight and polarized monolayers, when cultured on permeable supports. T_{84} cells were used for numerous electrophysiological studies and resemble a model for electrolyte transport in the colonic epithelium (23). They show many aspects of native epithelial cells such as a relatively hyperpolarized membrane voltage and Cl^- secretion by cAMP-dependent cystic fibrosis transmembrane conductance regulator (CFTR) channels. When stimulated by secretagogues, which increase the intracellular Ca^{2+} concentration such as ATP or carbachol, predominantly K^+ channels are activated, hyperpolarizing the membrane voltage. This is comparable to colonic crypt cells, which also activate Ca^{2+} activated K^+ channels upon stimulation of basolateral muscarinic M3 and apical purinergic $P2Y_2$ receptors (60;101). In contrast, T_{84} cells that had undergone spontaneous transformation were remarkably different: They proliferated much faster, were unable to polarize and to form tight monolayers when grown on permeable support, showed typical features of malignancy and had different membrane conductances.

Anderson and Welsh as well as Morris and Frizzell reported earlier that expression of ion channels in epithelial cells is significantly affected by the underlying substrate (4;84). Thus Ca^{2+} activated Cl^- channels were prominent in non-differentiated HT_{29} colonic carcinoma cells but disappeared with polarization (32). Although T_{84}-fast cells did not polarize when grown on permeable supports, a change in best1 expression upon differentiation of filter grown HT_{29} cells may explain earlier results (32).

A change in membrane ion conductance has also been reported for spontaneously transformed Madin-Darby canine kidney (MDCK) cells. These fast growing MDCK-F cells express Ca^{2+} activated K^+ channels that largely enhance cell migration (121). The fast growing T_{84} cells described in the present study, showed a strong increase in the expression of the best1 Cl^- channel, along with Eag1 potassium channels. Eag1 currents were detected despite a relatively high (100 nM) Ca^{2+} concentration in resting cells. However up to 1 µM $[Ca^{2+}]_i$ are required for complete inhibition of Eag1 and thus a fraction (~ 40%) of the Eag1 conductance is still detectable in T_{84}-fast cells (125). Notably, the Cl^- channels were already active in non-stimulated cells, i.e. without purinergic stimulation. Additional increase of intracellular Ca^{2+} by ATP or carbachol did not further increase Cl^- conductance. A similar result was obtained when best1 was overexpressed in T_{84}-slow cells, and has also been observed when best1 was expressed in Hek293 cells (63). It suggests that additional

components may be required for Ca^{2+} -regulation of best1 currents, which may not be present in cancer cells. The presence of these DIDS-sensitive Cl^- currents along with astemizole inhibited Eag1 K^+ currents clearly augmented cell proliferation

Ion channels induce malignancy and metastatic cell growth

Clonal selection of fast proliferating T_{84} cells (T84SF) has previously been reported (3). These cells demonstrate invasive and metastatic cell growth, when transferred into nude mice. Basal tyrosine phosphorylation and expression of src kinase were enhanced in these T84SF cells (3). Along this line, the src-inhibitor PP2 reduced cell growth, invasion and cell adhesion of T84SF cells (14). In Jurkat T lymphocytes, src kinase controls voltage-dependent Kv1.3 K^+ channels, which also affect cell proliferation (134). Src kinase may also be up-regulated in fast growing T_{84} cells and may be responsible for changes in membrane conductance. It will be interesting to examine in subsequent studies the impact of Eag1 and best1 on cell migration and tissue invasion, since we previously found that genomic amplification of Eag1 in human colorectal carcinoma is an independent marker of adverse prognosis (90).

How do ion channels determine malignancy?

K^+ and Cl^- channels are essential for cell migration and metastasis of cancer (120). It has been shown that enhanced intracellular Ca^{2+} activates Kv channels during intestinal wound healing (112). Cell migration and formation of tumor metastasis is due to fluctuations in the activity of membrane transporters and ion channels, since they cause localized cell swelling and shrinkage (120). These changes in cell volume appear to be a prerequisite for cell migration and malignant invasion. There are only a few studies investigating the role of Cl^- channels in cell migration. Cl^- channels are probably necessary for cell movement, since K^+ transport needs to be accompanied by a counterion (121). Notably, bestrophin has been shown to operate as a volume sensitive Cl^- channel (31).

A novel function of bestrophin for cell proliferation?

Cl^- currents induced by expression of bestrophins share many of the properties attributed to Ca^{2+} activated Cl^- channels, such as an anion selectivity of $I^- > Cl^-$ and inhibition by NFA and DIDS (11;104;130;139). There is, however, an ongoing controversy whether bestrophins are actually channel forming proteins or rather regulators of ion channels. Moreover, other proteins have also been proposed as molecular candidates for the Ca^{2+} activated Cl^- channel (reviewed in (63). The present results would support the role of best1 as a Cl^- channel. As known from previous studies, Ca^{2+} and volume regulated Cl^- channels support cell proliferation, and bestrophin is activated by increase in intracellular Ca^{2+} as well as cell

swelling (15;58). In an ongoing study with M1 collecting duct cells expressing high levels of best1, we found inhibition of proliferation by the Cl^- channel blockers DIDS and NFA (unpublished results). Thus bestrophins may provide the molecular basis for an understanding of the role of Ca^{2+} and volume regulated Cl^- channels in cell proliferation.

References

1. Al Jumaily, M., Kozlenkov, A., Mechaly, I., Fichard, A., Matha, V., Scamps, F., Valmier, J., Carroll, P. (2007). Expression of three distinct families of calcium-activated chloride channel genes in the mouse dorsal root ganglion. *Neurosci.Bull.* 23, 293-299

2. AlDehni, F., Spitzner, M., Martins, J. R., Barro-Soria R., Schreiber R., Kunzelmann K (2008). Role of bestrophin for proliferation and in epithelial to mesenchymal transition. *J Am Soc Nephrol. (submitted)*

3. Alessandro, R., Flugy, A. M., Russo, D., Stassi, G., De Leo, A., Corrado, C., Alaimo, G., De Leo, G. (2005). Identification and phenotypic characterization of a subpopulation of T84 human colon cancer cells, after selection on activated endothelial cells. *J Cell Physiol.* 203, 261-272

4. Anderson, M. P., Welsh, M. J. (1991). Calcium and cAMP activate different chloride channels in the apical membrane of normal and cystic fibrosis epithelia. *Proc.Natl.Acad.Sci.USA.* 88, 6003-6007

5. Arreola, J., Melvin, J. E., Begenisich, T. (1996). Activation of calcium-dependent chloride channels in rat parotid acinar cells. *J Gen.Physiol.* 108, 35-47

6. Bakall, B., McLaughlin, P., Stanton, J. B., Zhang, Y., Hartzell, H. C., Marmorstein, L. Y., Marmorstein, A. D. (2008). Bestrophin-2 is involved in the generation of intraocular pressure. *Invest Ophthalmol.Vis.Sci.* 49, 1563-1570

7. Ball, J. M., Tian, P., Zeng, C. Q., Morris, A. P., Estes, M. K. (1996). Age-dependent diarrhea induced by a rotaviral nonstructural glycoprotein. *Science.* 272, 101-104

8. Bao, L., Kaldany, C., Holmstrand, E. C., Cox, D. H. (2004). Mapping the BKCa channel's "Ca^{2+} bowl": side-chains essential for Ca^{2+} sensing. *J.Gen.Physiol.* 123, 475-489

9. Barriere, H., Belfodil, R., Rubera, I., Tauc, M., Poujeol, C., Bidet, M., Poujeol, P. (2003). CFTR null mutation altered cAMP-sensitive and swelling-activated Cl^- currents in primary cultures of mouse nephron. *Am.J Physiol Renal Physiol.* 284, F796-F811

10. Barro-Soria, R., Schreiber R., Kunzelmann K. (2008). Bestrophin 1 and 2 are components of the Ca^{2+}-activated Cl^- conductance in mouse airways. *BBA. (submitted)*

11. Barro-Soria, R., Spitzner, M., Schreiber, R., Kunzelmann, K. (2006). Bestrophin 1 enables Ca^{2+} activated Cl^- conductance in epithelia. *J Biol Chem.* 281, 17460-17467

12. Berschneider, H. M., Knowles, M. R., Azizkhan, R. G., Boucher, R. C., Tobey, N. A., Orlando, R. C., Powell, D. W. (1988). Altered intestinal chloride transport in cystic fibrosis. *FASEB J.* 2, 2625-2629

13. Bidet, M., Tauc, M., Rubera, I., De Renzis, G., Poujeol, C., Bohn, M. T., Poujeol, P. (1996). Calcium-activated chloride currents in primary cultures of rabbit distal convoluted tubule. *Am.J Physiol.* 271, F940-F950

14. Boyd, D. D., Wang, H., Avila, H., Parikh, N. U., Kessler, H., Magdolen, V., Gallick, G. E. (2004). Combination of an SRC kinase inhibitor with a novel pharmacological antagonist of the urokinase receptor diminishes in vitro colon cancer invasiveness. *Clin.Cancer Res.* 10, 1545-1555

15. Chien, L. T., Hartzell, H. C. (2007). Drosophila bestrophin-1 chloride current is dually regulated by calcium and cell volume. *J Gen.Physiol.* 130, 513-524

16. Chien, L. T., Zhang, Z. R., Hartzell, H. C. (2006). Single Cl^- channels activated by Ca^{2+} in *Drosophila* S2 cells are mediated by bestrophins. *J Gen.Physiol.* 128, 247-259

17. Clarke, L. L., Grubb, B. R., Gabriel, S. E., Smithies, O., Koller, B. H., Boucher, R. C. (1992). Defective epithelial chloride transport in a gene-targeted mouse model of cystic fibrosis. *Science.* 257, 11251128

18. Clarke, L. L., Grubb, B. R., Yankaskas, J. R., Cotton, C. U., McKenzie, A., Boucher, R. C. (1994). Relationship of a non-cystic fibrosis transmembrane conductance regulator-mediated chloride conductance to organ-level didease in *cftr (-/-)* mice. *Proc.Natl.Acad.Sci.USA.* 91, 479-483

19. Cressman, V. L., Lazarowski, E. R., Homolya, L., Boucher, R. C., Koller, B. H., Grubb, B. R. (1999). Effect of loss of $P2Y_2$ receptor gene expression on nucleotide regulation of murine epithelial Cl^- transport. *J Biol Chem.* 274, 26461-26468

20. Cunningham, S. A., Awayda, M. S., Bubien, J. K., Ismailov, I. I., Arrate, M. P., Berdiev, B. K., Benos, D. J., Fuller, C. M. (1995). Cloning of an epithelial chloride channel from bovine trachea. *J.Biol.Chem.* 270, 31016-31026

21. Dawson, D. C., Smith, S. S., Mansoura, M. K. (1999). CFTR: mechanism of anion conduction. *Physiol.Rev.* 79, S47-S75

22. de la, Fuente, R., Namkung, W., Mills, A., Verkman, A. S. (2007). Small-molecule screen identifies inhibitors of a human intestinal calcium-activated chloride channel. *Mol Pharmacol.* 73, 758-768

23. Dharmsathaphorn, K., McRoberts, J. A., Mandel, K. G., Tisdale, L. D., Masui, H. (1984). A human colonic tumor cell line that maintains vectorial electrolyte transport. *Am J Physiol.* 246, G204-G208

24. Dong, Y., Zeng, C. Q., Ball, J. M., Estes, M. K., Morris, A. P. (1997). The rotavirus enterotoxin NSP4 mobilizes intracellular calcium in human intestinal cells by stimulating phospholipase C-mediated inositol 1,4,5- trisphosphate production. *Proc.Natl.Acad Sci.U.S.A.* 94, 3960-3965

25. Doughty, J. M., Miller, A. L., Langton, P. D. (1998). Non-specificity of chloride channel blockers in rat cerebral arteries: block of the L-type calcium channel. *J.Physiol.* 507, 433-439

26. Duta, V., Duta, F., Puttagunta, L., Befus, A. D., Duszyk, M. (2007). Regulation of Basolateral Cl(-) Channels in Airway Epithelial Cells: The Role of Nitric Oxide. *J Membr.Biol.* 213, 165-174

27. Duta, V., Szkotak, A. J., Nahirney, D., Duszyk, M. (2004). The role of bestrophin in airway epithelial ion transport. *FEBS Lett.* 577, 551-554

28. Eggermont, J. (2004). Calcium-activated chloride channels: (un)known, (un)loved? *Proc.Am.Thorac.Soc.* 1, 22-27

29. Evans, M. G., Marty, A. (1986). Calcium-dependent chloride currents in isolated cells from rat lacrimal glands. *J Physiol.* 378, 437-460

30. Fahlke, C. (2001). Ion permeation and selectivity in ClC-type chloride channels. *Am.J.Physiol Renal Physiol.* 280, F748-F757

31. Fischmeister, R., Hartzell, H. C. (2005). Volume sensitivity of the bestrophin family of chloride channels. *J.Physiol.* 562, 477-491

32. Fraser, G. M., Portnoy, M., Bleich, M., Ecke, D., Niv, Y., Greger, R., Schwartz, B. (1997). Characterization of sodium and chloride conductances in preneoplastic and neoplastic murine colonocytes. *Pflügers Arch.* 434, 801-808

33. Frings, S., Reuter, D., Kleene, S. J. (2000) Neuronal Ca^{2+} -activated Cl^- channels--homing in on an elusive channel species. *Prog.Neurobiol.* 60, 247-289

34. Frizzell, R. A., Rechkemmer, G. R., Shoemaker, R. L. (1986). Altered regulation of airway epithelial cell chloride channels in cystic fibrosis. *Science.* 233, 558-560

35. Fujii, S., Gallemore, R. P., Hughes, B. A., Steinberg, R. H. (1992). Direct evidence for a basolateral membrane Cl^- conductance in toad retinal pigment epithelium. *Am J Physiol.* 262, C374-C383

36. Gabriel, S. E., McDaniel, J., Wasilchen, T., Kreda, S. M., Quinney, N. (2006). Bestrophin-mediated Ca^{2+} activated Cl^- conductance of the airway epithelium. *FASEB J.* 16.

37. Galietta, L. J., Haggie, P. M., Verkman, A. S. (2001). Green fluorescent protein-based halide indicators with improved chloride and iodide affinities. *FEBS Lett.* 499, 220-224

38. Greenberg, N. M., DeMayo, F., Finegold, M. J., Medina, D., Tilley, W. D., Aspinall, J. O., Cunha, G. R., Donjacour, A. A., Matusik, R. J., Rosen, J. M. (1995). Prostate cancer in a transgenic mouse. *Proc.Natl.Acad.Sci.U.S.A.* 92, 3439-3443

39. Greger, R. (1996). The membrane transporters regulating epithelial NaCl secretion. *Pflugers Arch.* 432, 579-588

40. Grubb, B. R., Boucher, R. C. (1999). Pathophysiology of gene-targeted mouse models for cystic fibrosis. *Physiol.Rev.* 79, S193-S214

41. Grubb, B. R., Rogers, T. D., Diggs, P. C., Boucher, R. C., Ostrowski, L. E. (2006). Culture of murine nasal epithelia: a model for cystic fibrosis. *Am J Physiol Lung Cell Mol.Physiol.* 290, L270-L277

42. Grubb, B. R., Vick, R. N., Boucher, R. C. (1994). Hyperabsorption of Na^+ and raised Ca^{2+} mediated Cl^- secretion in nasal epithelia of CF mice. *Am.J.Physiol.* 266, C1478-C1483

43. Guo, X., Merlin, D., Harvey, R. D., Laboisse, C., Hopfer, U. (1997). Pharmacological evidence that calcium is not required for P2-receptor-stimulated Cl^- secretion in HT29-Cl.16E. *J Membr.Biol.* 155, 239-246

44. Guziewicz, K. E., Zangerl, B., Lindauer, S. J., Mullins, R. F., Sandmeyer, L. S., Grahn, B. H., Stone, E. M., Acland, G. M., Aguirre, G. D. (2007). Bestrophin gene mutations cause canine multifocal retinopathy: a novel animal model for best disease. *Invest Ophthalmol.Vis.Sci.* 48, 1959-1967

45. Hartzell, H. C. (1996). Activation of different Cl currents in Xenopus oocytes by Ca liberated from stores and by capacitative Ca influx. *J.Gen.Physiol.* 108, 157-175

46. Hartzell, H. C., Putzier, I., Arreola, J. (2005). Calcium-Activated Chloride Channels. *Annu.Rev.Physiol.* 67, 719-758

47. Hartzell, H. C., Qu, Z., Putzier, I., Artinian, L., Chien, L. T., Cui, Y. (2005). Looking chloride channels straight in the eye: bestrophins, lipofuscinosis, and retinal degeneration. *Physiology.(Bethesda.)* 20, 292-302

48. Hartzell, H. C., Qu, Z., Yu, K., Xiao, Q., Chien, L. T. (2008). Molecular Physiology of bestrophins: multifunctional membrane proteins linked to best disease and other retinopathies. *Physiological Reviews.* 88, 639-672

49. Hiraoka, M., Kawano, S., Hirano, Y., Furukawa, T. (1998). Role of cardiac chloride currents in changes in action potential characteristics and arrhythmias. *Cardiovasc.Res.* 40, 23-33

50. Ho, M. W., Kaetzel, M. A., Armstrong, D. L., Shears, S. B. (2001). Regulation of a human chloride channel. a paradigm for integrating input from calcium, type ii calmodulin-dependent protein kinase, and inositol 3,4,5,6-tetrakisphosphate. *J Biol Chem.* 276, 18673-18680

51. Huang, P., Liu, J., Di, A., Robinson, N. C., Musch, M. W., Kaetzel, M. A., Nelson, D. J. (2001). Regulation of human CLC-3 channels by multifunctional Ca^{2+}/calmodulin-dependent protein kinase. *J Biol Chem.* 276, 20093-20100

52. Jentsch, T. J., Stein, V., Weinreich, F., Zdebik, A. A. (2001). Molecular structure and physiological function of chloride channels. *Physiol Rev.* 82, 503-568

53. Kitamura, K., Yamazaki, J. (2001). Chloride channels and their functional roles in smooth muscle tone in the vasculature. *Jpn.J.Pharmacol.* 85, 351-357

54. Knowles, M. R., Boucher, R. C. (2002) Mucus clearance as a primary innate defense mechanism for mammalian airways. *J Clin.Invest.* 109, 571-577

55. Kramer, F., White, K., Pauleikhoff, D., Gehrig, A., Passmore, L., Rivera, A., Rudolph, G., Kellner, U., Andrassi, M., Lorenz, B., Rohrschneider, K., Blankenagel, A., Jurklies, B., Schilling, H., Schutt, F., Holz, F. G., Weber, B. H. (2000). Mutations in the VMD2 gene are associated with juvenile-onset vitelliform macular dystrophy (Best disease) and adult vitelliform macular dystrophy but not age-related macular degeneration. *Eur.J.Hum.Genet.* 8, 286-292

56. Kubitz, R., Warth, R., Kunzelmann, K., Grolik, M., Greger, R. (1992). Small conductance Cl^- channels induced by cAMP, Ca^{2+}, and hypotonicity in HT_{29} cells: ion selectivity, additivity and stilbene sensitivity. *Pflügers Arch* 421, 447-454

57. Kunzelmann, K. (1999). The Cystic Fibrosis Transmembrane Conductance Regulator and its function in epithelial transport. *Rev.Physiol.Biochem.Pharmacol.* 137, 1-70.

58. Kunzelmann, K. (2005). Ion channels and cancer. *J Membr.Biol.* 205, 159-173

59. Kunzelmann, K., Kubitz, R., Grolik, M., Warth, R., Greger, R. (1992). Small conductance Cl^- channels in HT_{29} cells: activation by Ca^{2+}, hypotonic cell swelling and 8-Br-cGMP. *Pflügers Arch.* 421, 238-246

60. Kunzelmann, K., Mall, M. (2002). Electrolyte transport in the colon: Mechanisms and implications for disease. *Physiological Reviews.* 82, 245-289.

61. Kunzelmann, K., Mall, M. (2003). Pharmacotherapy of the ion transport defect in cystic fibrosis: role of purinergic receptor agonists and other potential therapeutics. *American Journal of Respiratory Medicine.* 2, 299-309

62. Kunzelmann, K., Mall, M., Briel, M., Hipper, A., Nitschke, R., Ricken, S., Greger, R. (1997). The cystic fibrosis transmembrane conductance regulator attenuates the endogenous Ca^{2+} activated Cl^- conductance in *Xenopus* ooyctes. *Pflügers Arch.* 434, 178-181

63. Kunzelmann, K., Milenkovic, V. M., Spitzner, M., Barro Soria, R., Schreiber, R. (2007). Calcium dependent chloride conductance in epithelia: Is there a contribution by Bestrophin? *Pflügers Arch.* 454, 879-889

64. Kunzelmann, K., Schreiber, R., Cook, D. I. (2002). Mechanisms for inhibition of amiloride-sensitive Na^+ absorption by extracellular nuceotides in mouse trachea. *Pflügers Arch* 444, 220-226

65. Kuruma, A., Hartzell, H. C. (2000). Bimodal Control of a Ca(2+)-activated Cl(-) Channel by Different Ca(2+) Signals. *J Gen.Physiol* 115, 59-80

66. Lazarowski, E. R., Boucher, R. C., Harden, T. K. (2000). Constitutive release of ATP and evidence for major contribution of ecto-nucleotide pyrophosphatase and nucleoside diphosphokinase to extracellular nucleotide concentrations. *J Biol Chem.* 275, 31061-31068

67. Lazarowski, E. R., Tarran, R., Grubb, B. R., Van Heusden, C. A., Okada, S., Boucher, R. C. (2004). Nucleotide release provides a mechanism for airway surface liquid homeostasis. *J Biol Chem.* 279, 36855-36864

68. Leblanc, N., Ledoux, J., Saleh, S., Sanguinetti, A., Angermann, J., O'Driscoll, K., Britton, F., Perrino, B. A., Greenwood, I. A. (2005). Regulation of calcium-activated chloride channels in smooth muscle cells: a complex picture is emerging. *Can.J Physiol Pharmacol.* 83, 541-556

69. Leipziger, J. (2003). Control of epithelial transport via luminal P2 receptors. *Am.J Physiol.Renal Physiol.* 284, F419-F432

70. Loewen, M. E., Forsyth, G. W. (2005). Structure and function of CLCA proteins. *Physiol Rev.* 85, 1061-1092

71. Lu, L., Markakis, D., Guggino, W. B. (1993). Identification and regulation of whole-cell Cl^- and Ca(2+)-activated K^+ currents in cultured medullary thick ascending limb cells. *J Membr.Biol.* 135, 181-189

72. Mall, M., Bleich, M., Greger, R., Schürlein, M., Kühr, J., Seydewitz, H. H., Brandis, M., Kunzelmann, K. (1998). Cholinergic ion secretion in human colon requires co-activation by cAMP. *Am J Physiol.* 275, G1274-G1281

73. Mall, M., Gonska, T., Thomas, J., Schreiber, R., Seydewitz, H. H., Kuehr, J., Brandis, M., Kunzelmann, K. (2003). Role of basolateral K^+ channels in Ca^{2+} activated Cl^- secretion in human normal and cystic fibrosis airway epithelia. *Pediatric Research.* 53, 608-618

74. Mall, M., Wissner, A., Seydewitz, H. H., Kühr, J., Brandis, M., Greger, R., Kunzelmann, K. (2000). Defective cholinergic Cl^- secretion and detection of K^+ secretion in rectal biopsies from cystic fibrosis patients. *Am.J.Physiol.* 278, G617-G624

75. Marmorstein, A. D., Marmorstein, L. Y., Rayborn, M., Wang, X., Hollyfield, J. G., Petrukhin, K. (2000). Bestrophin, the product of the Best vitelliform macular dystrophy gene (VMD2), localizes to the basolateral plasma membrane of the retinal pigment epithelium. *Proc.Natl.Acad.Sci.U.S.A.* 97, 12758-12763

76. Marmorstein, L. Y., McLaughlin, P. J., Stanton, J. B., Yan, L., Crabb, J. W., Marmorstein, A. D. (2002). Bestrophin interacts physically and functionally with protein phosphatase 2A. *J Biol Chem.* 277, 30591-30597

77. Marmorstein, L. Y., Wu, J., McLaughlin, P., Yocom, J., Karl, M. O., Neussert, R., Wimmers, S., Stanton, J. B., Gregg, R. G., Strauss, O., Peachey, N. S., Marmorstein, A. D. (2006). The Light Peak of the Electroretinogram Is Dependent on Voltage-gated Calcium Channels and Antagonized by Bestrophin (Best-1). *J Gen.Physiol.* 127, 577-589

78. McBride, D. W., Jr., Roper, S. D. (1991). Ca(2+)-dependent chloride conductance in Necturus taste cells. *J.Membr.Biol.* 124, 85-93

79. Melvin, J. E., Yule, D., Shuttleworth, T., Begenisich, T. (2005). Regulation of fluid and electrolyte secretion in salivary gland acinar cells. *Annu.Rev.Physiol.* 67, 445-469

80. Milenkovic, V. M., Langmann, T., Schreiber, R., Kunzelmann, K., Weber, B. H. F. (2008). Molecular evolution and functional divergence of the bestrophin protein family. *BMC Evolutionary Biology* 8, 72-78

81. Milenkovic, V. M., Rivera, A., Horling, F., Weber, B. H. (2007). Insertion and topology of normal and mutant bestrophin-1 in the endoplasmic reticulum membrane. *J Biol Chem.* 282, 1313-1321

82. Milenkovic, V. M., Schreiber R., Barro-Soria R., Aldehni F., Kunzelmann, K. (2008). Functional assembly and purinergic activation of bestrophins. *BBA. (submitted)*

83. Mizukawa, Y., Nishizawa, T., Nagao, T., Kitamura, K., Urushidani, T. (2002). Cellular distribution of parchorin, a chloride intracellular channel-related protein, in various tissues. *Am.J Physiol Cell Physiol.* 282, C786-C795

84. Morris, A. P., Frizzell, R. A. (1993). Ca(2+)-dependent Cl^- channels in undifferentiated human colonic cells (HT-29). I. Single-channel properties. *Am J Physiol.* 264, C968-C976

85. Motoshima, H., Goldstein, B. J., Igata, M., Araki, E. (2006). AMPK and cell proliferation--AMPK as a therapeutic target for atherosclerosis and cancer. *J Physiol.* 574, 63-71

86. Nakamoto, T., Srivastava, A., Romanenko, V. G., Ovitt, C. E., Perez-Cornejo, P., Arreola, J., Begenisich, T., Melvin, J. E. (2007). Functional and molecular characterization of the fluid secretion mechanism in human parotid acinar cells. *Am J Physiol Regul.Integr.Comp Physiol.* 292, R2380-R2390

87. Nilius, B., Droogmans, G. (2003). Amazing chloride channels: an overview. *Acta Physiol Scand.* 177, 119-147

88. Nilius, B., Prenen, J., Wei, L., Tanzi, F., Voets, T., Droogmans, G. (1997). Calcium-activated chloride channels in bovine pulmonary artery endothelial cells. *J.Physiol.* 498, 381-396

89. Nilius, B., Voets, T. (2005). TRP channels: a TR(I)P through a world of multifunctional cation channels. *Pflugers Arch.* 451, 1-10

90. Ousingsawat, J., Spitzner, M., Puntheeranurak, S., Terracciano, L., Tornillo, L., Bubendorf, L., Kunzelmann, K., Schreiber, R. (2007). Expression of voltage gated potassium channels in human and mouse colonic carcinoma. *Clinical Cancer Research.* 13, 824-831

91. Paradiso, A. M., Ribeiro, C. M., Boucher, R. C. (2001). Polarized Signaling via Purinoceptors in Normal and Cystic Fibrosis Airway Epithelia. *J Gen.Physiol.* 117, 53-68

92. Pardo, L. A. (2004). Voltage-gated potassium channels in cell proliferation. *Physiology (Bethesda.)* 19, 285-292

93. Pardo, L. A., Contreras-Jurado, C., Zientkowska, M., Alves, F., Stuhmer, W. (2005). Role of voltage-gated potassium channels in cancer. *J Membr.Biol.* 205, 115-124

94. Pauli, B. U., Abdel-Ghany, M., Cheng, H. C., Gruber, A. D., Archibald, H. A., Elble, R. C. (2000). Molecular characteristics and functional diversity of CLCA family members. *Clin Exp Pharmacol Physiol.* 27, 901-905

95. Petersen, O. H. (2005). Ca^{2+} signalling and Ca^{2+}-activated ion channels in exocrine acinar cells. *Cell Calcium.* 38, 171-200

96. Peterson, W. M., Meggyesy, C., Yu, K., Miller, S. S. (1997). Extracellular ATP activates calcium signaling, ion, and fluid transport in retinal pigment epithelium. *J Neurosci.* 17, 2324-2337

97. Petrukhin, K., Koisti, M. J., Bakall, B., Li, W., Xie, G., Marknell, T., Sandgren, O., Forsman, K., Holmgren, G., Andreasson, S., Vujic, M., Bergen, A. A., McGarty-Dugan, V., Figueroa, D., Austin, C. P., Metzker, M. L., Caskey, C. T., Wadelius, C. (1998). Identification of the gene responsible for Best macular dystrophy. *Nat.Genet.* 19, 241-247

98. Pifferi, S., Pascarella, G., Boccaccio, A., Mazzatenta, A., Gustincich, S., Menini, A., Zucchelli, S. (2006). Bestrophin-2 is a candidate calcium-activated chloride channel involved in olfactory transduction. *Proc.Natl.Acad.Sci.U.S.A.* 103, 12929-12934

99. Piper, A. S., Greenwood, I. A., Large, W. A. (2002). Dual effect of blocking agents on Ca^{2+}-activated Cl(-) currents in rabbit pulmonary artery smooth muscle cells. *J.Physiol.* 539, 119-131

100. Piper, A. S., Large, W. A. (2003). Multiple conductance states of single Ca^{2+}-activated Cl^- channels in rabbit pulmonary artery smooth muscle cells. *J.Physiol.* 547, 181-196

101. Puntheeranurak, S., Schreiber, R., Kunzelmann, K., Krishnamra, N. (2007). Control of ion transport in mouse proximal and distal colon by prolactin. *Cell Physiol Biochem.* 19, 77-88

102. Qu, Z., Chien, L. T., Cui, Y., Hartzell, H. C. (2006). The anion-selective pore of the bestrophins, a family of chloride channels associated with retinal degeneration. *J Neurosci.* 26, 5411-5419

103. Qu, Z., Cui, Y., Hartzell, H. C. (2006). A short motif in the C-terminus of mouse bestrophin 3 [corrected] inhibits its activation as a Cl channel. *FEBS Lett.* 580, 2141-2146

104. Qu, Z., Fischmeister, R., Hartzell, H. C. (2004). Mouse bestrophin-2 is a bona fide Cl^- channel: identification of a residue important in anion binding and conduction. *J Gen Physiol.* 123, 327-340

105. Qu, Z., Hartzell, H. C. (2000). Anion permeation in Ca(2+)-activated Cl^- channels. *J Gen.Physiol.* 116, 825-844

106. Qu, Z., Hartzell, H. C. (2001). Functional geometry of the permeation pathway of Ca^{2+}-activated Cl^- channels inferred from analysis of voltage-dependent block. *J Biol Chem.* 276, 18423-18429

107. Qu, Z., Hartzell, H. C. (2004). Determinants of anion permeation in the second transmembrane domain of the mouse bestrophin-2 chloride channel. *J Gen.Physiol.* 124, 371-382

108. Qu, Z., Hartzell, H. C. (2008). Bestrophin Cl^- Channels are Highly Permeable to HCO3-. *Am.J.Physiol Cell Physiol. (in press)*.

109. Qu, Z., Wei, R. W., Hartzell, H. C. (2003). Characterization of Ca^{2+}-activated Cl^- Currents in Mouse Kidney Inner Medullary Collecting Duct Cells. *Am.J Physiol Renal Physiol* 285, F326-F335

110. Qu, Z., Wei, R. W., Mann, W., Hartzell, H. C. (2003). Two bestrophins cloned from Xenopus laevis Oocytes express Ca-activated Cl currents. *J Biol Chem.* 278, 49563-49572

111. Qu, Z., Yu, K., Cui, Y., Ying, C., Hartzell, H. C. (2007). Activation of bestrophin Cl channels is regulated by C-terminal domains. *J Biol Chem.* 282, 17460-17467

112. Rao, J. N., Platoshyn, O., Li, L., Guo, X., Golovina, V. A., Yuan, J. X., Wang, J. Y. (2002). Activation of K(+) channels and increased migration of differentiated intestinal epithelial cells after wounding. *Am.J Physiol Cell Physiol.* 282, C885-C898

113. Reigada, D., Lu, W., Mitchell, C. H. (2006). Glutamate acts at NMDA receptors on fresh bovine and on cultured human retinal pigment epithelial cells to trigger release of ATP. *J Physiol.* 575, 707-720

114. Roper, S. D. (2007). Signal transduction and information processing in mammalian taste buds. *Pflugers Arch.* 454, 759-776

115. Rosenthal, R., Bakall, B., Kinnick, T., Peachey, N., Wimmers, S., Wadelius, C., Marmorstein, A. D., Strauss, O. (2005). Expression of bestrophin-1, the product of the VMD2 gene, modulates voltage-dependent Ca^{2+} channels in retinal pigment epithelial cells. *FASEB J.* 20, 178-180

116. Rozmahel, R., Wilschanski, M., Matin, A., Plyte, S., Oliver, M., Auerbach, W., Moore, A., Forstner, J., Durie, P., Nadeau, J., Bear, C., Tsui, L. C. (1996). Modulation of disease severity in cystic fibrosis transmembrane conductance regulator deficient mice by a secondary genetic factor. *Nat.Genet.* 12, 280-287

117. Schlatter, E., Greger, R., Schafer, J. A. (1990). Principal cells of cortical collecting ducts of the rat are not a route of transepithelial Cl^- transport. *Pflugers Arch.* 417, 317-323

118. Schonherr, R. (2005). Clinical relevance of ion channels for diagnosis and therapy of cancer. *J Membr.Biol.* 205, 175-184

119. Schreiber, R., Kunzelmann, K. (2005). Purinergic P2Y6 receptors induce Ca^{2+} and CFTR dependent Cl^- secretion in mouse trachea. *Cell Physiol Biochem.* 16, 99-108

120. Schwab, A. (2001). Ion channels and transporters on the move. *News Physiol Sci.* 16, 29-33

121. Schwab, A., Wojnowski, L., Gabriel, K., Oberleithner, H. (1994). Oscillating activity of a Ca(2+)-sensitive K^+ channel. A prerequisite for migration of transformed Madin-Darby canine kidney focus cells. *J Clin.Invest.* 93, 1631-1636

122. Smyth, J. T., Dehaven, W. I., Jones, B. F., Mercer, J. C., Trebak, M., Vazquez, G., Putney, J. W., Jr. (2006). Emerging perspectives in store-operated Ca^{2+} entry: roles of Orai, Stim and TRP. *Biochim.Biophys.Acta.* 1763, 1147-1160

123. Spitzner, M., Martins, J. R., Soria, R. B., Ousingsawat, J., Scheidt, K., Schreiber, R., Kunzelmann, K. (2008). Eag1 and Bestrophin 1 are up-regulated in fast-growing colonic cancer cells. *J.Biol.Chem.* 283, 7421-7428

124. Spitzner, M., Ousingsawat, J., Scheidt, K., Kunzelmann, K., Schreiber, R. (2006). Role of voltage gated K^+ channels for proliferation of colonic cancer cells. *FASEB J.* 21, 35-44

125. Stansfeld, C. E., Roper, J., Ludwig, J., Weseloh, R. M., Marsh, S. J., Brown, D. A., Pongs, O. (1996). Elevation of intracellular calcium by muscarinic receptor activation induces a block of voltage-activated rat ether-a-go-go channels in a stably transfected cell line. *Proc.Natl.Acad.Sci.U.S.A.* 93, 9910-9914

126. Stanton, J. B., Goldberg, A. F., Hoppe, G., Marmorstein, L. Y., Marmorstein, A. D. (2006). Hydrodynamic properties of porcine bestrophin-1 in Triton X-100. *Biochim.Biophys.Acta.* 1758, 241-247

127. Strauss, O. (2005). The retinal pigment epithelium in visual function. *Physiol Rev.* 85, 845-881

128. Stuhmer, W., Alves, F., Hartung, F., Zientkowska, M., Pardo, L. A. (2006). Potassium channels as tumour markers. *FEBS Lett.* 580, 2850-2852

129. Stutts, M. J., Fitz, J. G., Paradiso, A. M., Boucher, R. C. (1994). Multiple modes of regulation of airway epithelial chloride secretion by ATP. *Am.J.Physiol.* 267, C1442-C1451

130. Sun, H., Tsunenari, T., Yau, K. W., Nathans, J. (2002). The vitelliform macular dystrophy protein defines a new family of chloride channels. *Proc.Natl.Acad.Sci.U.S.A.* 99, 4008-4013

131. Suzuki, M., Mizuno, A. (2004) A novel human Cl(-) channel family related to Drosophila flightless locus. *J Biol Chem.* 279, 22461-22468

132. Suzuki, M., Mizuno, A. (2004). A novel human Cl(-) channel family related to Drosophila flightless locus. *J Biol Chem.* 279, 22461-22468

133. Suzuki, M., Morita, T., Iwamoto, T. (2006). Diversity of Cl(-) channels. *Cell Mol.Life Sci.* 63, 12-24

134. Szabo, I., Gulbins, E., Apfel, H., Zhang, X., Barth, P., Busch, A. E., Schlottmann, K., Pongs, O., Lang, F. (1996). Tyrosine phosphorylation-dependent suppression of a voltage-gated K^+ channel in T lymphocytes upon Fas stimulation. *J Biol Chem.* 271, 20465-20469

135. Tarran, R., Button, B., Boucher, R. C. (2006). Regulation of normal and cystic fibrosis airway surface liquid volume by phasic shear stress. *Annu.Rev.Physiol.* 68, 543-561

136. Tarran, R., Button, B., Picher, M., Paradiso, A. M., Ribeiro, C. M., Lazarowski, E. R., Zhang, L., Collins, P. L., Pickles, R. J., Fredburg, J. J., Boucher, R. C. (2005). Normal and cystic fbrosis airway surface liquid homeostasis: The effects of phasic shear stress and viral infections. *J Biol Chem.* 280, 35751-35759

137. Tarran, R., Loewen, M. E., Paradiso, A. M., Olsen, J. C., Gray, M. A., Argent, B. E., Boucher, R. C., Gabriel, S. E. (2002). Regulation of murine airway surface liquid volume by CFTR and Ca^{2+}-activated Cl^- conductances. *J Gen.Physiol.* 120, 407-418

138. Tsunenari, T., Nathans, J., Yau, K. W. (2006). Ca^{2+}-activated Cl^- Current from Human Bestrophin-4 in Excised Membrane Patches. *J Gen.Physiol.* 127, 749-754

139. Tsunenari, T., Sun, H., Williams, J., Cahill, H., Smallwood, P., Yau, K. W., Nathans, J. (2003). Structure-function analysis of the bestrophin family of anion channels. *J Biol Chem.* 278, 41114-41125

140. Wang, Y. X., Kotlikoff, M. I. (1997) Inactivation of calcium-activated chloride channels in smooth muscle by calcium/calmodulin-dependent protein kinase. *Proc.Natl.Acad.Sci.U.S.A.* 94, 14918-14923

141. Wang, Z. (2004). Roles of K^+ channels in regulating tumour cell proliferation and apoptosis. *Pflugers Arch.* 448, 274-286

142. Webb, D. J., Nuccitelli, R. (1985). Fertilization potential and electrical properties of the Xenopus laevis egg. *Dev.Biol.* 107, 395-406

143. Wei, L., Vankeerberghen, A., Cuppens, H., Eggermont, J., Cassiman, J. J., Droogmans, G., Nilius, B. (1999). Interaction between calcium-activated chloride channels and the cystic fibrosis transmembrane conductance regulator. *Pflugers Arch.* 438, 635-641

144. White, M. M., Aylwin, M. (1990). Niflumic and flufenamic acids are potent reversible blockers of Ca2(+)-activated Cl^- channels in Xenopus oocytes. *Mol.Pharmacol.* 37, 720-724

145. Wonderlin, W. F., Strobl, J. S. (1996). Potassium channels, proliferation and G1 progression. *J Membr.Biol.* 154, 91-107

146. Wong, C. H., Ko, W. H. (2002). Stimulation of Cl^- secretion via membrane-restricted Ca^{2+} signaling mediated by P2Y receptors in polarized epithelia. *J Biol Chem.* 277, 9016-9021

147. Worrell, R. T., Frizzell, R. A. (1991). CaMKII mediates stimulation of chloride conductance by calcium in T_{84}. *Am.J.Physiol.* 260, C877-C882

148. Wu, J., Marmorstein, A. D., Striessnig, J., Peachey, N. S. (2007). Voltage-dependent calcium channel CaV1.3 subunits regulate the light peak of the electroretinogram. *J Neurophysiol.* 97, 3731-3735

149. Yardley, J., Leroy, B. P., Hart-Holden, N., Lafaut, B. A., Loeys, B., Messiaen, L. M., Perveen, R., Reddy, M. A., Bhattacharya, S. S., Traboulsi, E., Baralle, D., De Laey, J. J., Puech, B., Kestelyn, P., Moore, A. T., Manson, F. D., Black, G. C. (2004). Mutations of VMD2 splicing regulators cause nanophthalmos and autosomal dominant vitreoretinochoroidopathy (ADVIRC). *Invest Ophthalmol.Vis.Sci.* 45, 3683-3689

150. Yau, K. W. (1994). Phototransduction mechanism in retinal rods and cones. The Friedenwald Lecture. *Invest Ophthalmol.Vis.Sci.* 35, 9-32

151. Yu, K., Cui, Y., Hartzell, H. C. (2006). The Bestrophin Mutation A243V, Linked to Adult-Onset Vitelliform Macular Dystrophy, Impairs Its Chloride Channel Function. *Invest Ophthalmol.Vis.Sci.* 47, 4956-4961

152. Zhang, S. L., Yu, Y., Roos, J., Kozak, J. A., Deerinck, T. J., Ellisman, M. H., Stauderman, K. A., Cahalan, M. D. (2005). STIM1 is a Ca^{2+} sensor that activates CRAC channels and migrates from the Ca^{2+} store to the plasma membrane. *Nature.* 437, 902-905

153. Zygmunt, A. C. (1994). Intracellular calcium activates a chloride current in canine ventricular myocytes. *Am.J.Physiol.* 267, H1984-H1995

154. Zygmunt, A. C., Robitelle, D. C., Eddlestone, G. T. (1997). Ito1 dictates behavior of ICl(Ca) during early repolarization of canine ventricle. *Am.J.Physiol.* 273, H1096-H1106

Acknowledgements/ Agradecimientos

I want to express my gratitude to those people who where next to me during this tough but also beautiful period of my life.

First of all I want to thank my tutor, prof. Dr. K. Kunzelmann for giving me the opportunity to work in his group. Through his guidance I started to love and understand Physiology. With no doubt, this thesis is possible thanks to his invaluable advice. I am very thankful as well for all the time out of the lab we spent together.

I want to acknowledge prof. Dr. R. Warth, prof. Dr. O. Strauss, prof. Dr. S. Schneuwly and prof. Dr. G. Längst for their kindness in accepting the revision of my thesis.

Spetial mention to the Friedrich-Ebert Stiftung for finance my studies. To Herr. J. Minzenbach for his constant support and attentions. My gratitude for the financial support to: DFG SFB699 A6 and A7, DFG KU 756/9-1 and Else-Kröner-Fresenius Stiftung.

Special Thanks to Dr. Rainer Schreiber for his wise advices and excellent guidance. My gratitude to Agnes Paech and Ernestine Tartler for their invaluable technical help and love. The lab's mates and neighbour colleages, for their support and patience with me. Thanks to: Ji, Melanie, Tanja, Joana, Fadi, Aim, Raquel, Marisa, Diana, Higgl, Vladi, Marcela, Rosi, Kerstin, Simone und Markus für die Übersetzung meiner Zusammenfassung. Again thanks to prof. Dr. R. Warth for his corrections and oppropiate suggestions as well as for his friendship.

A Noki fofita, por las sugerencias, críticas y noches dedicadas a esta Tesis. Marisa, Raquel y J. Garcia. A mis amigos Mary, Ste y su lindo Joseph por estar ahí siempre para mi. A mi profesora O. Castañeda por su confianza. A la "mami" Adyi y el "papi" Roge. A mis hermanos Ulises, Alian, Migue, Ashley, Ilenana, Veit y todos los de la pandilla. Un cariño especial a Mailita. Para Christine todo mi amor y agradecimiento, vielen Dank meine freund. A mis brothers del día a día, Nesty y J.R, gracias chamas. A mi querida Tanja, du bis ganz tief im mein Herz. Mein Doktorarbeit war auch möglich wegen dir. Vielen Dank Tanjta.

Por último mi amor inconmensurable y agradecimiento a mi mamá y papá, por todo el apoyo en estos casi 4 años de dura separación. Su confianza y amor fortalecieron mi, por momentos, lánguido espíritu y permitieron que esta tesis se realizara. A mis hermanas y sobrinos por su amor y presencia. A toda mi familia que es la alegria de mi vida, muchas gracias.

Publications

Publications used in this thesis

Barro-Soria,R., Spitzner,M., Schreiber,R. and Kunzelmann,K. (2006) Bestrophin 1 enables Ca^{2+}-activated Cl^- conductance in epithelia. J Biol Chem 281:17460-17467.

Barro-Soria,R., Schreiber,R. and Kunzelmann,K. (2008) Bestrophin 1 and 2 are components of the Ca^{2+}-activated Cl^- conductance in mouse airways. BBA (submitted).

Milenkovic,V.M., Schreiber,R., **Barro-Soria,R.**, AlDehni,F., and Kunzelmann,K. (2008) Functional assembly and purinergic activation of bestrophins. BBA (submitted).

Spitzner,M., Martins,J.R., **Barro-Soria,R.**, Ousingsawat,J., Scheidt,K., Schreiber,R. and Kunzelmann, K. (2008) Eag1 and Bestrophin1 are up-regulated in fast-growing colonic cancer cells. J Biol Chem 283: 7421-7428.

Other publications

AlDehni,F., Spitzner,M., Martins,J.R., **Barro-Soria,R.**, Schreiber,R. and Kunzelmann, K. (2008) Role of bestrophin for proliferation and in epithelial to mesenchymal transition. J Am Soc Nephrol (submitted).

Grangeia,A., **Barro-Soria,R.**, Carvalho,F., Damas,A.M., Mauricio,A.C., Kunzelmann,K., Sousa,M. and Barros,A. (2007) Novel CFTR mutations causing CBAVD. Cell Physiol Biochem (submitted).

Kunzelmann,K., Milenkovic,V.M., Spitzner,M., **Barro-Soria,R.** and Schreiber,R. (2007) Calcium dependent chloride conductance in epithelia: Is there a contribution by Bestrophin? Pflügers Arch 454:879-889.

Presentations at scientific conferences

Barro-Soria,R., Schreiber,R. and Kunzelmann,K. Cellular role of the putative Ca^{2+}-activated Cl^- channel bestrophin. Poster presentation at: ARVO annual meeting. Eyes on innovation. 2008, Fort Lauderdale, USA.

Barro-Soria,R., Schreiber,R. and Kunzelmann,K. Bestrophin 1 and 2 are both involved in the calcium-activated chloride secretion in mouse airways. Oral presentation at: The 87th annual meeting of the *Deutsche Physiologische Gesellschaft*. 2008, Cologne.

Barro-Soria,R., Schreiber,R. and Kunzelmann,K. Bestrophin 1 and 2 are important components of the Ca^{2+} activated Cl^- channel in mouse airways epithelium. Oral presentation at: ECFS Conference - New Frontiers in Basic Science of Cystic Fibrosis, 2007, Tavira, Portugal.

Barro-Soria,R., Schreiber,R. and Kunzelmann,K. Bestrophin 1 and 2 are both components of the Ca^{2+}-activated Cl^- channel in mouse airways epithelium. Oral presentation at: The 86th annual meeting of the *Deutsche Physiologische Gesellschaft*. 2007, Hannover, Germany.

Barro-Soria,R., Schreiber,R. and Kunzelmann,K. Bestrophin may form the calcium-activated chloride channel in epithelial cells. Oral presentation at: The 85th annual meeting of the *Deutsche Physiologische Gesellschaft*. 2006, Munich, Germany.

Erklärung

Hiermit versichere ich, dass ich die vorliegende Arbeit selbstständig verfasst und keine anderen als die angegebenen Hilfsmittel verwendet habe.

Regensburg, im Mai 2008 _____